The Astrophysical Journal Supplement Series, 161:271–303, 2005 December

THE X-RAY BINARY POPULATION IN M33. I. SOURCE LIST AND LUMINOSITY FUNCTION

H.-J. Grimm,[1] J. McDowell,[1] A. Zezas,[1] D.-W. Kim,[1] and G. Fabbiano[1]

Received 2005 January 25; accepted 2005 June 26

ABSTRACT

In this paper we present the source list for three *Chandra* observations of the Local Group galaxy M33. The observations are centered on the nucleus and on the star-forming region NGC 604. We detect a total of 261 sources in an area of $\sim$0.2 deg^2 down to a flux limit of 3×10^{-16} ergs s^{-1} cm^{-2}, which corresponds to a luminosity of $\sim 2 \times 10^{34}$ ergs s^{-1} at a distance of 840 kpc. From the source list we construct the luminosity functions of sources observed in M33. If we take into account background contamination, the luminosity functions are consistent with those of other star-forming galaxies. In addition, the combination of X-ray color analysis and the existence of "blue" optical counterparts strongly indicates that the X-ray point-source population in M33 consists of young objects. Above 3×10^{35} ergs s^{-1} there are few X-ray sources in the locus of the X-ray hardness ratio diagram that is generally populated by low-mass X-ray binaries.

Subject heading: galaxies: individual (M33, NGC 598)

Online material: color figures, machine-readable tables

1. INTRODUCTION

M33 is a late-type spiral galaxy, type Sc II–III, and the third largest galaxy in the Local Group. In the Local Group it occupies a unique place since morphologically it is of intermediate type between the large early-type spiral galaxies (Milky Way and M31) and the numerous irregular galaxies. In contrast to M31 and the Milky Way, M33 does not have a stellar bulge and also does not contain a supermassive black hole at the center (Gebhardt et al. 2001). Other galaxies of this type cannot be investigated with the same depth even with *Chandra*: at a distance of 840 kpc (Freedman et al. 1991) M33 is the second nearest spiral galaxy; it spans roughly $73' \times 45'$ on the sky; the line-of-sight absorption column density[2] is small, $N_{\rm H} \sim 6 \times 10^{20}$ cm^{-2}. M33 is more actively star forming (SFR ~ 0.3–$0.7\ M_\odot$ yr^{-1}) than either the Milky Way or M31 (Hippelein et al. 2003), particularly compared to its much smaller mass. This star formation activity is visible in a number of large H II regions in the disk of M33.

As a large nearby galaxy, M33 has been observed with a number of X-ray satellites. The *Einstein Observatory* detected 17 point sources (Trinchieri et al. 1988), among them a clear eclipsing binary (M33 X-7; Peres et al. 1989). Markert & Rallis (1983) established the existence of an X-ray binary population based on X-ray variability and noted the association of the X-ray sources with young stellar populations. *Röntgensatellit* (*ROSAT*) observations led to the detection of a total of 184 fainter sources coincident with Population I markers; a number of these X-ray sources are identified with supernova remnants (SNRs; Long et al. 1996; Haberl & Pietsch 2001). *BeppoSAX* spectroscopy showed that the spectra of the brighter X-ray sources in M33 are consistent with X-ray binaries and that up to five sources are variable (Parmar et al. 2001).

M33's proximity, angular size, and low line-of-sight column density provide unique advantages for the study of the X-ray population of this late-type spiral galaxy: (1) The same amount of detail is achievable in M33 as in M31 ($1'' = 4.1$ pc). (2) The smaller angular size of M33 allows the observation of a larger fraction of the galaxy in a single exposure, unlike M31 or the LMC or SMC. (3) The low line-of-sight $N_{\rm H}$ and the proximity of M33 allow the study of a luminosity range (few 10^{34}–10^{38} ergs s^{-1}) inaccessible in more distant galaxies. Sources in this luminosity range are more difficult to survey in both the Milky Way and M31 because of their larger angular sizes, which require very long observing times. Moreover, in the Milky Way distance uncertainties for individual sources, and partly high $N_{\rm H}$, make this type of study more uncertain. (4) The higher star formation rate of M33 results in a different population of X-ray sources compared to those in the Milky Way and M31. (5) Its proximity combined with the positional accuracy and sensitivity of *Chandra* allows a detailed comparison of the X-ray sources with cataloged sources at other wavelengths. This is crucial to understand the X-ray source population in detail and to gain a complete picture of the X-ray binary population.

In this paper we present the source list, luminosities, X-ray luminosity functions, and identifications of X-ray point sources in M33. An accompanying paper will investigate the detailed properties and X-ray spectra of the point source population.

2. *CHANDRA* DATA AND ANALYSIS

For this study we used three of the *Chandra* observations of M33 (Table 1). A short ($\sim$12 ks) fourth observation, ObsID 787, was disregarded. This observation was aimed at studying the nucleus and suffers from both high background and small field of view (FOV; $\sim$54 arcmin^2). Due to the angular extent of M33, all active Advanced CCD Imaging Spectrometer (ACIS) chips cover areas of M33. These include the standard ACIS-S configuration for ObsID 786 and the standard ACIS-I configuration for ObsIDs 1730 and 2023. There is considerable overlap between the different observations. However, because of the decreasing resolution/sensitivity with increasing off-axis angle, only the inner parts of M33 ($\sim 8'$–$10'$) have a significant number of detected sources in two observations, 786 and 1730.

We used CIAO versions 3.0.1 and 3.0.2 and CALDB versions 2.24 and 2.25 to analyze the data. There were no changes to the ACIS data preparation software or to the source detection software or to relevant files in the CALDB between these versions.

[1] Harvard-Smithsonian Center for Astrophysics, 60 Garden Street, Cambridge, MA 02138.

[2] Obtained from the `colden` tool (http://cxc.harvard.edu/toolkit/colden.jsp) based on NRAO data compiled by Dickey & Lockman (1990).

TABLE 1
List of ACIS Observations of M33

ObsID	Date	Aim Point	Duration (ks)	Chips	Data Mode
786.....	2000 Aug 30	Nucleus	45	ACIS-I 2–3, ACIS-S 1–4	FAINT
1730.....	2000 Jul 12	Nucleus	45	ACIS-I 0–3, ACIS-S 2–3	VFAINT
2023.....	2001 Jul 6	NGC 604	90	ACIS-I 0–3, ACIS-S 2–3	FAINT

We do not correct for enhanced absorption due to the hydrocarbon accumulation on the chips. The observations do not suffer from strong background flares, but short times of higher background (3 σ above the mean) have been excluded. The effective exposure times are ~45, ~43, and ~89 ks for observations 786, 1730, and 2023, respectively. We correct for time-dependent variations of the gain with the `corr_tgain` program developed by A. Vikhlinin.[3]

Source detection was performed with `wavdetect` on scales of 1, 2, 4, 8, 10, 12, and 16 pixels. The full energy range, 0.3–8.0 keV, was also subdivided in a soft band, 0.3–2 keV, and a hard band, 2–8 keV. Source detection was done in all three bands. The chance detection threshold was set to 10^{-6}, equivalent to 1 spurious detection per million pixels. Due to strong pile-up, these scales fail to detect the nucleus of M33 unambiguously. Moreover, the H II regions NGC 604 and IC 131, which are more extended than the scales used, were detected by visual inspection and interactive analysis. The nucleus of M33 is strongly piled up and was therefore excluded from the analysis. For details on the nuclear sources refer, e.g., to Dubus et al. (2004) and La Parola et al. (2003). The source regions correspond to the 3 σ ellipses output from `wavdetect`. All source regions were inspected by eye and, if necessary, adjusted for overlapping with nearby regions and to cover the whole extent of a source. Due to the partly crowded fields, particularly near the aim point, we chose background regions on each chip in a large source-free area to ensure a sufficient number of background counts. This background region was used for all sources on the corresponding chip. Since M33 has no significant intrinsic diffuse emission due to hot gas, with the exception of the inner 2′ around the nucleus, the background does not vary significantly over our FOV. Therefore, our approach does not introduce significant errors in the intensity of the sources. Note that for ObsID 786 most of the sources are on the back-illuminated ACIS-S3 chip, whereas the majority of sources in the other observations is on the ACIS-I chips. The source counts were computed according to

$$C_{\rm source} = C - \frac{A_{\rm source}}{A_{\rm bkg}} C_{\rm bkg} \frac{E_{\rm source}}{E_{\rm bkg}}, \qquad (1)$$

where $C_{\rm source}$ and $C_{\rm bkg}$ are the source and background counts, C is the observed counts, $A_{\rm source}$ and $A_{\rm bkg}$ are the source and background region areas of the extraction apertures, and $E_{\rm source}$ and $E_{\rm bkg}$ are the exposures for the source and background areas. For sources that are not detected in one of the energy bands, we compute upper limits on the number of source counts following the approach of Kraft et al. (1991). A few of these sources show nonzero lower limits, which indicate the presence of a source. In these cases we used the most probable value for the source counts obtained with the method of Kraft et al. (1991). These sources are marked in Table 3 below.

In order to obtain proper positional uncertainties for our sources, which are important for identifications with objects at other wavelengths, we use the formula of Kim et al. (2004a). This formula assumes that variations in the absolute astrometric accuracy from observation to observation are small and therefore that the uncertainties depend only on count rate and off-axis angle. The positional uncertainty is given as a function of off-axis angle in the high- and low-count regimes. We use 100 counts to discriminate between low- and high-count sources. The density of point sources is small enough that sources are identified unambiguously, with the possible exception of the nucleus and the H II region NGC 604. These two cases, however, are problematic only in terms of the background they provide for other sources. In the cases where a source is observed in two or three observations, we take as the positional uncertainty the smallest value of the available observations.

To derive X-ray colors we subdivided the observations into three energy bands—soft (0.3–1.0 keV), medium (1.0–2.1 keV), and hard (2.1–8.0 keV)—and measured the number of counts within the source aperture in each band. For count extraction we use the source regions in the total band from 0.3 to 8.0 keV. Since very faint sources, i.e., sources with fewer than 20 counts in the total band, are not used in the color analysis, this choice does not introduce a significant error in the extracted counts. Of the 288 sources detected in the whole band in all observations, 99 sources have fewer than 20 counts. Most of the sources are too faint to be investigated for spectral variability. Spectral variability of brighter sources for which spectra can be extracted will be discussed in a separate paper.

3. POINT SOURCE DETECTIONS

The number of sources detected with `wavdetect` in the different energy bands is given in Table 2. Note that because of the overlapping fields of view some of the sources appear in more than one observation. Also some sources are detected only in one of the three energy bands. The combined number of individual

TABLE 2
Number of Sources Detected in Different Energy Bands and Observations

	Energy Band (keV)			
ObsID	0.3–2.0	2.0–8.0	0.3–8.0	Total Number of Sources
786.....	79 (53)	47 (32)	96 (60)	121
1730.....	68 (37)	48 (30)	84 (47)	98
2023.....	99 (30)	68 (21)	112 (33)	129

Notes.—Note that due to overlapping observations some of the sources appear in more than one observation. Their number for each band is given in parentheses.

[3] See http://asc.harvard.edu/cont-soft/software/corr_tgain.1.0.html.

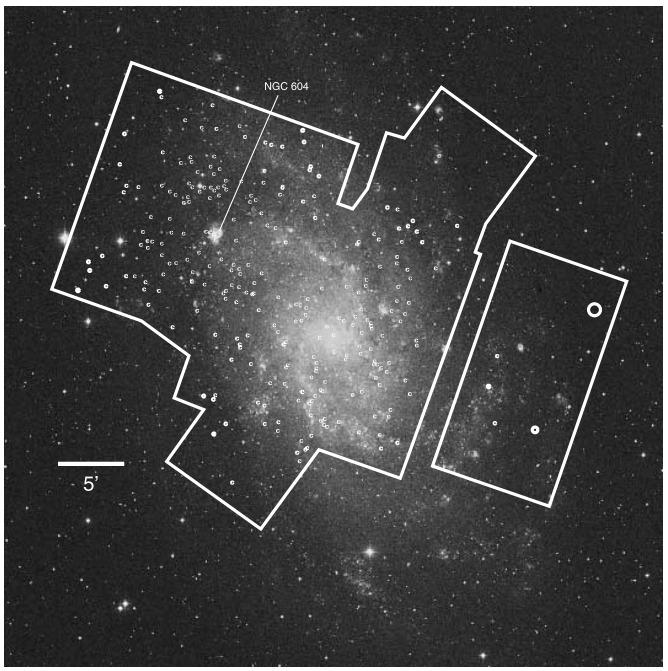

FIG. 1.—DSS image of M33 overlaid with source regions and the envelope of the *Chandra* field of view. North is up, and east is to the left. [*See the electronic edition of the Supplement for a color version of this figure.*]

sources from all observations is 261. Among these sources 25 are detected only in the soft (0.3–2.0 keV) band and 16 only in the hard (2.0–8.0 keV) band. These hard sources have either intrinsically hard spectra or are attenuated by the interstellar medium within M33, since the Galactic absorption toward M33 is relatively small. Figure 1 shows a Digitized Sky Survey image of M33 overlaid with the source regions and the detector outline for the three observations.

The source list, including position, counts, and fluxes, is presented in Table 3 in the Appendix: column (1) gives the *Chandra* source name, column (2) the sky position and positional uncertainty, column (3) the Obs ID, columns (4), (5), and (6) the number of counts in the total, soft, and hard bands for the three observations, columns (7), (8), and (9) the number of counts in the color bands, columns (10), (11), and (12) the flux in the total, soft, and hard bands, and column (13) the luminosity in the total band. The errors given on the counts are computed using the Gehrels approximation, $\sigma = 1 + (N + 0.75)^{1/2}$ (Gehrels 1986). Upper limits of 99% on the counts were calculated in one of two ways: (1) Because observations 1730 and 786 have the same aim point, the extent of sources is comparable between these observation; thus, if a source was detected in observations 1730 or 786 in another energy band, this source region was used to compute the upper limits for observations 1730 and/or 786. (2) If the source was not detected in either of these observations, upper limits were calculated from counts in a 2″ region around the source position.

The observation time of ObsID 2023 is twice as long as in the other two observations. This explains the larger number of sources compared to observation 1730, which uses the same instrumental configuration. The similar number of source detections in ObsIDs 786 and 2023 is both due to the use in ObsID 786 of the two back-illuminated (BI) chips S3 and S5 that have a higher sensitivity at low energies than the front-illuminated (FI) chips and to the aim at the center of M33, where the source density might be higher. Because of the different exposure times, upper limits for non-detections in the 2023 observation are smaller than in the other observations. Moreover, the ~100% completeness of this observation reaches down to $\sim(2-3)\times10^{-15}$ ergs s^{-1} cm^{-2}, compared to $\sim(6-7)\times10^{-15}$ ergs s^{-1} cm^{-2} for both other observations. The completeness estimate is derived from simulations for correcting the luminosity function according to Kim & Fabbiano (2003). The correction is based on simulations of the detection probability of point sources with a range of flux values for various off-axis angles from the aim point. The simulations are performed with the MARX simulator.[4] The effects taken into account in the simulations are the decreasing sensitivity with increasing off-axis angle, diffuse background (not important here), uneven sky coverage of the S3 chip, and telescope vignetting as described in the exposure maps.

For sources with more than 80 counts we extracted radial profiles of the source counts and fitted them with a Gaussian plus background. We compared the FWHM of the Gaussian with a Gaussian fit of the point-spread function. For the 59 sources with sufficient counts we find no evidence of extended emission.

Given the large area covered by the observations, we expect to have serious contamination by background active galactic nuclei (AGNs), in particular at fainter luminosities. Based on data from the *Chandra* Deep Field–North (CDF-N; Alexander et al. 2003) we estimate that of order 50% of the sources detected with luminosities in the range 10^{34} ergs s^{-1} $\leq L_X \leq$ 5×10^{35} ergs s^{-1} are background AGNs. Pietsch et al. (2004) arrive at a comparable fraction for the *XMM-Newton* field, which is roughly 4 times larger than the area covered by *Chandra*. The *XMM-Newton* observation is on average less deep than the *Chandra* observations. Cosmic variance may change the number of background AGNs slightly, but on the basis of data from the *Chandra* Multiwavelength Project survey, cosmic variance does not appear to be a strong effect (Kim et al. 2004b). A more detailed estimate of the actual number of background objects requires a more detailed knowledge of the source properties. Above $L_X \geq 5\times10^{35}$ ergs s^{-1}, contamination of the luminosity function is small because the AGN $\log N - \log S$ is much steeper than the luminosity function of Galactic X-ray sources.

4. POINT SOURCE COLORS

Hardness-ratio diagrams are a straightforward way to classify sources in general, especially for sources that do not have sufficient number of counts to allow spectral fitting (Kim et al. 1992; Prestwich et al. 2003). From the counts extracted from the three different bands mentioned in § 2 we construct two colors, a soft color and a hard color. The soft color is defined as

$$\mathrm{HR1} = \frac{M - S}{S + M + H} \tag{2}$$

and the hard color as

$$\mathrm{HR2} = \frac{H - M}{S + M + H}, \tag{3}$$

where S, M, and H are the counts in a soft (0.3–1.0 keV), medium (1.0–2.1 keV), and hard (2.1–8.0 keV) energy bands, respectively. The energy bands were selected to achieve an optimal separation between soft/thermal and hard/power-law components (A. H. Prestwich 2004, private communication). The results for the different observations are shown in Figure 2. Following Prestwich et al. (2003), we consider here only sources

[4] See http://space.mit.edu/ASC/MARX/.

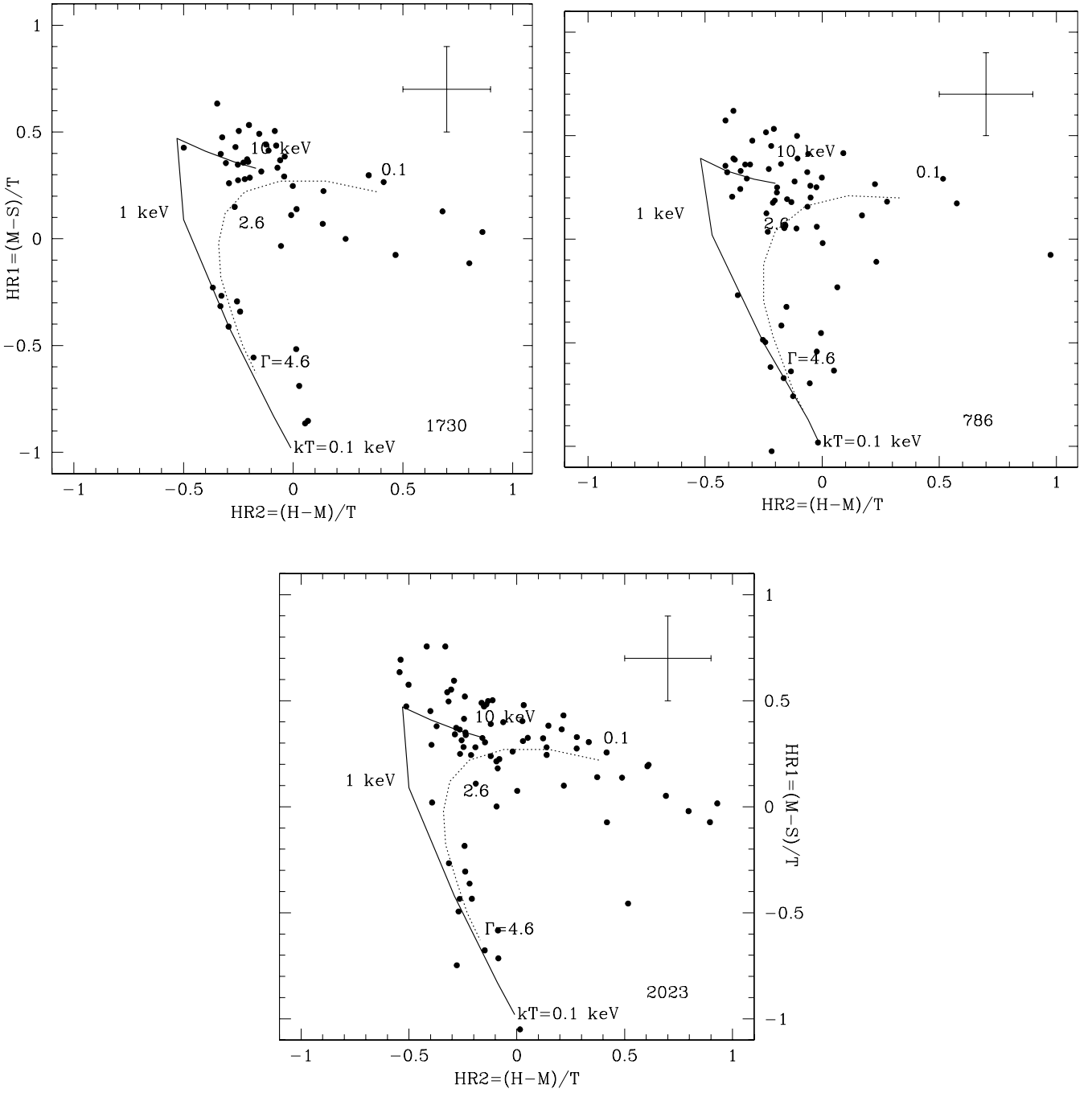

FIG. 2.—Hardness ratio diagrams for the three *Chandra* observations. The solid line shows a model path for a blackbody spectrum and the dotted line shows a model for a power law, both with Galactic absorption and taking into account different responses of the main CCDs in the observations. The CCD response is not a strong effect. Increasing absorption moves the lines to the top left corner. The cross represents a typical error bar for a source with 35–40 counts. [*See the electronic edition of the Supplement for a color version of this figure.*]

with more than 20 detected counts in the full band to somewhat reduce statistical errors on the colors. The errors on the counts are computed with the Gehrels approximation (Gehrels 1986); errors on the colors are computed using standard error propagation. Note that for small number of counts the errors must not be regarded as Gaussian 68% limits. We disregard sources that have upper limits in any of the bands. Typical net counts for the sources are in the range from 30 to 50 counts. The detected number of counts is dependent on the response of the CCD. This difference is expected to be largest between FI and BI chips. Therefore, we plot the hardness ratios in separate panels. The model tracks in Figure 2 were computed separately for the BI (ObsID 786) and FI chips (ObsIDs 1730 and 2023). The strong similarity of the tracks indicates that differences in the CCD response between our observations do not have a strong effect on the colors, at least for sources with more than ~20 counts. In § 7 we will use optical identification together with colors to investigate the color relations of different source types in more detail.

5. LUMINOSITY FUNCTION

Since the *Chandra* observations have different exposure times and cover somewhat different areas, we present here the luminosity functions for each observation separately. Figure 3 shows

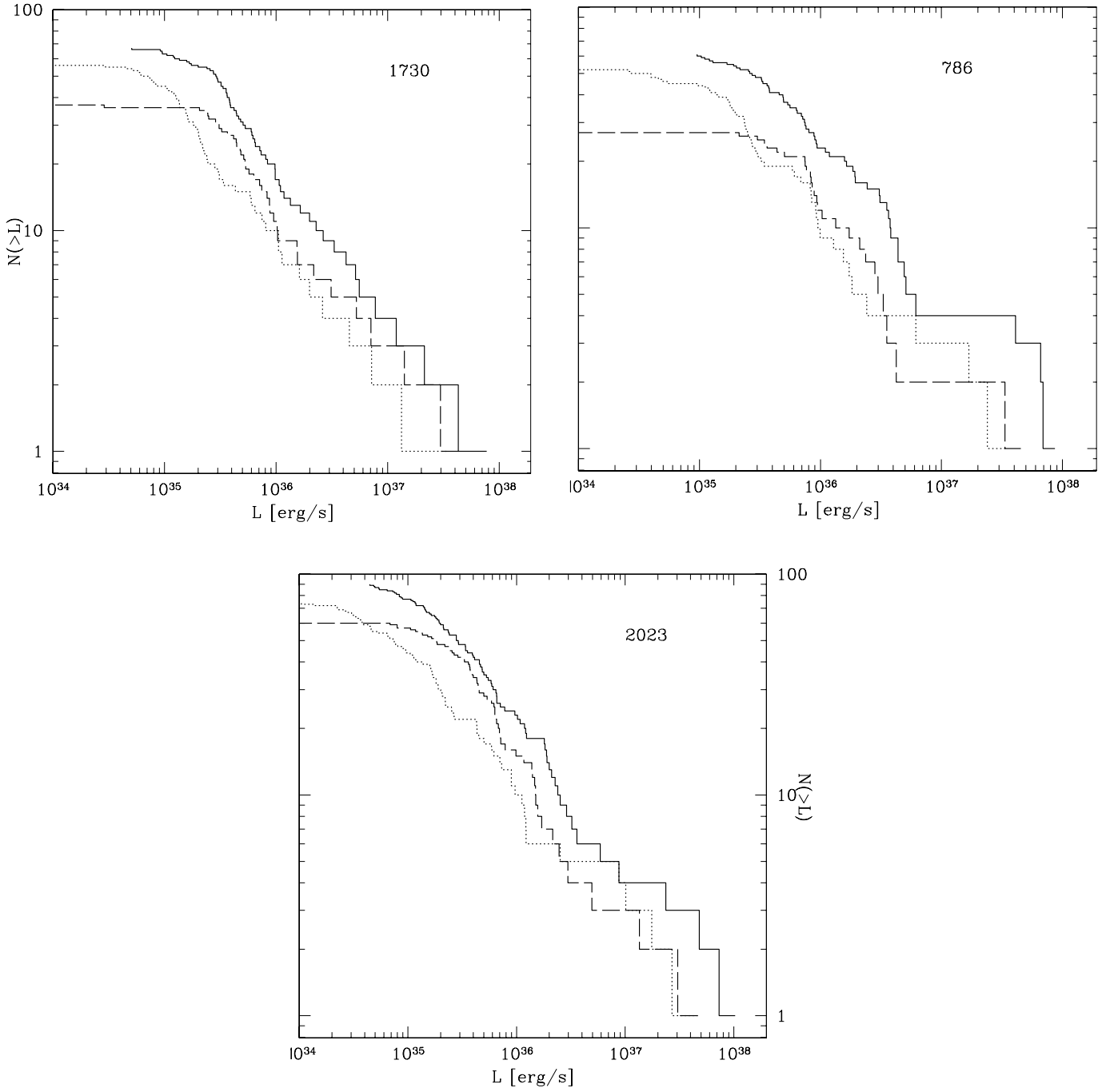

FIG. 3.—Luminosity functions for the three *Chandra* observations. The black line shows the sources detected in the whole band (0.3–8.0 keV), the dotted line shows sources detected in the soft band (0.3–2.0 keV), and the dashed line shows sources detected in the hard band (2.0–8.0 keV). [*See the electronic edition of the Supplement for a color version of this figure.*]

the observed luminosity functions. The black line shows the sources detected in the whole band (0.3–8.0 keV), the dotted line shows sources detected in the soft band (0.3–2.0 keV), and the dashed line shows sources detected in the hard band (2.0–8.0 keV).

The count to luminosity conversion was established based on the fit of source spectra with more than 100 counts with XSPEC version 11.3.0. The typical spectrum for the fainter sources in this range, ~100–200 counts, is an absorbed power law with Galactic absorption, 6×10^{20} cm^{-2}, and a photon index of ~2.0. This spectrum roughly describes an X-ray binary spectrum, the sources of particular interest. These values are assumed for fainter sources for the conversion from counts to flux. The values quoted in the following for sources with more than 100 counts are the fitted observed values. As a rule of thumb, 100 counts correspond to a luminosity of $(1-2) \times 10^{36}$ ergs s^{-1}. The spectra of the brighter sources are roughly consistent with such a spectrum. The details of spectral fitting will be discussed in a separate paper.

In Figure 4 we present the luminosity functions in the full band after correcting for incompleteness by applying the procedure outlined in Kim & Fabbiano (2003). A comparison with Figure 3 shows the importance of this correction for obtaining the actual shape of the luminosity function.

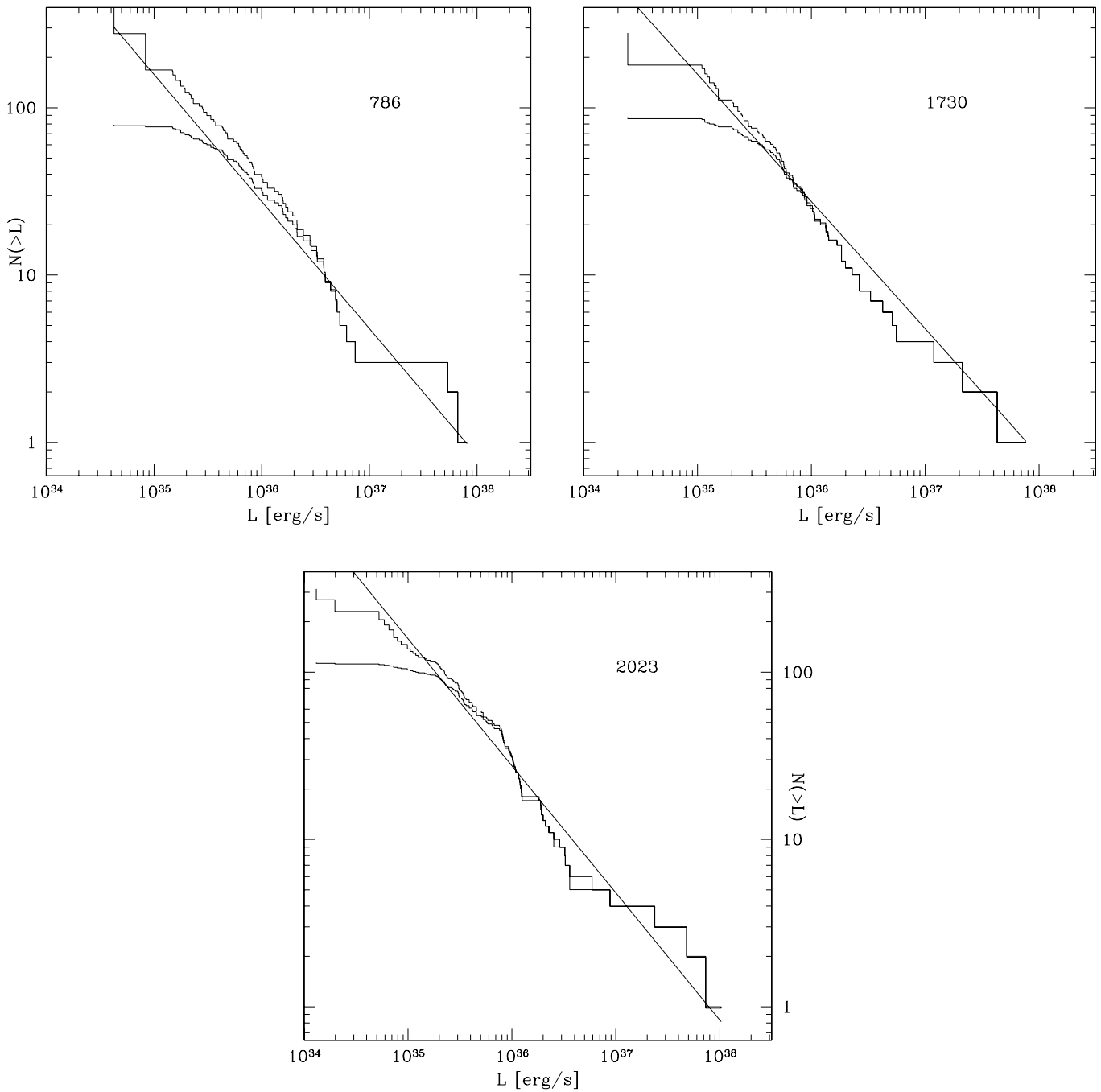

FIG. 4.—Corrected and uncorrected luminosity functions for the three *Chandra* observations. The histograms show the sources detected in the whole band (0.3–8.0 keV). The solid line (the same in each panel) shows the best-fit power law for the luminosity function of ObsID 1730. The scale is the same in all panels.

A Kolmogorov-Smirnov test shows that the luminosity functions have a probability higher than 95% to be drawn from the same distribution. The slopes of the luminosity functions are relatively steep for an actively star-forming galaxy. A maximum likelihood fit gives slopes for cumulative luminosity function for the ObsIDs 786, 1730, and 2023 of 0.78 ± 0.17, 0.76 ± 0.14, and 0.74 ± 0.13, respectively. The effect of interloper contamination on these slopes is discussed in § 7.2.

6. COUNTERPARTS

In order to gain more information about the nature of the X-ray sources, we cross-correlate our sources with a number of different catalogs available for M33. Given the proximity of M33 and the resulting good resolution, there is a large amount of data in many wavebands. We used the SIMBAD database to find catalogs pertaining to M33, and we also cross-correlated the positions of individual *Chandra* sources against the whole SIMBAD database. We discuss below the results of these comparisons with X-ray catalogs and multiwavelength databases separately.

We cross-correlated our source list with the following catalogs: The *XMM-Newton* survey of M33 (Pietsch et al. 2004), the *ROSAT* source catalog (Haberl & Pietsch 2001), the catalog of SNRs by Gordon et al. (1999), H II regions from Hodge et al. (1999), giant molecular clouds from Engargiola et al. (2003), globular clusters from Mochejska et al. (1998), star clusters

from Chandar et al. (1999, 2001), blue and red supergiants from Ivanov et al. (1993), red supergiants from Massey (1998), Wolf-Rayet stars from Massey & Johnson (1998), UV-bright stars from Massey et al. (1996), hot stars from Massey et al. (1995), OB associations from Regan & Wilson (1993), planetary nebulae from Magrini et al. (2001), Hα emitters from Calzetti et al. (1995), and the DIRECT star catalog from Macri et al. (2001).

The cross-correlation is done using the uncertainty of the *Chandra* source position, computed according to Kim et al. (2004a). In addition the source uncertainty of catalog positions was quadratically added to the *Chandra* positional uncertainty. If no such number is available in the catalogs, an uncertainty of $1''$ was added. If there is more than one source in the error circle we make no further assumption about the likelihood of any of the sources *within* the error circle being a real counterpart of the X-ray source.

6.1. *X-Ray Counterparts*

M33 has been observed with various X-ray missions, most notably *ROSAT* and recently *XMM-Newton*. Haberl & Pietsch (2001) have analyzed all available *ROSAT* observations and extracted a total of 184 sources. The *ROSAT* observations cover a much larger area of M33 than our *Chandra* observations. Also note that the *ROSAT* (0.1–2.4 keV) and *Chandra* energy bands (0.3–8.0 keV) are different. Only 115 *ROSAT* sources are in the field of view of the *Chandra* observations. Of these 115 sources, we detect 50 with *Chandra*: 12 of these are SNRs as classified by Haberl & Pietsch (2001), three supersoft sources (SSSs), two X-ray binaries (XRB), including M33 X-7 (Peres et al. 1989), the first such identification, and two foreground stars. Of the *ROSAT* detections, 20 sources are far off-axis ($\gtrsim 8'$) in any *Chandra* observation, and 22 are observable in only one observation. Table 5 in the Appendix contains the matches of *Chandra* and *ROSAT* sources. Column (1) is the *Chandra* source name, column (2) the *Chandra* positional uncertainty, column (3) the right ascension and declination of the *ROSAT* source, column (4) the *ROSAT* positional uncertainty, column (5) the *ROSAT* name, and column (6) the HRI flux and the corresponding 1 σ error. The typical astrometric error for the *ROSAT* sources is $\sim 5''$ with a long tail to larger errors; 32 sources have positional uncertainties larger than or equal to $20''$.

The *XMM-Newton* observations of M33 were of relatively shallow exposure, lasting generally between $\sim$10 and 15 ks (Pietsch et al. 2004). Their detection limit of $\sim 1.4 \times 10^{-15}$ ergs s^{-1} cm^{-2} for a power law with $\Gamma = 1.7$ and $N_{\rm H} = 6 \times 10^{20}$ cm^{-2} compares to our $\sim 3 \times 10^{-16}$ ergs s^{-1} cm^{-2}. Like the *ROSAT* observations, this *XMM-Newton* survey also covers a larger area than *Chandra*. Of the 408 sources detected by *XMM-Newton*, 184 are in the *Chandra* fields of view. Of these 184 sources, 102 are detected with *Chandra*, including 13 SNRs, 2 SSSs, 1 XRB, 3 foreground stars, 4 background AGNs, and 35 hard sources as defined by Pietsch et al. (2004). Table 6 in the Appendix contains the *Chandra* and *XMM-Newton* matches. Column (1) is the *Chandra* source name, column (2) the *Chandra* positional uncertainty, column (3) the right ascension and declination of the *XMM-Newton* source position, column (4) the *XMM-Newton* energy flux and 1 σ error, and column (5) the *XMM-Newton* X-ray identification.

6.2. *Other Wavebands*

The correlation with the radio data from Gordon et al. (1999) yields 24 matches, 14 of which are SNRs or candidate SNRs based on their radio spectral slope. One SNR matches two *Chandra* sources. Five SNRs are associated with H II regions. Nine matches are foreground/background objects. The radius assigned for sources of the whole catalog is $3''$. The optical radius of the SNRs is on average $4\farcs5$. Taking the actual optical radius to match *Chandra* sources with selected SNRs in Table 4 of Gordon et al. (1999) does not change the result for the SNR matches. We expect fewer than three chance coincidences at 95% for the whole catalog and fewer than two for the selected SNRs.

There is one association with a globular cluster in M33 from the sample of Mochejska et al. (1998). The assumed radius of the clusters is $2''$. The number of expected chance coincidences is <1. This source is also the only match with the samples of Chandar et al. (1999, 2001; also $2''$ radius). This source does not match any other catalog; however, its location in a globular cluster suggests that it is either a bright cataclysmic variable or a low-mass X-ray binary (LMXB).

There are nine matches with blue stars in M33 from the sample of Ivanov et al. (1993) for seven *Chandra* sources; two *Chandra* sources match two blue stars each. The accuracy for the blue star positions is $1\farcs5$ (Ivanov et al. 1993). None of the red stars in the Ivanov et al. (1993) sample match any *Chandra* source. Due to the highly clustered nature of the blue supergiants, it is not straightforward to calculate the probability of chance coincidences. However, it is possible that the majority of matches are not real.

Due to the large number of objects, roughly 60,000, a matching with DIRECT sources yields ambiguous results. The limiting magnitude of the catalog is 23.6 in *V*. For off-axis angle sources ($\sim 4'$), where the *Chandra* beam is large, there are numerous associations. But for *Chandra* sources closer to the aim point, and a correspondingly smaller error radius ($\leq 1''$), there are also 43 unique counterparts. However, because of the very high density of DIRECT objects, most of them are likely chance coincidences.

Similarly to the DIRECT sources, OB stars from Regan & Wilson (1993) have a high density and give multiple matches. In total there are 14 matches with 9 *Chandra* sources, 6 of which are unique matches. The positional accuracy of the OB stars is within $2''$ (Regan & Wilson 1993). The high source density and overlapping source regions indicate that the majority of matches are chance coincidences.

The H II region sample of Hodge et al. (1999) gives three matches. As radius for the H II regions we use the optical radius if given; otherwise we use $1''$. Despite the small radius, the number of expected chance coincidences is still three because of the large number of H II regions ($\sim$1200).

The UV stars in M33 in the sample of Massey et al. (1996) yield six matches (uncertainty $1\farcs4$, two chance coincidences expected). One of the sources is identified with a B1 supergiant, another with a luminous bluevariable candidate, and another one with an H II region. One of the *Chandra* sources is also the only match with the Wolf-Rayet star sample of Massey & Johnson (1998). There is also only one match with the catalog of hot stars of Massey et al. (1995). For the two later catalogs an uncertainty of $1''$ was assumed and one chance coincidence is expected in each.

7. DISCUSSION

7.1. *Source Types*

Due to the comparable number of expected background sources and sources associated with M33 in our data set, it is important to distinguish the different source types. Only by identifying the

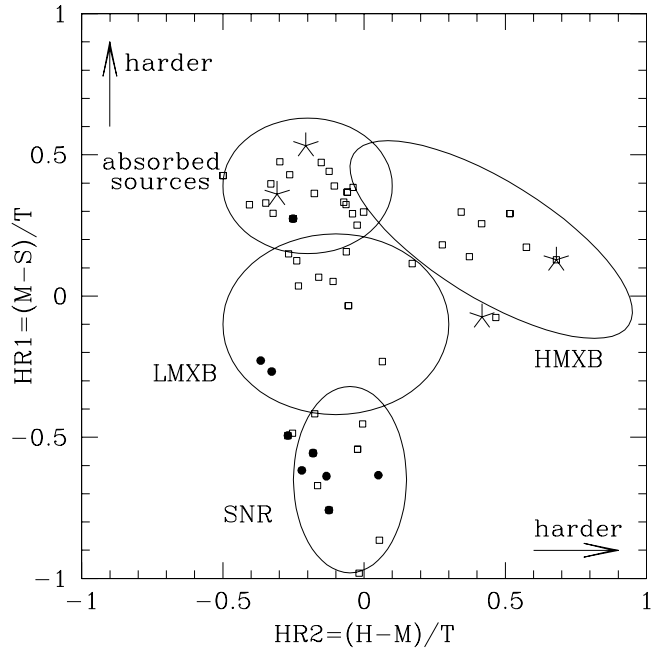

FIG. 5.—Hardness-ratio diagram of sources with identifications. *Filled circles*, SNRs; *stars*, background/foreground objects; *open squares*, "blue" counterparts. The elliptical areas indicate the expected locations of various source types. The areas are taken from Prestwich et al. (2003). Only sources with no upper limits in any flux band are shown. For more details see § 7.1.

X-ray sources is it possible to learn more about the true source population of M33. As a first step we compare X-ray colors with the expected location of different source types in the hardness-ratio diagram. Again sources with upper limits in any band are disregarded. In Figure 5 we show different source types, derived from identifications in other wavelengths: filled circles show supernova remnants; stars show background and foreground objects; open squares shows objects with a "blue" counterpart, blue meaning either an Hα, UV, *U*, or *B* band counterpart detected in M33. As can be easily seen from the picture, SNRs do populate the expected locus in the hardness-ratio diagram based on the prescription of Prestwich et al. (2003). There is only one exception of an SNR from the Gordon catalog, which has a harder X-ray spectrum than expected of a thermal SNR and might either be a plerionic SNR or an SNR harboring an X-ray binary.

Comparing the X-ray hardness ratio diagram with the regions Prestwich et al. (2003) identified with certain source types in Figure 5 shows that the region that covers LMXBs, around $(-0.3, 0)$ in HR2–HR1, is only sparsely populated, whereas all other regions are well populated with sources. The distribution of points in the color diagram, and in particular the avoidance of the LMXB locus, is reinforced if we consider Figure 2, which contains both identified and unidentified sources. AGNs and pulsar-like X-ray binaries are not distinct in the hardness ratio diagram, both being consistent with hard and/or possibly absorbed sources. Note that very strongly absorbed sources ($N_{\rm H} \geq 10^{22}$ cm^{-2}) would not be plotted because they would not be detected in the soft band if they were not very bright. This implies that LMXBs do not contribute significantly to the X-ray source population in M33. This is consistent with the estimate of its stellar mass and star formation rate, which suggests a prevalent young stellar population.

Although the regions shown in Figure 5 do not represent a quantitative expectation value for different source locations, we can nevertheless quantify our expectations for the number of high-mass X-ray binaries (HMXBs) and LMXBs from the universal luminosity functions for HMXBs (Grimm et al. 2003) and LMXBs (Gilfanov 2004). We take the star formation rate of M33 to be $\sim$0.3 $M_\odot$ yr^{-1} (Hippelein et al. 2003), and the *K*-band magnitude to be $m_K = 4.1$ (Jarrett et al. 2003). Using equation (22) of Grimm et al. (2003) and equation (21) with the normalization for late-type galaxies of Gilfanov (2004), we expect to observe $\sim$6–7 HMXBs and $\sim$3 LMXBs above 10^{37} ergs s^{-1}. At 10^{37} ergs s^{-1} we expect no strong contamination by background sources. These numbers are in good agreement with the observed number of six sources above 10^{37} ergs s^{-1}. Although the *Chandra* observations do not cover M33 in its entirety, they cover more than 80% of M33. The expected total luminosity is $\sim 3.5 \times 10^{38}$ ergs s^{-1} for HMXBs and $\sim 10^{38}$ ergs s^{-1} for LMXBs. These values agree very well with the observed total X-ray luminosity of point sources (excluding the nucleus) of $\sim 3\text{–}4 \times 10^{38}$ ergs s^{-1}. Using the formulae of Colbert et al. (2004) for the relation of total X-ray luminosities with *K*-band luminosity, FIR+UV luminosities, as well as with stellar mass and star formation rate give basically identical results. An exception is the X-ray–stellar mass relation, which predicts an LMXB X-ray luminosity of $\sim 1.2 \times 10^{39}$ ergs s^{-1}, an order of magnitude larger than predicted by other relations, and 3–4 times larger than the observed luminosity.

7.2. *Luminosity Function*

Based on spectrophotometry and comparison with theoretical SEDs, M33 is expected to be dominated by a young stellar population (Li et al. 2004), in agreement with the source colors as discussed in § 7.1. Therefore, most X-ray sources in M33 should be HMXBs. We would then expect the luminosity

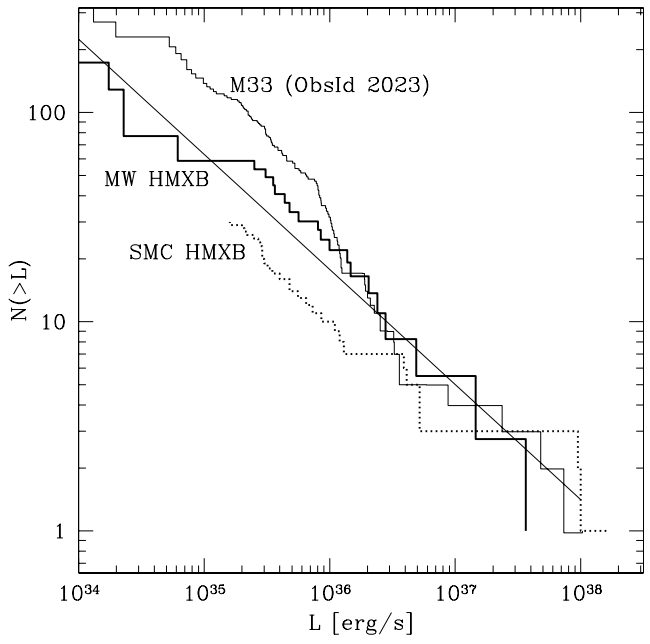

FIG. 6.—Luminosity functions of X-ray sources in M33 from ObsID 2023 (*solid histograms*) compared with the HMXB luminosity function of the Milky Way (*thick solid histogram*; Grimm et al. 2002) and X-ray binary candidates in the SMC (*thick dotted histogram*; Yokogawa et al. 2000). The solid line is a representation of the expected intrinsic luminosity function of M33 after subtraction of background AGNs with a cumulative slope of 0.55. The normalization of the expected intrinsic luminosity function of M33 is defined by the high-luminosity end of the luminosity function of ObsID 2023. [*See the electronic edition of the Supplement for a color version of this figure.*]

function of the M33 sources to be similar to the luminosity function of HMXBs in the Milky Way. Figure 6 shows the corrected luminosity functions of M33 and the luminosity functions of HMXBs in the Milky Way (*thick solid histogram*) and in the SMC (*dotted histogram*). The luminosity functions differ slightly in shape but have a similar slope within the errors. The SMC luminosity function seems to be somewhat flatter, but there is a large contribution from the four brightest sources in the SMC. On the other hand, the M33 luminosity functions obtained from maximum likelihood fits are steeper ($\sim 0.76 \pm 0.14$) than the Milky Way HMXB luminosity function (0.64 ± 0.15), though still consistent within the errors.

These values for the slope of the M33 luminosity functions lie in between what is found for star-forming galaxies, $\alpha \sim 0.5$–0.6 (Kilgard et al. 2005), and for elliptical galaxies, $\alpha \sim 1$ (Kim & Fabbiano 2004). The reason for the steep luminosity function is most likely the expected large number of background objects ($\sim$50%), which steepen the luminosity function due to their steep number-flux relation (Alexander et al. 2003). A significant contribution of LMXBs is unlikely since the stellar mass of M33 is roughly one-tenth that of the Milky Way and therefore the number of LMXBs is expected to be similarly small ($\sim$10 above 10^{36} ergs s^{-1} in all of M33). Moreover, at low luminosities ($L_X < 10^{37}$ ergs s^{-1}) the LMXB luminosity function flattens as well (Grimm et al. 2002; Kong et al. 2002).

We compared our number-flux relation with the 2Ms CDF-N source catalog of Alexander et al. (2003) in the full band.[5] In order to compare the CDF-N data with our analysis of M33 we take into account different assumptions about spectral shape, different fields of view, and different column densities. Alexander et al. (2003) assume a power-law spectrum with a photon index of $\Gamma = 1.4$ and a Galactic absorption column density of $N_H = 1.6 \times 10^{20}$ cm^{-2} and compute the flux in the energy range from 0.5 to 8.0 keV. Converting the fluxes to our values of $\Gamma = 2$ and $N_H = 6 \times 10^{20}$ cm^{-2} in the energy range from 0.3 to 8.0 keV results in a correction factor of $\sim$0.5 for the CDF-N data. Moreover, the different fields of view used in the CFD-N analysis and our analysis (note that we correct our observations individually) yield another factor of $\sim$0.6 with respect to the CDF-N data for the number of sources. The first factor obviously depends only on assumptions about spectral shape and energy band used. The second factor, however, is subject to uncertainties arising from the (non-)existence of cosmic variance. This background can significantly affect the normalization of the background $\log N - \log S$.

We find that after subtracting the corrected CDF-N number-flux relation from the M33 ones the slope flattens to $\sim$0.5–0.6. Note that this is an estimate of slope, not a fit. The slopes are flatter for higher background normalizations. However, the range is relatively robust for reasonable assumptions about the normalization of the background $\log N - \log S$ arising from cosmic variance, i.e., changes in normalization of a factor of 2–3. We also compare the soft-band (0.3–2.0 keV) luminosity function with *ROSAT* All-Sky Survey data from fields adjacent to M33. Slope and normalization of the RASS $\log N - \log S$ are consistent with the values from the CDF-N in the overlapping flux range. The solid line in Figure 6 gives an approximation to the *intrinsic* M33 luminosity function with a slope of 0.55 and a normalization fixed by the brightest sources. A more detailed study of luminosity functions and background $\log N - \log S$ is necessary to quantify these results further.

[5] The data were obtained from Neil Brandt's Web site, http://www.astro.psu.edu/users/niel/hdf/hdf-chandra.html.

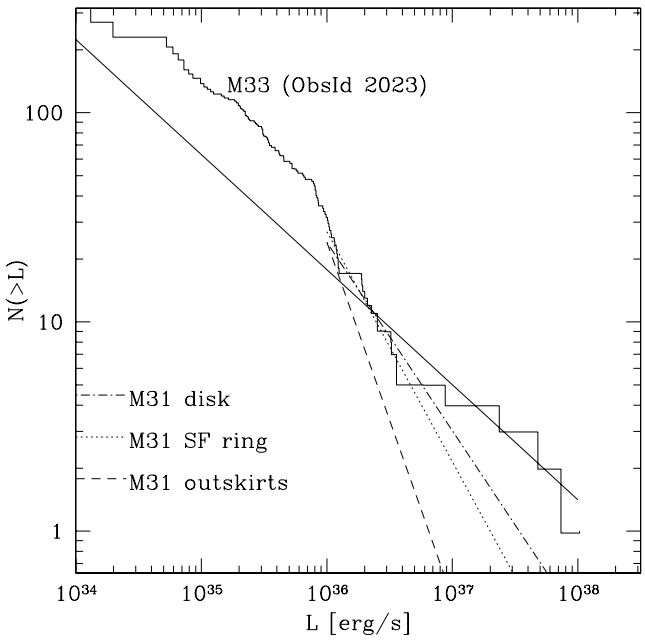

FIG. 7.—Luminosity functions of X-ray sources in M33 from ObsID 2023 compared with luminosity function fits from regions in M31 by Kong et al. (2003). The dashed line shows the luminosity function (slope of 1.1) for a region in the outer parts of M31, the dash-dotted line shows that for a region in the disk of M31, and the dotted line shows that for a region including parts of the star-forming ring around the bulge of M31. The solid line is a representation of the expected intrinsic luminosity function of M33 after subtraction of background AGNs with a cumulative slope of 0.55 and a normalization defined by the high-luminosity end of the observed luminosity function. [*See the electronic edition of the Supplement for a color version of this figure.*]

Figure 7 shows the luminosity function of M33 overlaid with the fitted luminosity functions for different regions of M31 (Kong et al. 2003). The dashed line shows the luminosity function for a region in the outer parts of M31 and has a slope of 1.1, the dash-dotted line shows that for a region in the disk of M31, and the dotted line shows that for a region including parts of the star-forming ring around the bulge of M31. The solid line gives again the approximation to the *intrinsic* M33 luminosity function. The dash-dotted and dotted lines, dominated by young stellar populations, resemble the luminosity functions of M33 most closely.

The similarity of the *intrinsic* slopes in M33 and the shapes of the luminosity function with HMXB luminosity functions in the Milky Way and starburst galaxies shows that the X-ray source population in M33 is dominated by HMXBs and other young X-ray sources. It also agrees with the assumption that LMXBs do not contribute significantly to the X-ray binary population in M33.

7.3. *Supernova Remnants*

Supernova remnants are another source type associated with young stellar populations. The X-ray luminosity distribution of 16 SNRs detected both in radio (Gordon et al. 1999) and with *Chandra* is shown in Figure 8. Due to the construction of the correction of the intensity distribution by Kim et al. (2004a), it is not possible to correct the luminosity function of a subset of sources. Therefore, the SNR luminosity function is not corrected for incompleteness.

For comparison, we show the luminosity function of SNRs in M33, and in the Magellanic Clouds and M31 obtained from *ROSAT* data in Figure 8. The data for M31 (*dotted histogram*) are

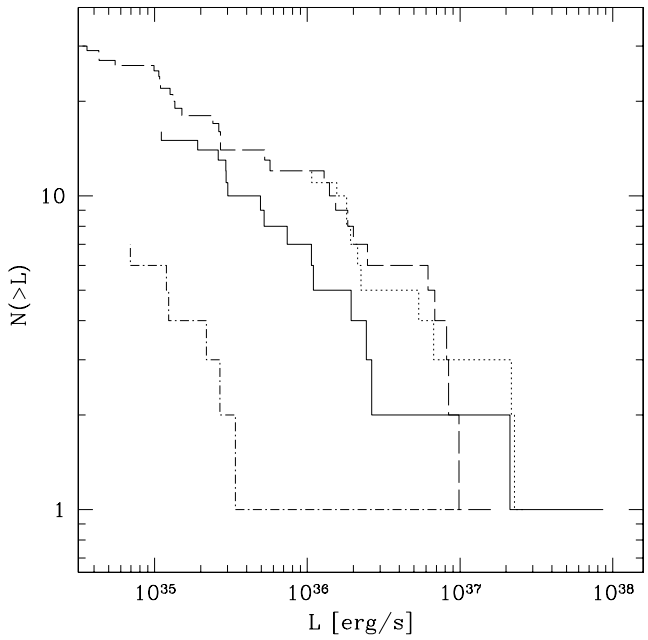

FIG. 8.—Observed luminosity function of radio SNRs in M33 combined from the three *Chandra* observations. For comparison we show the observed luminosity of the Magellanic Clouds (*dot-dashed histogram*, SMC; *dashed histogram*, LMC) from Sasaki et al. (2000a, 2000b), and of M31 (*dotted histogram*) from Supper et al. (2001). [*See the electronic edition of the Supplement for a color version of this figure.*]

taken from observations by Supper et al. (2001) and the data on the Magellanic Clouds (*dashed histogram for LMC, dot-dashed histogram for SMC*) are from Sasaki et al. (2000a, 2000b). The data are not corrected for the different energy bands of *Chandra* and *ROSAT*. For thermal supernova remnants most of the flux is in the soft band, so the extended *Chandra* response toward hard X-rays will not significantly change the luminosity for these sources. Also different assumptions about spectral shape do not strongly affect the luminosities in this energy range. Although numerous SNRs are known in the Milky Way, their poorly determined distances and nonuniform sampling do not allow a comprehensive comparison with the population with extragalactic SNRs.

Although there are relatively few sources, SNRs in the SMC are underluminous compared with SNRs in the other galaxies. This has been noted already by Haberl & Pietsch (2001), and the authors attribute this to higher metal abundances in the LMC. Although the luminosities in M33, M31, and the LMC are comparable, a two-sample Kolmogorov-Smirnov test gives a probability of only $\sim$1% for the luminosity functions of M31 and M33 and the Magellanic Clouds to have the same underlying distribution. However, for M33 and the Magellanic Clouds the probability increases to $\sim$10%, and for LMC and SMC the probability increases to over 60%. Even considering the different incompleteness limits and instrumental effects (M31–PSPC, the Magellanic Clouds–HRI), there nevertheless might be a difference in the SNR population in star-forming and older galaxies. For a complete and more concise discussion of the SNRs in M33, refer to Ghavamian et al. (2005), who investigate the properties of the SNRs individually.

8. CONCLUSION

The sensitivity of the *Chandra* observations of M33, and the wealth of multiwavelength data for this galaxy does allow a uniquely detailed study of the X-ray point source population. Here we present the source list, counterparts, X-ray colors, and X-ray luminosity functions of sources in M33 observed with *Chandra*. In total 261 individual sources are detected in three partly overlapping observations down to a flux of 3×10^{-16} ergs s^{-1} cm^{-2}, corresponding to a luminosity of $\sim 2 \times 10^{34}$ ergs s^{-1} at a distance of 840 kpc. The observations are centered on the nucleus and the star-forming region NGC 604. The luminosity functions of the observations are statistically consistent with each other. Because of the large area covered by the observation, $\sim$0.2 deg^2, the number of background objects is large. On the basis of CDF-N data, we conclude that around 50% of the detected sources are background objects at low luminosities (10^{34} ergs s^{-1} $\leq L_X \leq 5 \times 10^{35}$ ergs s^{-1}).

Taking into account the contribution of background AGNs to the luminosity function of M33, the slope of the luminosity function, cumulatively $\sim$0.5–0.6, is consistent with HMXB luminosity functions in the Milky Way and the Magellanic Clouds. Color analysis of the sources shows a lack of sources at the location populated by low-mass X-ray binaries in the X-ray color-color diagram. Also cross-correlations with catalogs at other wavelengths result preferably in matches with objects associated with young stellar populations: e.g., SNRs, blue stars, and H II regions. We therefore conclude that the X-ray source population in M33 is dominated by a young population, similar to other star-forming galaxies. This is also in agreement with expectations based on the stellar mass and star formation rate of M33.

We also find that the shape of the luminosity function of SNRs in M33 is more similar to the SNR luminosity functions in the Magellanic Clouds (Sasaki et al. 2000a, 2000b) than to the SNRs in M31 (Supper et al. 2001). This might be related to abundance differences in these galaxies (Haberl & Pietsch 2001). The spectral properties, along with temporal properties, of sources with a sufficient number of counts will be discussed in a following paper.

This work has been supported by NASA grant GO2-3135X. The authors want to thank Ralph Kraft for his program to compute upper limits, and Wolfgang Pietsch for providing the *XMM-Newton* source list before publication. We also thank the referee for constructive comments on the paper.

APPENDIX

Table 3 lists the sources in order of increasing right ascension. Table 4 lists *Chandra* sources with optical counterparts. Table 5 shows matches of *Chandra* and *ROSAT* sources. Finally, Table 6 shows matches of *Chandra* and *XMM-Newton* sources.

TABLE 3

SOURCE LIST ORDERED WITH INCREASING RIGHT ASCENSION

SOURCE			COUNTS						FLUX[a] (10^{-7} counts s^{-1} cm^{-2})			L[a] (ergs s^{-1})
CXO J	R.A., Decl., Uncertainty (arcsec)	ObsID	0.3–8.0	0.3–2.0	2.0–8.0	0.3–1.0	1.0–2.1	2.1–8.0	0.3–8.0	0.3–2.0	2.0–8.0	0.3–8.0
013219.6+304153	01 32 19.668	1730	8.2 (4.3)	<7.5	6.9 (4.0)	...	...	...	8.6 (4.4)	<5.6	8.4 (3.4)	1.54E+35
	30 41 53.57	786	...	...	...	...	...	...	...	...	...	...
	27.0	2023	...	...	...	...	...	...	...	...	...	...
013239.7+303245	01 32 39.787	1730	11.0[b] (3.3)	<9.3	9.6 (4.7)	...	...	...	8.2[b]	<7.0	9.6 (3.6)	1.47E+35[b]
	30 32 45.78	786	...	...	...	...	...	...	...	...	...	...
	12.7	2023	...	...	...	...	...	...	...	...	...	...
013253.4+303817	01 32 53.481	1730	969.6 (32.8)	703.5 (27.8)	237.5 (17.1)	226.9 (16.3)	492.8 (23.4)	246.9 (17.7)	800 (27)	560 (21)	220 (15)	1.43E+37
	30 38 17.07	786	...	...	...	...	...	...	...	...	...	...
	2.6	2023	...	...	...	...	...	...	...	...	...	...
013253.9+303312	01 32 53.931	1730	665.4 (28.5)	584.9 (26.3)	146.2 (15.2)	216.1 (16.4)	315.7 (19.3)	140.7 (14.7)	440 (19)	350 (15)	150 (14)	7.79E+36
	30 33 12.29	786	...	...	...	...	...	...	...	...	...	...
	3.0	2023	...	...	...	...	...	...	...	...	...	...
013256.3+303558	01 32 56.324	1730	<43.1	<14.3	20.5 (8.2)	...	...	...	<32.3	<10.7	18 (6.5)	<5.78E+35
	30 35 58.64	786	...	...	...	...	...	...	...	...	...	...
	5.6	2023	...	...	...	...	...	...	...	...	...	...
013308.3+304802	01 33 08.375	1730	...	...	...	...	...	...	...	...	...	...
	30 48 02.69	786	127.2 (15.0)	136.3 (14.3)	21.0[b] (4.6)	39.3 (8.5)	65.9 (9.9)	11.2 (8.8)	66 (8.4)	67 (7.3)	15.7[b]	1.19E+36
	2.5	2023	<6.0	<6.6	<4.6	...	...	...	<4.5	<5.0	<3.5	<8.10E+34
013315.1+305317	01 33 15.139	1730	...	...	...	...	...	...	...	...	...	...
	30 53 17.94	786	4824.9 (74.1)	3852.6 (64.5)	929.0 (36.7)	1216.3 (37.7)	2778.4 (54.7)	818.7 (35.1)	3000 (46)	2200 (36)	900 (36)	5.33E+37
	0.7	2023	9210.7 (99.3)	6994.6 (85.6)	2167.0 (50.2)	1550.3 (41.4)	5705.2 (77.0)	2059.4 (48.8)	5800 (62)	4100 (50)	1700 (38)	1.03E+38
013315.5+304448	01 33 15.584	1730	215.7 (20.8)	170.9 (16.3)	44.8 (13.7)	44.9 (8.6)	95.3 (11.4)	31.6 (9.6)	180 (18)	140 (13)	44 (12)	3.28E+36
	30 44 48.28	786	200.9 (22.8)	174.9 (18.2)	25.9 (14.7)	34.5 (8.9)	91.5 (11.5)	20.4 (9.9)	170 (19)	130 (14)	33 (14)	2.99E+36
	1.5	2023	<5.7	<4.6	<6.0	...	...	...	<4.3	<3.5	<4.5	<7.70E+34
013320.5+304646	01 33 20.522	1730	<12.2	<4.6	3.5 (3.2)	...	...	...	<9.2	<3.5	3.1 (1.8)	<1.65E+35
	30 46 46.36	786	<6.0	<6.6	<4.6	...	...	...	<4.5	<5.0	<3.5	<8.10E+34
	2.4	2023	<6.0	<6.6	<4.6	...	...	...	<4.5	<5.0	<3.5	<8.10E+34
013321.7+303858	01 33 21.716	1730	31.0 (6.8)	<12.2	26.6 (6.4)	0.6 (2.3)	4.6 (3.4)	25.8 (6.3)	24 (5.2)	<9.2	21 (4.2)	4.25E+35
	30 38 58.24	786	...	...	...	...	...	...	...	...	...	...
	1.4	2023	<8.3	<7.5	<6.0	...	...	...	<6.2	<5.6	<4.5	<1.11E+35
013321.9+303921	01 33 21.943	1730	28.5 (6.6)	14.5 (5.0)	13.9 (5.0)	2.5 (2.9)	13.5 (4.8)	12.4 (4.8)	22 (5.0)	11 (2.9)	11 (3.0)	3.86E+35
	30 39 21.12	786	...	...	...	...	...	...	...	...	...	...
	1.4	2023	<5.7	<6.0	<4.6	...	...	...	<4.3	<4.5	<3.5	<7.70E+34
013323.8+303517	01 33 23.887	1730	21.3 (6.0)	13.1 (4.8)	10.9 (5.4)	3.3 (3.2)	9.5 (4.3)	8.7 (4.3)	17 (4.6)	10 (2.9)	9.0 (3.4)	2.97E+35
	30 35 17.36	786	...	...	...	...	...	...	...	...	...	...
	1.6	2023	...	...	...	...	...	...	...	...	...	...
013323.9+304821	01 33 23.996	1730	...	...	...	...	...	...	...	...	...	...
	30 48 21.74	786	57.2 (9.6)	35.5 (7.8)	27.3 (7.8)	2.7 (3.6)	31.0 (6.8)	26.3 (6.8)	46 (7.4)	27 (5.8)	25 (6.6)	8.15E+35
	3.2	2023	<12.2	<6.6	<12.2	...	...	...	<9.2	<5.0	<9.2	<1.65E+35
013324.4+304401	01 33 24.447	1730	2023.7 (46.1)	1339.0 (37.6)	689.3 (27.4)	313.9 (18.8)	1067.9 (33.7)	643.2 (26.5)	1700 (39)	1100 (31)	590 (23)	3.03E+37
	30 44 01.47	786	3864.0 (63.3)	2629.1 (52.3)	1233.8 (36.3)	708.2 (27.7)	2018.7 (46.0)	1137.8 (34.9)	2800 (45)	1800 (37)	960 (28)	4.95E+37
	0.7	2023	7800.0 (93.0)	5672.6 (78.0)	2016.8 (49.7)	1984.4 (48.1)	3929.4 (64.9)	1867.2 (48.7)	2500 (31)	1700 (23)	1000 (25)	4.56E+37

TABLE 3—*Continued*

Source			Counts						Flux[a] (10^{-7} counts s^{-1} cm^{-2})			L[a] (ergs s^{-1})
CXO J	R.A., Decl., Uncertainty (arcsec)	ObsID	0.3–8.0	0.3–2.0	2.0–8.0	0.3–1.0	1.0–2.1	2.1–8.0	0.3–8.0	0.3–2.0	2.0–8.0	0.3–8.0
013324.7+304210	01 33 24.799	1730	<9.7	<4.6	<12.2	...	...	...	<7.3	<3.5	<9.2	<1.31E+35
	30 42 10.73	786	8.0 (4.4)	<12.2	<14.2	...	...	...	5.7 (3.1)	<9.2	<10.7	1.02E+35
	1.3	2023	<6.6	<4.6	<7.5	...	...	...	<5.0	<3.5	<5.6	<9.00E+34
013325.5+303618	01 33 25.569	1730	24.6 (6.3)	15.0 (5.1)	10.0[b] (3.2)	3.4 (3.2)	11.5 (4.6)	9.8 (4.4)	19 (4.8)	11 (3.0)	7.5[b]	3.36E+35
	30 36 18.15	786	...	...	...	...	...	...	...	...	...	...
	1.4	2023	...	...	...	...	...	...	...	...	...	...
013325.5+304439	01 33 25.582	1730	12.0[b] (3.5)	9.0[b] (3.0)	<13.4	...	...	...	9.0[b]	6.7[b]	<10.1	1.61E+35[b]
	30 44 39.95	786	13.8 (6.0)	<17.8	<18.2	...	...	...	10 (4.2)	<13.4	<13.7	1.78E+35
	1.6	2023	<6.6	<7.5	<4.6	...	...	...	<5.0	<5.6	<3.5	<9.00E+34
013325.6+304756	01 33 25.641	1730	...	...	...	...	...	...	...	...	...	...
	30 47 56.28	786	16.8 (6.5)	11.1 (5.5)	5.0[b] (2.2)	...	...	...	13 (4.8)	8.5 (4.0)	3.8[b]	2.38E+35
	2.8	2023	<4.6	<4.6	<4.6	...	...	...	<3.5	<3.5	<3.5	<6.30E+34
013326.0+304119	01 33 26.062	1730	<10.2	3.9 (3.2)	<4.6	...	...	...	<7.7	2.9 (1.5)	<3.5	<1.38E+35
	30 41 19.01	786	<6.6	<6.6	<4.6	...	...	...	<5.0	<5.0	<3.5	<9.00E+34
	1.2	2023	<15.7	<13.8	<7.5	...	...	...	<11.8	<10.4	<5.6	<2.11E+35
013327.6+304045	01 33 27.647	1730	<12.2	3.8 (3.2)	<6.6	...	...	...	<9.2	2.7 (1.5)	<5.0	<1.65E+35
	30 40 45.82	786	<4.6	<4.6	<4.6	...	...	...	<3.5	<3.5	<3.5	<6.30E+34
	1.1	2023	<9.7	<9.1	<6.0	...	...	...	<7.3	<6.8	<4.5	<1.31E+35
013327.7+304645	01 33 27.728	1730	18.0 (5.4)	16.5 (5.2)	<9.1	...	...	...	14 (4.3)	13 (3.2)	<6.8	2.52E+35
	30 46 45.84	786	25.0 (7.2)	24.9 (6.7)	<9.8	16.1 (5.5)	9.2 (4.4)	0.9 (3.8)	20 (5.4)	18 (4.8)	<7.4	3.49E+35
	1.3	2023	122.5 (15.0)	90.5 (12.0)	33.0[b] (5.7)	43.4 (8.8)	43.6 (8.8)	28.6 (9.8)	52 (6.6)	38 (5.1)	24.7[b]	9.21E+35
013327.9+303135	01 33 27.922	1730	18.7 (6.1)	17.8 (5.8)	<9.3	...	...	...	15 (4.9)	15 (3.8)	<7.0	2.77E+35
	30 31 35.77	786	...	...	...	...	...	...	...	...	...	...
	2.3	2023	...	...	...	...	...	...	...	...	...	...
013328.6+304321	01 33 28.686	1730	26.5 (6.4)	5.8 (3.6)	7.7 (4.0)	6.7 (3.8)	6.7 (3.8)	13.0 (4.8)	20 (4.7)	4.3 (1.8)	5.8 (2.1)	3.50E+35
	30 43 21.30	786	28.4 (7.2)	17.1 (5.3)	<18.0	5.7 (4.0)	16.6 (5.3)	6.0 (4.4)	19 (4.9)	11 (3.6)	<13.5	3.47E+35
	1.2	2023	<4.6	<4.6	<4.6	...	...	...	<3.5	<3.5	<3.5	<6.30E+34
013328.7+304746	01 33 28.786	1730	...	...	...	...	...	...	...	...	...	...
	30 47 46.01	786	70.0 (10.9)	61.7 (9.6)	<19.8	47.3 (8.4)	18.0 (5.8)	7.2 (5.7)	53 (8.0)	45 (6.8)	<14.9	9.46E+35
	2.4	2023	80.8 (14.7)	60.6 (9.7)	<25.3	66.3 (10.5)	8.6 (6.7)	−3.1 (9.3)	33 (6.6)	26 (4.2)	<19.0	5.85E+35
013329.0+304216	01 33 29.009	1730	199.4 (15.2)	202.2 (15.3)	<6.0	140.7 (12.9)	58.7 (8.7)	−0.1 (2.3)	150 (12)	150 (11)	<4.5	2.72E+36
	30 42 16.54	786	242.5 (16.7)	240.6 (16.6)	<10.2	180.8 (14.5)	60.3 (8.9)	1.3 (3.2)	160 (11)	160 (11)	<7.7	2.93E+36
	1.0	2023	615.1 (31.4)	610.5 (28.6)	<37.1	512.3 (25.7)	96.1 (13.6)	0.4 (14.3)	200 (10)	180 (8.6)	<27.8	3.61E+36
013329.2+304537	01 33 29.278	1730	44.1 (7.9)	30.3 (6.6)	12.6 (4.8)	5.5 (3.6)	26.4 (6.3)	12.1 (4.8)	34 (6.0)	23 (4.2)	9.8 (2.9)	6.01E+35
	30 45 37.10	786	55.1 (9.3)	34.3 (7.2)	21.6 (6.4)	2.7 (3.6)	32.0 (6.9)	20.9 (6.4)	39 (6.5)	24 (5.0)	17 (4.9)	7.00E+35
	1.6	2023	<8.3	<4.6	<9.1	...	...	...	<6.2	<3.5	<6.8	<1.11E+35
013329.2+304508	01 33 29.299	1730	188.3 (14.9)	123.1 (12.2)	67.0 (9.5)	30.3 (6.6)	98.3 (11.0)	59.5 (8.9)	140 (11)	93 (8.4)	52 (6.5)	2.55E+36
	30 45 08.07	786	243.9 (17.0)	171.4 (14.3)	70.1 (9.7)	60.4 (9.0)	115.4 (11.9)	68.4 (9.7)	170 (12)	120 (9.7)	53 (7.3)	3.05E+36
	1.1	2023	351.2 (24.7)	207.9 (17.6)	80.0[b] (8.9)	113.1 (14.4	151.8 (14.9)	82.8 (15.0)	120 (8.2)	60 (5.1)	60.0[b]	2.06E+36
013329.4+304912	01 33 29.434	1730	...	...	...	...	...	...	...	...	...	...
	30 49 12.03	786	103.0 (12.8)	103.7 (11.9)	<12.1	85.5 (10.7)	21.5 (6.2)	1.8 (5.3)	82 (9.8)	78 (8.9)	<9.1	1.47E+36
	1.7	2023	186.0 (18.9)	189.2 (16.7)	<35.2	127.1 (13.5)	46.4 (9.7)	2.7 (10.6)	80 (8.5)	82 (7.3)	<26.4	1.42E+36

TABLE 3—*Continued*

Source			Counts						Flux[a] (10^{-7} counts s^{-1} cm^{-2})			L[a] (ergs s^{-1})
CXO J	R.A., Decl., Uncertainty (arcsec)	ObsID	0.3–8.0	0.3–2.0	2.0–8.0	0.3–1.0	1.0–2.1	2.1–8.0	0.3–8.0	0.3–2.0	2.0–8.0	0.3–8.0
013330.5+303404	01 33 30.588	1730	64.5 (9.2)	23.6 (6.2)	54.6 (8.6)	1.4 (2.7)	20.5 (5.7)	42.8 (7.7)	50 (7.2)	19 (4.0)	44 (6.1)	9.02E+35
	30 34 04.62	786	...	...	...	...	...	...	...	...	...	...
	1.5	2023	...	...	...	...	...	...	...	...	...	...
013330.8+304132	01 33 30.873	1730	<4.6	<4.6	<4.6	...	...	...	<3.5	<3.5	<3.5	<6.30E+34
	30 41 32.02	786	6.0[b] (2.5)	<6.6	5.6 (3.6)	...	...	...	4.5[b]	<5.0	4.0 (2.6)	8.06E+34[b]
	1.1	2023	<9.7	<7.5	<7.5	...	...	...	<7.3	<5.6	<5.6	<1.31E+35
013331.1+303333	01 33 31.161	1730	261.0 (17.3)	259.3 (17.2)	<11.6	158.7 (13.7)	99.0 (11.0)	3.5 (3.6)	200 (13)	200 (13)	<8.7	3.61E+36
	30 33 33.51	786	...	...	...	...	...	...	...	...	...	...
	1.1	2023	...	...	...	...	...	...	...	...	...	...
013331.3+303737	01 33 31.366	1730	14.5 (5.1)	9.0[b] (3.0)	<13.8	...	...	...	11 (3.7)	6.8[b]	<10.4	1.90E+35
	30 37 37.54	786	...	...	...	...	...	...	...	...	...	...
	1.1	2023	<9.7	<4.6	<12.2	...	...	...	<7.3	<3.5	<9.2	<1.31E+35
013332.1+303656	01 33 32.112	1730	19.2 (5.6)	<11.8	15.5 (5.1)	...	...	...	14 (4.1)	<8.9	12 (3.0)	2.53E+35
	30 36 56.47	786	...	...	...	...	...	...	...	...	...	...
	1.1	2023	...	...	...	...	...	...	...	...	...	...
013333.0+304920	01 33 33.008	1730	...	...	...	...	...	...	...	...	...	...
	30 49 20.38	786	35.6 (8.)1	22.0 (6.9)	13.0[b] (3.6)	2.8 (3.6)	21.0 (5.9)	13.4 (5.6)	28 (6.0)	17 (5.0)	9.8[b]	4.94E+35
	3.0	2023	<9.1	<6.6	<7.5	...	...	...	<6.8	<5.0	<5.6	<1.22E+35
013333.6+303108	01 33 33.606	1730	86.3 (10.9)	50.5 (8.6)	38.5 (7.7)	9.5 (4.6)	41.2 (7.6)	36.5 (7.5)	70 (8.7)	40 (6.0)	32 (5.5)	1.25E+36
	30 31 08.76	786	...	...	...	...	...	...	...	...	...	...
	2.2	2023	...	...	...	...	...	...	...	...	...	...
013333.9+303938	01 33 33.924	1730	3.9 (3.2)	<8.5	<8.5	...	...	...	2.8 (2.3)	<6.4	<6.4	4.93E+34
	30 39 38.97	786	<4.6	<4.6	<4.6	...	...	...	<3.5	<3.5	<3.5	<6.30E+34
	1.0	2023	<6.6	<7.5	<4.6	...	...	...	<5.0	<5.6	<3.5	<9.00E+34
013334.1+303714	01 33 34.112	1730	59.1 (8.8)	36.4 (7.1)	23.9 (6.1)	4.7 (3.4)	30.8 (6.6)	23.5 (6.0)	43 (6.4)	26 (4.4)	18 (3.7)	7.71E+35
	30 37 14.3	786	...	...	...	...	...	...	...	...	...	...
	1.0	2023	<5.7	<4.6	<6.0	...	...	...	<4.3	<3.5	<4.5	<7.70E+34
013334.1+303210	01 33 34.155	1730	5036.7 (72.1)	3691.1 (61.8)	1348.6 (37.9)	899.7 (31.1)	2900.9 (54.9)	1238.0 (36.3)	4100 (59)	3000 (49)	1100 (31)	7.37E+37
	30 32 10.51	786	...	...	...	...	...	...	...	...	...	...
	0.7	2023	...	...	...	...	...	...	...	...	...	...
013334.5+303556	01 33 34.525	1730	18.1 (5.4)	17.0[b] (4.1)	<8.5	...	...	...	13 (4.0)	12.8[b]	<6.4	2.39E+35
	30 35 56.22	786	...	...	...	...	...	...	...	...	...	...
	1.1	2023	...	...	...	...	...	...	...	...	...	...
013335.1+304451	01 33 35.152	1730	<4.6	<4.6	<4.6	...	...	...	<3.5	<3.5	<3.5	<6.30E+34
	30 44 51.71	786	<11.1	4.3 (3.4)	<4.6	...	...	...	<8.3	3.0 (2.3)	<3.5	<1.49E+35
	1.2	2023	<9.7	<9.1	<6.0	...	...	...	<7.3	<6.8	<4.5	<1.31E+35
013335.5+303728	01 33 35.502	1730	16.2 (5.2)	9.7 (4.3)	6.0[b] (2.5)	...	...	...	12 (4.0)	7.4 (2.4)	4.5[b]	2.21E+35
	30 37 28.84	786	38.1 (7.5)	24.4 (6.2)	12.2 (4.8)	13.2 (4.8)	12.5 (4.7)	12.6 (4.8)	19 (3.7)	11 (2.9)	8.8 (3.5)	3.43E+35
	1.0	2023	<5.7	<6.0	<4.6	...	...	...	<4.3	<4.5	<3.5	<7.70E+34
013335.8+304654	01 33 35.830	1730	8.1 (4.3)	<12.2	<12.2	...	...	...	6.4 (3.4)	<9.2	<9.2	1.14E+35
	30 46 54.65	786	<14.6	<6.0	<12.6	...	...	...	<11.0	<4.5	<9.5	<1.97E+35
	1.6	2023	<4.6	<4.6	<4.6	...	...	...	<3.5	<3.5	<3.5	<6.30E+34
013335.9+303627	01 33 35.962	1730	100.4 (11.2)	96.6 (10.9)	<13.8	62.3 (9.0)	35.5 (7.1)	2.7 (3.2)	76 (8.4)	72 (7.4)	<10.4	1.35E+36
	30 36 27.35	786	...	...	...	...	...	...	...	...	...	...
	1.0	2023	...	...	...	...	...	...	...	...	...	...

TABLE 3—*Continued*

Source			Counts						Flux[a] (10^{-7} counts s^{-1} cm^{-2})			L[a] (ergs s^{-1})
CXO J	R.A., Decl., Uncertainty (arcsec)	ObsID	0.3–8.0	0.3–2.0	2.0–8.0	0.3–1.0	1.0–2.1	2.1–8.0	0.3–8.0	0.3–2.0	2.0–8.0	0.3–8.0
013336.0+303333	01 33 36.094	1730	24.0 (6.3)	19.9 (5.8)	<14.2	5.2 (3.6)	15.4 (5.1)	3.5 (3.4)	18 (4.8)	15 (3.6)	<10.7	3.28E+35
	30 33 33.43	786	...	...	...	...	...	...	...	...	...	...
	1.4	2023	...	...	...	...	...	...	...	...	...	...
013336.3+303742	01 33 36.398	1730	118.1 (11.9)	71.6 (9.5)	47.5 (8.0)	6.8 (3.8)	64.8 (9.1)	46.6 (7.9)	90 (9.1)	54 (6.4)	37 (5.4)	1.60E+36
	30 37 42.26	786	98.6 (11.2)	62.5 (9.1)	38.7 (7.5)	10.8 (4.6)	49.2 (8.1)	38.9 (7.5)	48 (5.5)	28 (4.1)	27 (5.2)	8.63E+35
	1.0	2023	<9.7	<9.1	<6.0	...	...	...	<7.3	<6.8	<4.5	<1.31E+35
013336.6+303729	01 33 36.694	1730	17.4 (5.3)	10.8 (4.4)	6.6 (3.8)	...	...	...	13 (4.0)	8.1 (2.5)	5.0 (2.0)	2.36E+35
	30 37 29.22	786	14.1 (5.1)	5.5 (3.6)	7.0[b] (2.7)	...	...	...	6.6 (2.4)	2.4 (1.6)	5.3[b]	1.19E+35
	1.0	2023	<11.1	<6.0	<12.2	...	...	...	<8.3	<4.5	<9.2	<1.49E+35
013337.4+304718	01 33 37.490	1730	92.0 (10.9)	68.8 (9.5)	26.0 (6.5)	17.1 (5.3)	49.0 (8.1)	25.8 (6.5)	71 (8.4)	53 (6.5)	20 (4.2)	1.27E+36
	30 47 18.27	786	145.3 (13.7)	104.8 (11.5)	38.9 (8.1)	28.5 (6.7)	80.9 (10.2)	36.7 (7.7)	100 (9.7)	73 (8.0)	31 (6.3)	1.85E+36
	1.2	2023	75.3 (12.3)	42.7 (9.5)	41.0[b] (6.4)	6.2 (5.4)	27.3 (7.3)	33.6 (9.5)	29 (5.2)	16 (3.9)	30.7[b]	5.13E+35
013337.6+304010	01 33 37.659	1730	7.0[b] (2.7)	<13.8	<9.1	...	...	...	5.3[b]	<10.4	<6.8	9.51E+34[b]
	30 40 10.18	786	22.1 (6.7)	8.6 (4.3)	<13.8	14.1 (5.2)	4.1 (3.6)	4.0 (4.1)	10 (3.2)	3.7 (1.8)	<10.4	1.86E+35
	1.0	2023	<9.7	<6.0	<9.1	...	...	...	<7.3	<4.5	<6.8	<1.31E+35
013337.8+303837	01 33 37.892	1730	6.6 (3.8)	<4.6	6.8 (3.8)	...	...	...	4.7 (2.7)	<3.5	5.0 (1.9)	8.45E+34
	30 38 37.49	786	11.5 (4.8)	<9.1	9.3 (4.4)	...	...	...	5.3 (2.2)	<6.8	6.1 (2.9)	9.51E+34
	1.0	2023	<11.1	<12.2	<6.0	...	...	...	<8.3	<9.2	<4.5	<1.49E+35
013337.9+304023	01 33 37.964	1730	7.8 (4.0)	<10.1	5.0[b] (2.2)	...	...	...	5.4 (2.8)	<7.6	3.8[b]	9.69E+34
	30 40 23.52	786	6.0[b] (2.5)	<9.1	<12.2	...	...	...	4.5[b]	<6.8	<9.2	8.06E+34[b]
	1.0	2023	<6.6	<4.6	<7.5	...	...	...	<5.0	<3.5	<5.6	<9.00E+34
013337.9+304035	01 33 37.992	1730	21.7 (5.8)	7.9 (4.0)	13.8 (4.8)	<1.9	8.9 (4.1)	12.8 (4.7)	15 (4.0)	5.5 (2.0)	9.6 (2.6)	2.70E+35
	30 40 35.58	786	11.6 (4.7)	<13.8	6.1 (3.8)	...	...	...	13 (5.1)	<10.4	10 (5.9)	2.40E+35
	1.0	2023	<11.1	<12.2	<6.0	...	...	...	<8.3	<9.2	<4.5	<1.49E+35
013339.2+304049	01 33 39.212	1730	72.6 (9.6)	41.9 (7.5)	29.7 (6.5)	6.9 (3.8)	36.9 (7.1)	28.7 (6.5)	50 (6.7)	29 (4.5)	21 (3.8)	9.01E+35
	30 40 49.48	786	42.5 (7.8)	30.9 (6.7)	12.1 (4.7)	3.9 (3.2)	28.8 (6.5)	11.4 (4.6)	47 (8.4)	32 (6.8)	17 (6.4)	8.48E+35
	1.0	2023	<8.3	<9.1	<4.6	...	...	...	<6.2	<6.8	<3.5	<1.11E+35
013339.8+304350	01 33 39.807	1730	6.7 (3.8)	<8.5	5.0[b] (2.2)	...	...	...	4.9 (2.8)	<6.4	3.8[b]	8.78E+34
	30 43 50.17	786	9.0 (4.3)	<16.5	<9.1	...	...	...	6.0 (2.8)	<12.4	<6.8	1.07E+35
	1.0	2023	<4.6	<4.6	<4.6	...	...	...	<3.5	<3.5	<3.5	<6.30E+34
013340.0+304323	01 33 40.084	1730	45.1 (7.8)	26.7 (6.3)	18.0[b] (4.2)	11.8 (4.6)	16.8 (5.2)	16.3 (5.2)	32 (5.6)	19 (3.7)	13.5[b]	5.71E+35
	30 43 23.11	786	35.7 (7.1)	24.3 (6.1)	12.2 (5.0)	1.6 (2.7)	23.8 (6.0)	10.2 (4.4)	23 (4.7)	16 (3.9)	8.5 (3.5)	4.19E+35
	1.0	2023	<12.6	<12.2	<7.5	...	...	...	<9.5	<9.2	<5.6	<1.70E+35
013340.7+303523	01 33 40.785	1730	14.1 (5.0)	9.5 (4.3)	5.0[b] (2.2)	...	...	...	10 (3.6)	6.9 (2.3)	<3.8	1.85E+35
	30 35 23.54	786	<13.8	4.5 (3.4)	<6.0	...	...	...	<10.4	5.7 (4.0)	<4.5	<1.86E+35
	1.1	2023	...	...	...	...	...	...	...	...	...	...
013341.2+303950	01 33 41.216	1730	<4.6	<4.6	<4.6	...	...	...	<3.5	<3.5	<3.5	<6.30E+34
	30 39 50.48	786	4.7 (3.6)	<9.1	<9.1	...	...	...	2.1 (1.6)	<6.8	<6.8	3.81E+34
	1.0	2023	<5.7	<6.0	<4.6	...	...	...	<4.3	<4.5	<3.5	<7.70E+34
013341.4+303815	01 33 41.447	1730	7.7 (4.0)	<8.5	5.8 (3.6)	...	...	...	5.4 (2.8)	<6.4	4.2 (1.7)	9.69E+34
	30 38 15.99	786	<4.6	<4.6	<4.6	...	...	...	<3.5	<3.5	<3.5	<6.30E+34
	1.0	2023	<6.6	<4.6	<7.5	...	...	...	<5.0	<3.5	<5.6	<9.00E+34
013341.5+303220	01 33 41.505	1730	21.3 (6.1)	15.4 (5.2)	<15.7	8.0 (4.1)	7.3 (4.0)	6.2 (4.0)	17 (4.7)	12 (3.2)	<11.8	2.96E+35
	30 32 20.5	786	...	...	...	...	...	...	...	...	...	...
	1.5	2023	...	...	...	...	...	...	...	...	...	...

TABLE 3—*Continued*

Source			Counts						Flux[a] (10^{-7} counts s^{-1} cm^{-2})			L[a] (ergs s^{-1})
CXO J	R.A., Decl., Uncertainty (arcsec)	ObsID	0.3–8.0	0.3–2.0	2.0–8.0	0.3–1.0	1.0–2.1	2.1–8.0	0.3–8.0	0.3–2.0	2.0–8.0	0.3–8.0
013341.5+304136	01 33 41.528	1730	37.6 (7.2)	21.8 (5.8)	18.6 (5.4)	0.9 (2.3)	19.9 (5.6)	16.7 (5.2)	26 (5.0)	15 (3.2)	13 (3.0)	4.65E+35
	30 41 36.23	786	56.1 (8.6)	34.3 (7.0)	22.5 (5.9)	9.8 (4.3)	23.9 (6.0)	22.5 (5.9)	37 (5.6)	22 (4.5)	16 (4.1)	6.56E+35
	1.0	2023	<14.2	<7.5	<12.2	...	...	...	<10.7	<5.6	<9.2	<2.95E+35
013341.8+303848	01 33 41.885	1730	99.6 (11.0)	95.7 (10.8)	5.9 (3.6)	63.9 (9.0)	29.9 (6.5)	5.8 (3.6)	70 (7.8)	67 (6.9)	4.2 (1.7)	1.25E+36
	30 38 48.71	786	318.8 (18.9)	318.6 (18.9)	<9.1	236.3 (16.4)	81.6 (10.1)	0.9 (2.7)	150 (8.7)	130 (8.0)	<6.8	2.61E+36
	1.0	2023	623.0 (31.1)	312.5 (20.1)	44.0[b] (6.6)	401.2 (23.2)	176.5 (16.3)	35.0 (14.9)	200 (10)	92 (6.0)	33.0[b]	3.57E+36
013342.5+304253	01 33 42.508	1730	19.6 (5.6)	12.8 (4.7)	8.7 (4.1)	...	...	...	15 (4.2)	9.7 (2.7)	6.6 (2.3)	2.65E+35
	30 42 53.11	786	87.3 (10.5)	35.2 (7.1)	50.9 (8.3)	2.3 (2.9)	38.5 (7.3)	46.3 (8.0)	56 (6.8)	22 (4.5)	35 (5.7)	1.01E+36
	1.0	2023	<15.7	7.0[b] (2.7)	<4.6	...	...	...	<11.8	<5.3	<3.5	<2.11E+35
013342.7+304642	01 33 42.741	1730	9.7 (4.4)	5.0[b] (2.2)	5.5 (3.6)	...	...	...	19 (7.9)	3.8[b]	11 (4.5)	3.34E+35
	30 46 42.14	786	33.9 (7.8)	14.5 (5.4)	21.8 (6.6)	4.2 (3.8)	10.3 (4.6)	20.2 (6.2)	25 (5.6)	10 (3.8)	18 (5.2)	4.51E+35
	1.4	2023	<12.2	<6.6	<9.1	...	...	...	<9.2	<5.0	<6.8	<1.65E+35
013343.4+304630	01 33 43.428	1730	8.8 (4.4)	10.4 (4.4)	<4.6	...	...	...	20 (8.8)	21 (6.6)	<3.5	3.60E+35
	30 46 30.83	786	86.1 (10.9)	79.7 (10.2)	<16.8	70.2 (9.6)	10.3 (4.6)	6.0 (4.6)	61 (7.7)	55 (7.0)	<12.6	1.09E+36
	1.1	2023	158.4 (17.5)	174.6 (16.2)	<12.2	154.0 (14.5)	32.8 (8.1)	<7.5	79 (7.5)	75 (6.4)	<9.2	1.42E+36
013343.5+304102	01 33 43.534	1730	7.0[b] (2.7)	8.0[b] (2.8)	<4.6	...	...	...	5.2[b]	6.0[b]	<3.5	9.30E+34[b]
	30 41 02.97	786	12.1 (5.2)	10.6 (4.6)	<6.5	...	...	...	5.7 (2.4)	4.6 (2.0)	<4.9	1.02E+35
	1.0	2023	<5.7	<4.6	<6.0	...	...	...	<4.3	<3.5	<4.5	<7.70E+34
013343.9+303508	01 33 43.938	1730	6.7 (3.8)	3.8 (3.2)	<10.1	...	...	...	4.9 (2.8)	2.8 (1.5)	<7.6	8.77E+34
	30 35 08.30	786	<7.5	<7.5	<4.6	...	...	...	<5.6	<5.6	<3.5	<1.00E+35
	1.1	2023	...	...	...	...	...	...	...	...	...	...
013344.2+304026	01 33 44.245	1730	16.0[b] (4.0)	<14.4	11.0[b] (3.3)	...	...	...	12.0[b]	<10.8	8.3[b]	3.31E+35[b]
	30 40 26.16	786	41.0[b] (6.4)	27.5 (8.2)	<30.2	...	...	...	30.8[b]	12 (3.5)	<22.7	5.52E+35[b]
	1.0	2023	<6.6	<4.6	<7.5	...	...	...	<5.0	<3.5	<5.6	<9.00E+34
013346.2+303807	01 33 46.252	1730	<4.6	<4.6	<4.6	...	...	...	<3.5	<3.5	<3.5	<6.30E+34
	30 38 07.18	786	<5.7	<4.6	<6.0	...	...	...	<4.3	<3.5	<4.5	<7.70E+34
	1.0	2023	143.0 (19.6)	150.3 (18.2)	<6.0	92.5 (12.8)	60.8 (10.5)	46.7 (12.0)	90 (9.0)	80 (7.7)	<4.5	1.62E+36
013346.5+303748	01 33 46.584	1730	157.4 (13.6)	107.8 (11.4)	49.7 (8.1)	32.8 (6.8)	77.9 (9.9)	46.7 (7.9)	120 (10)	80 (7.7)	38 (5.3)	2.09E+36
	30 37 48.33	786	198.5 (15.2)	124.9 (12.3)	72.8 (9.6)	49.6 (8.1)	80.7 (10.0)	68.2 (9.4)	93 (7.1)	54 (5.3)	48 (6.4)	1.65E+36
	1.0	2023	...	...	...	...	...	...	...	...	...	...
013346.7+304318	01 33 46.781	1730	5.8 (3.6)	<10.1	<10.1	...	...	...	4.1 (2.6)	<7.6	<7.6	7.35E+34
	30 43 18.09	786	<10.1	<8.5	<6.6	...	...	...	<7.6	<6.4	<5.0	<1.36E+35
	0.9	2023	<9.7	<7.5	<7.5	...	...	...	<7.3	<5.6	<5.6	<1.31E+35
013347.5+304042	01 33 47.574	1730	7.9 (4.0)	5.0[b] (2.2)	<10.1	...	...	...	5.3 (2.7)	3.8[b]	<7.6	9.56E+34
	30 40 42.75	786	13.5 (5.0)	11.9 (4.7)	<12.2	...	...	...	6.2 (2.3)	5.1 (2.0)	<9.2	1.11E+35
	1.0	2023	<11.1	<9.1	<7.5	...	...	...	<8.3	<6.8	<5.6	<1.49E+35
013348.6+303304	01 33 48.645	1730	29.0[b] (5.4)	27.9 (6.6)	<9.1	...	...	...	21.8[b]	21 (4.2)	<6.8	3.90E+35[b]
	30 33 04.70	786	<10.2	8.5 (6.4)	<6.0	...	...	...	<7.7	12 (4.7)	<4.5	<1.38E+35
	1.3	2023	...	...	...	...	...	...	...	...	...	...
013349.1+304055	01 33 49.122	1730	<8.5	<8.5	<4.6	...	...	...	<6.4	<6.4	<3.5	<1.15E+35
	30 40 55.19	786	6.0[b] (2.5)	5.7 (3.6)	<6.6	...	...	...	4.5[b]	2.4 (1.5)	<5.0	8.06E+34[b]
	1.0	2023	<9.7	<9.1	<6.0	...	...	...	<7.3	<6.8	<4.5	<1.31E+35
013350.5+303821	01 33 50.520	1730	39.6 (7.4)	29.7 (6.5)	10.7 (4.4)	7.9 (4.0)	21.9 (5.8)	9.8 (4.3)	27 (5.1)	20 (3.8)	7.4 (2.3)	4.88E+35
	30 38 21.42	786	123.4 (12.3)	92.8 (10.7)	30.0 (6.6)	42.2 (7.6)	50.5 (8.2)	30.6 (6.7)	57 (5.7)	40 (4.6)	20 (4.4)	1.02E+36
	1.0	2023	<15.7	6.0[b] (2.5)	<6.0	...	...	...	<11.8	4.5[b]	<4.5	<2.11E+35

TABLE 3—*Continued*

Source			Counts						Flux[a] (10^{-7} counts s^{-1} cm^{-2})			L[a] (ergs s^{-1})
CXO J	R.A., Decl., Uncertainty (arcsec)	ObsID	0.3–8.0	0.3–2.0	2.0–8.0	0.3–1.0	1.0–2.1	2.1–8.0	0.3–8.0	0.3–2.0	2.0–8.0	0.3–8.0
013351.0+303937[c]	01 33 51.001	1730	5786.1 (77.8)	3471.9 (60.4)	2314.3 (49.8)	...	...	...	4100 (56)	2400 (43)	1700 (36)	7.37E+37
	30 39 37.62	786	10300.6 (104.9)	6874.8 (85.4)	3425.8 (61.7)	...	...	...	4900 (50)	3000 (37)	2300 (41)	8.68E+37
	0.7	2023	171076.0 (415.1)	131846.5 (364.4)	39229.5 (199.6)	...	...	...	53000 (130)	37000 (100)	19000 (95)	9.40E+38
013352.7+303242	01 33 52.715	1730	<4.6	<4.6	<4.6	...	...	...	<3.5	<3.5	<3.5	<6.30E+34
	30 32 42.21	786	<12.1	<4.6	5.4 (4.1)	...	...	...	<9.1	<3.5	4.4 (3.1)	<1.63E+35
	1.4	2023	...	...	...	...	...	...	...	...	...	...
013353.3+304016	01 33 53.361	1730	<6.6	<4.6	<6.6	...	...	...	<5.0	<3.5	<5.0	<9.00E+34
	30 40 16.02	786	10.2 (4.4)	9.6 (4.3)	<6.6	...	...	...	4.9 (2.1)	4.3 (1.9)	<5.0	8.79E+34
	1.0	2023	<12.6	<13.8	<4.6	...	...	...	<9.5	<10.4	<3.5	<1.70E+35
013353.5+303317	01 33 53.518	1730	<4.6	<4.6	<4.6	...	...	...	<3.5	<3.5	<3.5	<6.30E+34
	30 33 17.67	786	<9.7	<4.6	2.9 (3.2)	...	...	...	<7.3	<3.5	2.1 (2.2)	<1.31E+35
	1.3	2023	...	...	...	...	...	...	...	...	...	...
013353.6+303605	01 33 53.662	1730	<13.8	<9.1	<9.1	...	...	...	<10.4	<6.8	<6.8	<1.86E+35
	30 36 05.79	786	21.7 (6.4)	11.0[b] (3.3)	10.0[b] (3.2)	7.1 (4.1)	4.8 (3.6)	9.7 (4.7)	9.9 (2.9)	8.3[b]	7.5[b]	1.76E+35
	1.0	2023	...	...	...	...	...	...	...	...	...	...
013353.7+303250	01 33 53.715	1730	<7.5	<4.6	<7.5	...	...	...	<5.6	<3.5	<5.6	<1.00E+35
	30 32 50.21	786	<11.2	<4.6	4.5 (3.8)	...	...	...	<8.4	<3.5	4.0 (3.1)	<1.50E+35
	1.4	2023	...	...	...	...	...	...	...	...	...	...
013354.5+303523	01 33 54.555	1730	12.5 (4.7)	9.8 (4.3)	<10.1	...	...	...	9.0 (3.4)	7.0 (2.3)	<7.6	1.61E+35
	30 35 23.01	786	7.0[b] (2.7)	<12.2	<12.2	...	...	...	<5.3	<9.2	<9.2	<9.50E+34
	1.0	2023	...	...	...	...	...	...	...	...	...	...
013354.6+304519	01 33 54.651	1730	9.0[b] (3.0)	9.5 (4.3)	<4.6	...	...	...	<6.8	6.9 (2.3)	<3.5	<1.22E+35
	30 45 19.25	786	19.5 (6.7)	22.0[b] (4.7)	<7.1	...	...	...	13 (4.6)	16.5[b]	<5.3	2.40E+35
	1.1	2023	...	...	...	...	...	...	...	...	...	...
013354.8+303309	01 33 54.872	1730	154.3 (13.6)	157.4 (13.7)	<8.3	101.0 (11.1)	52.3 (8.3)	1.2 (2.9)	120 (10)	120 (9.4)	<6.2	2.07E+36
	30 33 09.98	786	443.2 (23.5)	446.4 (22.7)	<15.7	391.5 (21.2)	55.1 (9.2)	2.4 (6.6)	230 (12)	210 (11)	<11.8	4.08E+36
	1.1	2023	...	...	...	...	...	...	...	...	...	...
013355.2+303528	01 33 55.217	1730	6.0[b] (2.5)	<6.6	4.8 (3.4)	...	...	...	4.5[b]	<5.0	3.5 (1.6)	8.06E+34[b]
	30 35 28.60	786	14.8 (5.5)	<12.6	11.0[b] (3.3)	...	...	...	7.3 (2.6)	<9.5	<8.3	1.30E+35
	1.0	2023	...	...	...	...	...	...	...	...	...	...
013355.4+304307	01 33 55.450	1730	<4.6	<4.6	<4.6	...	...	...	<3.5	<3.5	<3.5	<6.30E+34
	30 43 07.24	786	5.5 (3.8)	<9.1	<12.2	...	...	...	4.3 (2.7)	<6.8	<9.2	7.64E+34
	1.0	2023	...	...	...	...	...	...	...	...	...	...
013355.8+303924	01 33 55.822	1730	7.0[b] (2.7)	<20.4	<6.6	...	...	...	5.3[b]	<15.3	<5.0	9.51E+34[b]
	30 39 24.41	786	12.4 (5.0)	9.0[b] (3.0)	<12.2	...	...	...	5.8 (2.3)	6.8[b]	<9.2	1.03E+35
	1.0	2023	<4.6	<4.6	<4.6	...	...	...	<3.5	<3.5	<3.5	<6.30E+34
013356.3+305353	01 33 56.367	1730	...	...	...	...	...	...	...	...	...	...
	30 53 53.21	786	...	...	...	...	...	...	...	...	...	...
	4.9	2023	<15.0	<4.6	7.1 (4.6)	...	...	...	<11.3	<3.5	3.8 (2.2)	<2.02E+35
013356.8+303729	01 33 56.809	1730	27.6 (6.4)	15.7 (5.1)	12.8 (4.7)	1.9 (2.7)	14.0 (4.8)	11.9 (4.6)	37 (8.4)	21 (5.2)	17 (4.7)	6.57E+35
	30 37 29.75	786	183.3 (14.7)	127.3 (12.4)	56.3 (8.7)	46.6 (8.0)	82.1 (10.2)	54.5 (8.6)	83 (6.7)	53 (5.2)	36 (5.7)	1.49E+36
	1.0	2023	...	...	...	...	...	...	...	...	...	...
013356.8+303706	01 33 56.828	1730	49.4 (8.1)	25.7 (6.2)	22.8 (5.9)	6.8 (3.8)	17.9 (5.3)	24.7 (6.1)	38 (6.2)	20 (3.9)	18 (3.8)	6.76E+35
	30 37 06.38	786	85.6 (10.5)	61.4 (9.1)	27.0 (6.6)	28.7 (6.5)	33.1 (6.9)	23.7 (6.2)	38 (4.7)	25 (3.8)	17 (4.2)	6.89E+35
	1.0	2023	...	...	...	...	...	...	...	...	...	...

TABLE 3—*Continued*

Source			Counts						Flux[a] (10^{-7} counts s^{-1} cm^{-2})			L[a] (ergs s^{-1})
CXO J	R.A., Decl., Uncertainty (arcsec)	ObsID	0.3–8.0	0.3–2.0	2.0–8.0	0.3–1.0	1.0–2.1	2.1–8.0	0.3–8.0	0.3–2.0	2.0–8.0	0.3–8.0
013356.9+303652	01 33 56.933	1730	2.8 (2.9)	<8.5	<6.6	...	...	...	2.0 (2.1)	<6.4	<5.0	3.56E+34
	30 36 52.73	786	<4.6	<4.6	<4.6	...	...	...	<3.5	<3.5	<3.5	<6.30E+34
	1.0	2023	...	...	...	...	...	...	...	...	...	...
013357.0+303500	01 33 57.033	1730	<10.9	<8.5	<7.5	...	...	...	<8.2	<6.4	<5.6	<1.47E+35
	30 35 00.70	786	21.0[b] (4.6)	21.9 (8.0)	<15.9	...	...	...	15.8[b]	9.8 (3.5)	<11.9	2.83E+35[b]
	1.1	2023	...	...	...	...	...	...	...	...	...	...
013357.2+305136	01 33 57.240	1730	...	...	...	...	...	...	...	...	...	...
	30 51 36.46	786	32.1 (8.2)	24.0 (6.7)	8.0[b] (2.8)	9.0 (4.9)	16.9 (5.6)	5.0 (5.1)	26 (6.7)	19 (5.4)	6.0[b]	4.56E+35
	3.5	2023	58.1 (11.0)	25.9 (6.8)	31.8 (8.2)	11.6 (5.6)	17.3 (6.0)	31.6 (8.5)	25 (4.6)	11 (2.8)	14 (3.5)	4.43E+35
013357.8+303756	01 33 57.882	1730	8.0[b] (2.8)	<17.8	<7.5	...	...	...	6.0[b]	<13.4	<5.6	1.07E+35[b]
	30 37 56.85	786	27.0[b] (5.2)	26.0 (7.7)	<15.4	...	...	...	20.3[b]	11 (3.3)	<11.6	3.64E+35[b]
	1.0	2023	...	...	...	...	...	...	...	...	...	...
013358.1+303200	01 33 58.127	1730	40.4 (7.7)	<9.7	38.7 (7.5)	1.1 (2.7)	2.3 (2.9)	37.3 (7.3)	33 (6.3)	<7.3	31 (5.2)	5.92E+35
	30 32 00.73	786	36.9 (7.9)	8.0[b] (2.8)	28.8 (7.1)	0.7 (3.2)	7.2 (4.1)	27.7 (6.9)	27 (5.9)	6.0[b]	22 (5.5)	4.80E+35
	2.6	2023	...	...	...	...	...	...	...	...	...	...
013358.1+303438	01 33 58.189	1730	6.0[b] (2.5)	<7.5	<12.2	...	...	...	4.5[b]	<5.6	<9.2	8.06E+34[b]
	30 34 38.07	786	19.5 (6.1)	11.0[b] (3.3)	8.0[b] (2.8)	...	...	...	9.6 (3.0)	8.2[b]	6.0[b]	1.72E+35
	1.1	2023	...	...	...	...	...	...	...	...	...	...
013358.3+304826	01 33 58.320	1730	...	...	...	...	...	...	...	...	...	...
	30 48 26.94	786	...	...	...	...	...	...	...	...	...	...
	2.1	2023	29.2 (7.4)	13.0[b] (3.6)	18.0 (5.8)	0.8 (2.9)	8.2 (4.3)	20.7 (6.3)	12 (3.1)	<0.0	7.5 (2.4)	2.19E+35
013358.4+303333	01 33 58.491	1730	23.1 (6.2)	22.9 (6.1)	<8.3	14.2 (5.0)	7.4 (4.0)	1.5 (2.9)	17 (4.6)	17 (3.7)	<6.2	3.08E+35
	30 33 33.10	786	51.7 (10.1)	46.6 (8.9)	<21.9	38.7 (7.8)	9.8 (4.8)	11.4 (5.8)	38 (6.4)	30 (5.3)	<16.4	6.79E+35
	1.3	2023	...	...	...	...	...	...	...	...	...	...
013358.4+303624	01 33 58.495	1730	<9.3	<12.2	<4.6	...	...	...	<7.0	<9.2	<3.5	<1.25E+35
	30 36 24.05	786	17.0[b] (4.1)	18.8 (6.1)	<7.5	...	...	...	12.8[b]	7.9 (2.6)	<5.6	2.29E+35[b]
	1.0	2023	...	...	...	...	...	...	...	...	...	...
013358.8+305004	01 33 58.824	1730	...	...	...	...	...	...	...	...	...	...
	30 50 04.78	786	118.9 (12.4)	65.9 (9.4)	48.8 (8.3)	9.1 (4.6)	58.2 (8.8)	50.4 (8.6)	93 (9.8)	51 (7.4)	40 (6.8)	1.67E+36
	1.5	2023	88.7 (11.2)	47.8 (8.3)	38.1 (7.5)	3.2 (3.6)	47.8 (8.1)	38.2 (7.8)	36 (4.5)	19 (3.3)	16 (3.2)	6.48E+35
013359.0+303425	01 33 59.076	1730	<16.5	<12.6	<12.6	...	...	...	<12.4	<9.5	<9.5	<2.39E+35
	30 34 25.84	786	27.2 (8.1)	47.2 (9.5)	<7.5	29.9 (7.1)	2.0 (3.6)	<3.8	14 (4.0)	22 (4.3)	<5.6	2.50E+35
	1.2	2023	...	...	...	...	...	...	...	...	...	...
013359.4+303104	01 33 59.452	1730	...	...	...	...	...	...	...	...	...	...
	30 31 04.6	786	43.3 (10.3)	25.0[b] (5.0)	18.0[b] (4.2)	5.7 (5.5)	21.8 (6.5)	12.4 (7.3)	32 (8.1)	18.8[b]	13.5[b]	5.66E+35
	2.0	2023	...	...	...	...	...	...	...	...	...	...
013400.0+303057	01 34 00.081	1730	...	...	...	...	...	...	...	...	...	...
	30 30 57.01	786	22.0[b] (4.7)	16.9 (6.0)	6.0[b] (2.5)	...	...	...	16.5[b]	13 (4.7)	4.5[b]	3.18E+35[b]
	2.0	2023	...	...	...	...	...	...	...	...	...	...
013400.1+305218	01 34 00.186	1730	...	...	...	...	...	...	...	...	...	...
	30 52 18.15	786	<4.6	<4.6	<4.6	...	...	...	<3.5	<3.5	<3.5	<6.30E+34
	3.2	2023	18.9 (8.7)	<18.0	16.3 (6.6)	...	...	...	9.3 (3.7)	<13.5	7.9 (2.9)	1.67E+35
013400.2+304218	01 34 00.286	1730	11.2 (4.6)	16.4 (5.2)	<6.6	...	...	...	8.1 (3.3)	12 (3.0)	<5.0	1.46E+35
	30 42 18.05	786	52.0 (10.6)	53.0 (9.1)	<17.4	42.0 (8.3)	8.8 (5.1)	2.7 (5.7)	25 (5.0)	23 (4.0)	<13.1	4.54E+35
	1.0	2023	...	...	...	...	...	...	...	...	...	...

TABLE 3—*Continued*

Source			Counts						Flux[a] (10^{-7} counts s^{-1} cm^{-2})			L[a] (ergs s^{-1})
CXO J	R.A., Decl., Uncertainty (arcsec)	ObsID	0.3–8.0	0.3–2.0	2.0–8.0	0.3–1.0	1.0–2.1	2.1–8.0	0.3–8.0	0.3–2.0	2.0–8.0	0.3–8.0
013400.5+305203	01 34 00.506	1730	...	...	...	...	...	...	...	...	...	...
	30 52 03.39	786	<4.6	<4.6	<4.6	...	...	...	<3.5	<3.5	<3.5	<6.30E+34
	3.1	2023	<22.0	11.5 (5.0)	<7.4	...	...	...	<16.5	5.0 (2.1)	<5.6	<3.18E+35
013400.7+304138	01 34 00.794	1730	<4.6	<4.6	<4.6	...	...	...	<3.5	<3.5	<3.5	<6.30E+34
	30 41 38.38	786	<9.1	<5.7	1.7 (3.2)	...	...	...	<6.8	<4.3	1.3 (2.3)	<1.22E+35
	1.0	2023	...	...	...	...	...	...	...	...	...	...
013401.0+304107	01 34 01.009	1730	5.7 (3.6)	<6.6	5.0[b] (2.2)	...	...	...	6.8 (4.2)	<5.0	3.8[b]	1.22E+35
	30 41 07.82	786	<14.2	<6.0	<13.8	...	...	...	<10.7	<4.5	<10.4	<2.95E+35
	1.0	2023	...	...	...	...	...	...	...	...	...	...
013401.4+303517	01 34 01.477	1730	8.0[b] (2.8)	<12.2	<13.8	...	...	...	6.0[b]	<9.2	<10.4	1.07E+35[b]
	30 35 17.27	786	30.3 (7.4)	38.7 (9.1)	9.0[b] (3.0)	14.3 (5.2)	7.2 (4.1)	9.3 (4.8)	15 (3.6)	18 (4.1)	6.8[b]	2.67E+35
	1.1	2023	...	...	...	...	...	...	...	...	...	...
013401.5+303136	01 34 01.529	1730	...	...	...	...	...	...	...	...	...	...
	30 31 36.50	786	222.4 (16.9)	146.0 (13.5)	70.0 (10.2)	25.0 (6.9)	131.1 (12.7)	63.1 (10.0)	170 (13)	110 (10)	54 (8.1)	2.98E+36
	1.2	2023	...	...	...	...	...	...	...	...	...	...
013401.6+303516	01 34 01.608	1730	6.7 (3.8)	<10.1	<11.8	...	...	...	7.7 (4.3)	<7.6	<8.9	1.38E+35
	30 35 16.83	786	10.0[b] (3.2)	<13.8	<12.2	...	...	...	7.5[b]	<10.4	<9.2	1.34E+35[b]
	1.1	2023	...	...	...	...	...	...	...	...	...	...
013402.0+303004	01 34 02.060	1730	...	...	...	...	...	...	...	...	...	...
	30 30 04.82	786	167.7 (15.4)	129.5 (13.2)	38.9 (8.6)	37.8 (8.2)	93.4 (11.1)	33.8 (8.6)	130 (12)	99 (10)	31 (7.1)	2.32E+36
	1.4	2023	...	...	...	...	...	...	...	...	...	...
013402.4+304040	01 34 02.409	1730	6.9 (3.8)	6.9 (3.8)	<6.6	...	...	...	4.9 (2.7)	4.9 (1.9)	<5.0	8.81E+34
	30 40 40.63	786	<4.6	<4.6	<4.6	...	...	...	<3.5	<3.5	<3.5	<6.30E+34
	1.0	2023	...	...	...	...	...	...	...	...	...	...
013402.6+304939	01 34 02.653	1730	...	...	...	...	...	...	...	...	...	...
	30 49 39.55	786	25.2 (7.9)	<11.8	25.6 (7.3)	1.2 (3.8)	<3.0	22.9 (7.1)	19 (6.3)	<8.9	20 (6.0)	3.33E+35
	2.1	2023	86.5 (11.0)	14.7 (5.2)	70.1 (9.8)	0.5 (2.9)	17.0 (5.4)	69.8 (9.8)	37 (4.6)	6.1 (2.2)	30 (4.2)	6.53E+35
013402.7+305409	01 34 02.700	1730	...	...	...	...	...	...	...	...	...	...
	30 54 09.13	786	...	...	...	...	...	...	...	...	...	...
	3.7	2023	20.8 (7.3)	13.7 (5.5)	<20.9	<2.9	15.3 (5.3)	7.5 (5.2)	9.3 (3.1)	5.9 (2.3)	<15.7	1.67E+35
013402.8+303438	01 34 02.874	1730	2.9 (2.9)	8.6 (4.1)	<4.6	...	...	...	2.6 (2.6)	7.8 (2.7)	<3.5	4.69E+34
	30 34 38.64	786	<4.6	<4.6	<4.6	...	...	...	<3.5	<3.5	<3.5	<6.30E+34
	1.2	2023	...	...	...	...	...	...	...	...	...	...
013402.8+304151	01 34 02.888	1730	28.6 (6.5)	<6.6	27.7 (6.4)	<1.9	0.9 (2.3)	27.7 (6.4)	20 (4.5)	<5.0	19 (3.7)	3.57E+35
	30 41 51.10	786	25.0 (7.2)	5.3 (3.6)	19.1 (7.4)	<2.9	6.7 (4.1)	19.9 (6.2)	13 (3.6)	2.5 (1.7)	15 (5.4)	2.34E+35
	1.0	2023	...	...	...	...	...	...	...	...	...	...
013402.9+303042	01 34 02.968	1730	...	...	...	...	...	...	...	...	...	...
	30 30 42.91	786	15.0[b] (3.9)	10.4 (5.1)	<15.9	...	...	...	11.3[b]	7.6 (3.9)	<11.9	2.02E+35[b]
	2.2	2023	...	...	...	...	...	...	...	...	...	...
013403.2+305501	01 34 03.248	1730	...	...	...	...	...	...	...	...	...	...
	30 55 01.76	786	...	...	...	...	...	...	...	...	...	...
	4.2	2023	<11.8	3.8 (3.2)	<4.6	...	...	...	<8.9	2.3 (1.9)	<3.5	<1.59E+35
013404.3+304036	01 34 04.354	1730	<10.1	2.9 (2.9)	<4.6	...	...	...	<7.6	2.0 (1.2)	<3.5	<1.36E+35
	30 40 36.07	786	<6.0	<6.6	<4.6	...	...	...	<4.5	<5.0	<3.5	<8.10E+34
	1.0	2023	...	...	...	...	...	...	...	...	...	...

TABLE 3—*Continued*

Source			Counts						Flux[a] (10^{-7} counts s^{-1} cm^{-2})			L[a] (ergs s^{-1})
CXO J	R.A., Decl., Uncertainty (arcsec)	ObsID	0.3–8.0	0.3–2.0	2.0–8.0	0.3–1.0	1.0–2.1	2.1–8.0	0.3–8.0	0.3–2.0	2.0–8.0	0.3–8.0
013404.4+304153	01 34 04.414	1730	7.7 (4.0)	5.9 (3.6)	<10.1	...	...	...	5.4 (2.8)	4.1 (1.7)	<7.6	9.68E+34
	30 41 53.55	786	<12.6	<12.2	<6.0	...	...	...	<9.5	<9.2	<4.5	<1.70E+35
	1.0	2023	<12.2	<10.1	<6.0	...	...	...	<9.2	<7.6	<4.5	<1.65E+35
013406.8+303716	01 34 06.891	1730	<12.6	<12.2	<7.5	...	...	...	<9.5	<9.2	<5.6	<1.70E+35
	30 37 16.82	786	22.1 (6.7)	18.0[b] (4.2)	<13.8	20.2 (5.9)		4.3 (4.1)	11 (3.3)	13.5[b]	<10.4	1.99E+35
	1.1	2023	...	...	...	...	...	...	...	...	...	...
013407.4+303707	01 34 07.471	1730	<12.2	4.7 (3.4)	<4.6	...	...	...	<9.2	3.3 (1.6)	<3.5	<1.65E+35
	30 37 07.43	786	8.0[b] (2.8)	9.0[b] (3.0)	<4.6	...	...	...	6.0[b]	<6.8	<3.5	1.07E+35[b]
	1.1	2023	...	...	...	...	...	...	...	...	...	...
013407.6+303902	01 34 07.639	1730	8.7 (4.1)	<8.5	6.7 (3.8)	...	...	...	6.2 (2.9)	<6.4	4.8 (1.9)	1.11E+35
	30 39 02.19	786	18.8 (5.8)	8.8 (4.3)	10.8 (4.7)	...	...	...	8.7 (2.7)	3.7 (1.8)	7.3 (3.2)	1.55E+35
	1.0	2023	<4.6	<4.6	<4.6	...	...	...	<3.5	<3.5	<3.5	<6.30E+34
013407.8+303553	01 34 07.811	1730	43.4 (7.8)	31.2 (6.7)	12.4 (4.7)	9.6 (4.3)	21.7 (5.8)	12.2 (4.7)	31 (5.6)	2.2 (4.1)	8.9 (2.6)	5.57E+35
	30 35 53.76	786	71.1 (10.5)	52.8 (9.1)	20.2 (6.6)	23.7 (6.5)	32.5 (7.1)	16.2 (6.1)	36 (5.2)	24 (4.1)	15 (4.7)	6.39E+35
	1.2	2023	...	...	...	...	...	...	...	...	...	...
013408.2+303851	01 34 08.296	1730	9.7 (4.3)	<6.6	8.7 (4.1)	...	...	...	7.0 (3.1)	<5.0	6.3 (2.2)	1.25E+35
	30 38 51.73	786	15.4 (5.7)	<14.6	11.0[b] (3.3)	...	...	...	7.1 (2.6)	<11.0	8.3[b]	1.27E+35
	1.1	2023	<4.6	<4.6	<4.6	...	...	...	<3.5	<3.5	<3.5	<6.30E+34
013408.4+304632	01 34 08.415	1730	26.1 (6.5)	19.1 (5.6)	<12.6	20.4 (5.7)	2.4 (2.9)	3.0 (3.4)	20 (4.9)	14 (3.4)	<9.5	3.54E+35
	30 46 32.86	786	17.9 (5.9)	16.8 (5.7)	<9.3	...	...	...	17 (5.4)	17 (5.5)	<7.0	2.99E+35
	1.5	2023	15.9 (5.5)	17.4 (5.5)	<5.7	...	...	...	14 (4.5)	15 (4.5)	<4.3	2.57E+35
013408.5+303850	01 34 08.538	1730	8.0[b] (2.8)	<6.0	<6.0	...	...	...	6.0[b]	<4.5	<4.5	1.07E+35[b]
	30 38 50.45	786	19.0[b] (4.4)	<13.4	15.8 (5.6)	...	...	...	14.3[b]	<10.1	11 (3.7)	2.56E+35[b]
	1.1	2023	<4.6	<4.6	<4.6	...	...	...	<3.5	<3.5	<3.5	<6.30E+34
013409.7+303259	01 34 09.745	1730	29.5 (6.8)	16.5 (5.3)	8.0 (4.1)	5.1 (3.6)	14.4 (5.0)	10.3 (4.6)	23 (5.2)	13 (3.2)	6.2 (2.3)	4.08E+35
	30 32 59.20	786	23.8 (6.7)	18.8 (5.9)	<18.0	5.6 (4.0)	12.7 (4.8)	4.6 (4.1)	17 (5.0)	14 (4.3)	<13.5	3.07E+35
	1.8	2023	...	...	...	...	...	...	...	...	...	...
013409.8+305044	01 34 09.882	1730	...	...	...	...	...	...	...	...	...	...
	30 50 44.84	786	5.0[b] (2.2)	<10.1	<8.5	...	...	...	3.8[b]	<7.6	<6.4	6.80E+34[b]
	1.6	2023	72.9 (10.0)	45.5 (7.9)	28.0 (6.6)	2.7 (3.2)	45.9 (7.9)	25.1 (6.5)	33 (4.5)	21 (3.6)	13 (3.1)	5.95E+35
013409.9+303219	01 34 09.925	1730	...	...	...	...	...	...	...	...	...	...
	30 32 19.92	786	208.8 (16.0)	213.7 (16.0)	<9.3	207.2 (15.6)	2.4 (3.4)	<3.8	160 (13)	170 (12)	<7.0	2.93E+36
	1.3	2023	...	...	...	...	...	...	...	...	...	...
013409.9+305039	01 34 09.983	1730	...	...	...	...	...	...	...	...	...	...
	30 50 39.73	786	33.0 (8.5)	23.4 (7.0)	<25.6	6.3 (4.6)	15.5 (5.5)	11.4 (6.0)	27 (7.1)	19 (5.7)	<19.2	4.78E+35
	1.5	2023	<9.1	<8.5	<6.0	...	...	...	<6.8	<6.4	<4.5	<1.22E+35
013410.3+305346	01 34 10.350	1730	...	...	...	...	...	...	...	...	...	...
	30 53 46.13	786	<6.6	<6.6	<4.6	...	...	...	<5.0	<5.0	<3.5	<9.00E+34
	2.4	2023	58.0 (9.3)	38.0 (7.5)	20.1 (6.0)	12.9 (5.0)	25.3 (6.3)	20.1 (6.2)	23 (3.8)	15 (3.0)	8.4 (2.5)	4.20E+35
013410.5+303946	01 34 10.520	1730	100.2 (11.1)	76.4 (9.8)	24.4 (6.1)	25.8 (6.2)	51.9 (8.3)	22.6 (5.9)	72 (7.9)	55 (6.3)	17 (3.6)	1.28E+36
	30 39 46.57	786	248.9 (17.1)	194.1 (15.2)	53.0 (8.6)	96.3 (11.0)	105.3 (11.4)	47.7 (8.3)	120 (8.0)	83 (6.5)	37 (6.0)	2.09E+36
	1.0	2023	276.0 (18.4)	183.0 (14.9)	94.1 (11.5)	49.9 (8.5)	133.8 (12.8)	93.9 (11.4)	120 (7.7)	77 (6.2)	41 (5.0)	2.09E+36
013410.6+304223	01 34 10.672	1730	75.5 (9.8)	73.3 (9.6)	<9.1	57.7 (8.7)	15.7 (5.1)	1.9 (2.9)	56 (7.3)	55 (6.4)	<6.8	1.01E+36
	30 42 23.64	786	...	...	...	...	...	...	...	...	...	...
	1.0	2023	147.5 (14.1)	145.8 (13.5)	<14.6	105.0 (11.5)	40.9 (7.8)	1.8 (5.0)	60 (5.7)	59 (5.4)	<11.0	1.07E+36

TABLE 3—*Continued*

Source			Counts						Flux[a] (10^{-7} counts s^{-1} cm^{-2})			L[a] (ergs s^{-1})
CXO J	R.A., Decl., Uncertainty (arcsec)	ObsID	0.3–8.0	0.3–2.0	2.0–8.0	0.3–1.0	1.0–2.1	2.1–8.0	0.3–8.0	0.3–2.0	2.0–8.0	0.3–8.0
013410.7+305008	01 34 10.766	1730	...	...	...	...	...	...	...	...	...	...
	30 50 08.65	786	<4.6	<4.6	<4.6	...	...	...	<3.5	<3.5	<3.5	<6.30E+34
	1.4	2023	21.5 (6.0)	<12.2	15.8 (5.2)	1.5 (2.7)	2.6 (2.9)	17.7 (5.4)	9.9 (2.7)	<9.2	7.3 (2.4)	1.77E+35
013411.8+304016	01 34 11.809	1730	5.0[b] (2.2)	<6.6	3.8 (3.2)	...	...	...	3.8[b]	<5.0	2.7 (1.4)	6.80E+34[b]
	30 40 16.82	786	<7.5	<4.6	<7.5	...	...	...	<5.6	<3.5	<5.6	<1.00E+35
	1.1	2023	<6.0	<4.6	<6.0	...	...	...	<4.5	<3.5	<4.5	<8.10E+34
013412.1+304737	01 34 12.121	1730	...	...	...	...	...	...	...	...	...	...
	30 47 37.23	786	<6.6	<4.6	<6.6	...	...	...	<5.0	<3.5	<5.0	<9.00E+34
	1.2	2023	5.5 (3.6)	<8.5	<10.0	...	...	...	2.1 (1.4)	<6.4	<7.5	3.72E+34
013412.8+303554	01 34 12.860	1730	<22.8	7.3 (4.0)	<12.2	...	...	...	<17.1	5.5 (2.1)	<9.2	<3.06E+35
	30 35 54.57	786	<20.0	<14.4	<12.1	...	...	...	<15.0	<10.8	<9.1	<2.68E+35
	1.4	2023	...	...	...	...	...	...	...	...	...	...
013414.1+305352	01 34 14.180	1730	...	...	...	...	...	...	...	...	...	...
	30 53 52.49	786	<4.6	<4.6	<4.6	...	...	...	<3.5	<3.5	<3.5	<6.30E+34
	2.1	2023	27.4 (7.6)	24.8 (6.4)	<12.9	16.9 (5.6)	8.5 (4.4)	2.2 (4.4)	11 (3.0)	9.8 (2.5)	<9.7	1.95E+35
013414.5+303250	01 34 14.506	1730	...	...	...	...	...	...	...	...	...	...
	30 32 50.02	786	13.0[b] (3.6)	<9.3	11.8 (5.1)	...	...	...	<9.8	<7.0	9.3 (4.1)	<1.75E+35
	2.1	2023	...	...	...	...	...	...	...	...	...	...
013414.8+303412	01 34 14.806	1730	12.6 (4.8)	6.0[b] (2.5)	6.0[b] (2.5)	...	...	...	9.9 (3.7)	4.5[b]	4.5[b]	1.76E+35
	30 34 12.70	786	9.0[b] (3.0)	7.0[b] (2.7)	<7.5	...	...	...	6.8[b]	5.3[b]	<5.6	1.22E+35[b]
	1.8	2023	...	...	...	...	...	...	...	...	...	...
013415.0+304748	01 34 15.073	1730	...	...	...	...	...	...	...	...	...	...
	30 47 48.67	786	<4.6	<4.6	<4.6	...	...	...	<3.5	<3.5	<3.5	<6.30E+34
	1.1	2023	11.2 (4.7)	<9.1	8.2 (4.1)	...	...	...	6.1 (2.5)	<6.8	4.4 (2.2)	1.10E+35
013416.3+305403	01 34 16.307	1730	...	...	...	...	...	...	...	...	...	...
	30 54 03.43	786	<6.6	<4.6	<6.6	...	...	...	<5.0	<3.5	<5.0	<9.00E+34
	2.0	2023	9.0 (4.3)	<10.1	6.0[b] (2.5)	...	...	...	3.6 (1.7)	<7.6	4.5[b]	6.36E+34
013416.3+305154	01 34 16.374	1730	...	...	...	...	...	...	...	...	...	...
	30 51 54.72	786	<8.5	<6.6	<6.6	...	...	...	<6.4	<5.0	<5.0	<1.15E+35
	1.3	2023	39.6 (8.1)	41.7 (7.9)	<9.8	29.7 (6.7)	10.2 (4.6)	<3.6	15 (3.1)	16 (3.0)	<7.4	2.69E+35
013416.6+304410	01 34 16.682	1730	<4.6	<4.6	<4.6	...	...	...	<3.5	<3.5	<3.5	<6.30E+34
	30 44 10.23	786	<6.6	<6.6	<4.6	...	...	...	<5.0	<5.0	<3.5	<9.00E+34
	1.2	2023	14.8 (5.1)	8.7 (4.1)	6.0[b] (2.5)	...	...	...	5.7 (2.0)	3.3 (1.6)	4.5[b]	1.02E+35
013416.7+305101	01 34 16.735	1730	...	...	...	...	...	...	...	...	...	...
	30 51 01.53	786	<10.2	<10.1	<6.6	...	...	...	<7.7	<7.5	<5.0	<1.38E+35
	1.2	2023	72.2 (9.8)	42.0 (7.6)	28.5 (6.5)	8.1 (4.1)	36.3 (7.1)	27.5 (6.5)	27 (3.7)	16 (2.9)	11 (2.5)	4.88E+35
013417.0+303425	01 34 17.074	1730	24.1 (6.3)	7.6 (4.0)	11.6 (4.7)	<1.9	12.5 (4.7)	12.6 (4.8)	18 (4.7)	5.8 (2.1)	9.0 (2.8)	3.28E+35
	30 34 25.59	786	39.5 (7.8)	33.6 (7.9)	25.9 (7.3)	5.2 (3.8)	17.0 (5.3)	16.6 (5.6)	29 (5.8)	24 (5.8)	19 (5.7)	5.16E+35
	1.9	2023	...	...	...	...	...	...	...	...	...	...
013417.1+304842	01 34 17.142	1730	...	...	...	...	...	...	...	...	...	...
	30 48 42.02	786	<6.6	<6.6	<4.6	...	...	...	<5.0	<5.0	<3.5	<9.00E+34
	1.1	2023	19.8 (5.7)	6.0[b] (2.5)	14.4 (5.0)	...	...	...	7.3 (2.1)	4.5[b]	5.4 (1.9)	1.31E+35
013417.4+304124	01 34 17.444	1730	<7.5	<8.5	<4.6	...	...	...	<5.6	<6.4	<3.5	<1.00E+35
	30 41 24.04	786	...	...	...	...	...	...	...	...	...	...
	1.4	2023	12.0[b] (3.5)	13.8 (5.1)	<6.5	...	...	...	9.0[b]	5.5 (2.0)	<4.9	1.61E+35[b]

TABLE 3—*Continued*

Source			Counts						Flux[a] (10^{-7} counts s^{-1} cm^{-2})			L[a] (ergs s^{-1})
CXO J	R.A., Decl., Uncertainty (arcsec)	ObsID	0.3–8.0	0.3–2.0	2.0–8.0	0.3–1.0	1.0–2.1	2.1–8.0	0.3–8.0	0.3–2.0	2.0–8.0	0.3–8.0
013419.1+304326	01 34 19.182	1730	<6.5	<6.0	<5.7	...	...	...	<4.9	<4.5	<4.3	8.80E+34
	30 43 26.17	786	<20.9	<7.5	8.8 (4.4)	...	...	...	<15.7	<5.6	6.4 (3.4)	<2.81E+35
	1.3	2023	<4.6	<4.6	<4.6	...	...	...	<3.5	<3.5	<3.5	<6.30E+34
013419.2+304942	01 34 19.294	1730	...	...	...	...	...	...	...	...	...	...
	30 49 42.07	786	<6.6	<6.6	<4.6	...	...	...	<5.0	<5.0	<3.5	<9.00E+34
	1.0	2023	47.3 (8.1)	22.4 (5.9)	24.7 (6.2)	2.6 (2.9)	21.7 (5.8)	22.8 (6.0)	17 (3.0)	8.3 (2.2)	9.2 (2.3)	3.12E+35
013419.3+304239	01 34 19.300	1730	<4.6	<4.6	<4.6	...	...	...	<3.5	<3.5	<3.5	<6.30E+34
	30 42 39.02	786	<4.6	<4.6	<4.6	...	...	...	<3.5	<3.5	<3.5	<6.30E+34
	1.4	2023	9.0[b] (3.0)	8.8 (4.3)	<6.6	...	...	...	6.8[b]	3.4 (1.7)	<5.0	1.22E+35[b]
013419.7+303719	01 34 19.783	1730	8.2 (4.4)	7.4 (4.0)	<8.3	...	...	...	6.3 (3.4)	5.6 (2.1)	<6.2	1.14E+35
	30 37 19.60	786	<12.2	<10.5	<8.3	...	...	...	<9.2	<7.9	<6.2	<1.65E+35
	1.6	2023	...	...	...	...	...	...	...	...	...	...
013419.8+304234	01 34 19.846	1730	<4.6	<4.6	<4.6	...	...	...	<3.5	<3.5	<3.5	<6.30E+34
	30 42 34.96	786	<4.6	<4.6	<4.6	...	...	...	<3.5	<3.5	<3.5	<6.30E+34
	1.4	2023	8.9 (5.0)	7.0[b] (2.7)	<10.8	...	...	...	3.4 (1.9)	5.3[b]	<8.1	6.12E+34
013420.9+305001	01 34 20.946	1730	...	...	...	...	...	...	...	...	...	...
	30 50 01.65	786	<8.5	<4.6	<8.5	...	...	...	<6.4	<3.5	<6.4	<1.15E+35
	1.0	2023	15.0 (5.2)	9.4 (4.3)	7.1 (4.0)	...	...	...	5.5 (1.9)	3.4 (1.6)	2.6 (1.5)	9.82E+34
013421.1+303928	01 34 21.174	1730	<6.0	<6.6	<4.6	...	...	...	<4.5	<5.0	<3.5	<8.10E+34
	30 39 28.57	786	...	...	...	...	...	...	...	...	...	...
	1.6	2023	17.2 (6.0)	11.7 (5.6)	<17.8	...	...	...	7.2 (2.5)	4.9 (2.3)	<13.4	1.29E+35
013421.2+304932	01 34 21.261	1730	...	...	...	...	...	...	...	...	...	...
	30 49 32.61	786	27.9 (7.6)	11.0[b] (3.3)	18.1 (5.8)	2.3 (3.6)	9.7 (4.6)	15.8 (6.0)	23 (6.4)	8.3[b]	16 (5.1)	4.20E+35
	1.0	2023	119.0 (12.0)	40.6 (7.5)	78.1 (9.9)	2.5 (2.9)	41.6 (7.5)	74.6 (9.8)	44 (4.4)	15 (2.7)	29 (3.7)	7.80E+35
013421.4+304448	01 34 21.427	1730	<6.6	<6.6	<4.6	...	...	...	<5.0	<5.0	<3.5	<9.00E+34
	30 44 48.30	786	6.0[b] (2.5)	<8.5	<10.2	...	...	...	4.5[b]	<6.4	<7.7	8.06E+34[b]
	1.1	2023	6.4 (4.0)	<12.2	<9.1	...	...	...	2.6 (1.6)	<9.2	<6.8	4.62E+34
013421.9+304242	01 34 21.913	1730	<4.6	<4.6	<4.6	...	...	...	<3.5	<3.5	<3.5	<6.30E+34
	30 42 42.36	786	<8.5	<6.6	<6.6	...	...	...	<6.4	<5.0	<5.0	<1.15E+35
	1.3	2023	<10.1	2.9 (2.9)	<4.6	...	...	...	<7.6	1.2 (1.2)	<3.5	<1.36E+35
013423.5+305426	01 34 23.516	1730	...	...	...	...	...	...	...	...	...	...
	30 54 26.23	786	<4.6	<4.6	<4.6	...	...	...	<3.5	<3.5	<3.5	<6.30E+34
	1.7	2023	10.2 (4.7)	19.1 (5.8)	<11.1	...	...	...	4.5 (2.0)	8.7 (2.6)	<8.3	8.03E+34
013423.6+303833	01 34 23.678	1730	9.0[b] (3.0)	8.2 (4.1)	<7.5	...	...	...	6.8[b]	6.3 (2.3)	<5.6	1.22E+35[b]
	30 38 33.10	786	...	...	...	...	...	...	...	...	...	...
	1.9	2023	...	...	...	...	...	...	...	...	...	...
013423.8+303847	01 34 23.851	1730	28.8 (6.8)	19.7 (5.8)	12.8 (5.2)	4.1 (3.4)	16.4 (5.2)	9.2 (4.4)	23 (5.3)	15 (3.6)	10 (3.2)	4.05E+35
	30 38 47.12	786	...	...	...	...	...	...	...	...	...	...
	1.9	2023	21.0 (6.9)	16.3 (6.1)	7.3 (5.0)	2.7 (3.2)	16.9 (5.3)	8.6 (4.6)	25 (6.1)	16 (4.6)	14 (5.6)	4.46E+35
013424.2+304406	01 34 24.225	1730	<4.6	<4.6	<4.6	...	...	...	<3.5	<3.5	<3.5	<6.30E+34
	30 44 06.01	786	<6.6	<4.6	<6.6	...	...	...	<5.0	<3.5	<5.0	<9.00E+34
	1.1	2023	<10.1	2.9 (2.9)	<4.6	...	...	...	<7.6	1.1 (1.1)	<3.5	<1.36E+35
013424.4+305104	01 34 24.455	1730	...	...	...	...	...	...	...	...	...	...
	30 51 04.95	786	<4.6	<4.6	<4.6	...	...	...	<3.5	<3.5	<3.5	<6.30E+34
	1.0	2023	6.4 (3.8)	<10.2	<10.1	...	...	...	2.4 (1.4)	<7.7	<7.6	4.21E+34

TABLE 3—*Continued*

Source			Counts						Flux[a] (10^{-7} counts s^{-1} cm^{-2})			L[a] (ergs s^{-1})
CXO J	R.A., Decl., Uncertainty (arcsec)	ObsID	0.3–8.0	0.3–2.0	2.0–8.0	0.3–1.0	1.0–2.1	2.1–8.0	0.3–8.0	0.3–2.0	2.0–8.0	0.3–8.0
013424.5+304306	01 34 24.524	1730	9.6 (4.4)	<16.5	<12.2	...	...	...	7.3 (3.4)	<12.4	<9.2	1.30E+35
	30 43 06.39	786	25.8 (7.0)	22.2 (6.3)	<18.2	4.9 (3.8)	15.0 (5.2)	4.3 (4.4)	19 (5.3)	16 (4.7)	<13.7	3.33E+35
	1.2	2023	52.8 (8.5)	27.1 (6.4)	26.3 (6.4)	5.2 (3.6)	22.4 (5.9)	25.0 (6.3)	20 (3.3)	10 (2.4)	10 (2.5)	3.61E+35
013424.6+304428	01 34 24.628	1730	<6.8	<7.5	<5.2	...	...	...	<5.1	<5.6	<3.9	9.10E+34
	30 44 28.85	786	35.4 (7.8)	18.5 (5.8)	19.5 (6.1)	6.8 (4.1)	10.9 (4.7)	16.1 (5.9)	26 (6.0)	14 (4.4)	15 (4.8)	4.70E+35
	1.0	2023	<9.1	<10.1	<4.6	...	...	...	<6.8	<7.6	<3.5	<1.22E+35
013424.7+303913	01 34 24.785	1730	<7.5	<7.4	<6.6	...	...	...	<5.6	<5.6	<5.0	<1.00E+35
	30 39 13.01	786	...	...	...	...	...	...	...	...	...	...
	2.0	2023	16.0 (6.7)	<15.5	11.0[b] (3.3)	...	...	...	6.8 (2.7)	<11.6	<8.3	1.21E+35
013425.3+304157	01 34 25.368	1730	<20.3	<10.8	<16.5	...	...	...	<15.2	<8.1	<12.4	<2.72E+35
	30 41 57.82	786	44.9 (8.3)	33.0 (7.1)	15.8 (5.6)	11.4 (4.7)	19.4 (5.7)	12.7 (5.3)	33 (6.2)	24 (5.3)	12 (4.3)	5.91E+35
	1.4	2023	26.7 (7.0)	18.3 (5.6)	<16.5	3.2 (3.4)	18.5 (5.6)	5.1 (4.3)	11 (2.9)	7.6 (2.3)	<12.4	1.97E+35
013425.4+302821	01 34 25.481	1730	...	...	...	...	...	...	...	...	...	...
	30 28 21.70	786	112.7 (14.5)	83.6 (11.2)	29.0[b] (5.4)	32.0 (8.3)	52.7 (9.0)	31.7 (9.3)	100 (13)	72 (9.6)	<21.8	1.81E+36
	2.4	2023	...	...	...	...	...	...	...	...	...	...
013425.5+305514	01 34 25.501	1730	...	...	...	...	...	...	...	...	...	...
	30 55 14.88	786	1774.2 (44.4)	1332.9 (38.2)	432.9 (23.2)	366.0 (20.8)	1003.4 (32.9)	431.6 (22.9)	2000 (49)	1500 (41)	530 (28)	3.55E+37
	0.7	2023	4404.5 (67.5)	3283.3 (58.4)	1380.7 (38.4)	788.0 (29.1)	2391.4 (49.9)	1226.3 (36.1)	2000 (30)	1600 (28)	680 (19)	3.53E+37
013425.8+304636	01 34 25.875	1730	<4.6	<4.6	<4.6	...	...	...	<3.5	<3.5	<3.5	<6.30E+34
	30 46 36.73	786	<6.6	<4.6	<6.6	...	...	...	<5.0	<3.5	<5.0	<9.00E+34
	1.0	2023	<11.8	<4.6	3.7 (3.2)	...	...	...	<8.9	<3.5	1.4 (1.2)	<1.59E+35
013426.5+304446	01 34 26.575	1730	36.2 (7.7)	22.8 (6.2)	14.0[b] (3.7)	8.6 (4.3)	13.6 (5.0)	14.3 (5.4)	31 (6.5)	19 (4.2)	10.5[b]	5.50E+35
	30 44 46.97	786	42.5 (8.8)	28.4 (7.1)	16.0[b] (4.0)	4.2 (4.0)	23.3 (6.3)	13.0 (6.1)	33 (7.0)	22 (5.6)	12.0[b]	5.82E+35
	1.0	2023	91.2 (10.7)	67.0 (9.3)	23.9 (6.1)	18.3 (5.4)	49.4 (8.1)	23.2 (6.1)	34 (4.0)	25 (3.5)	9.0 (2.3)	6.07E+35
013426.6+303737	01 34 26.608	1730	19.9 (5.9)	16.8 (5.3)	<11.1	...	...	...	15 (4.5)	13 (3.2)	<8.3	2.75E+35
	30 37 37.70	786	...	...	...	...	...	...	...	...	...	...
	2.3	2023	...	...	...	...	...	...	...	...	...	...
013426.7+304811	01 34 26.799	1730	...	...	...	...	...	...	...	...	...	...
	30 48 11.93	786	<4.6	<4.6	<4.6	...	...	...	<3.5	<3.5	<3.5	<6.30E+34
	1.0	2023	38.2 (7.4)	18.6 (5.4)	13.6 (4.8)	2.6 (2.9)	20.7 (5.7)	14.8 (5.1)	14 (2.8)	7.0 (2.1)	5.2 (1.8)	2.57E+35
013427.0+304314	01 34 27.062	1730	27.7 (6.7)	20.5 (5.9)	9.0[b] (3.0)	2.4 (2.9)	16.4 (5.2)	9.9 (4.6)	25 (5.9)	18 (4.1)	6.8[b]	4.43E+35
	30 43 14.47	786	62.0 (9.7)	35.1 (7.5)	25.1 (6.7)	8.3 (4.4)	28.4 (6.6)	23.3 (6.7)	46 (7.4)	26 (5.7)	19 (5.3)	8.28E+35
	1.0	2023	107.9 (11.6)	77.8 (9.9)	30.5 (6.7)	19.3 (5.6)	59.4 (8.8)	29.0 (6.6)	41 (4.4)	30 (3.8)	12 (2.6)	7.33E+35
013427.2+304421	01 34 27.277	1730	<10.1	<10.1	<4.6	...	...	...	<7.6	<7.6	<3.5	<1.36E+35
	30 44 21.86	786	<6.6	<6.6	<4.6	...	...	...	<5.0	<5.0	<3.5	<9.00E+34
	1.0	2023	10.1 (4.4)	7.6 (4.0)	<9.1	...	...	...	3.7 (1.7)	2.8 (1.5)	<6.8	6.70E+34
013428.1+303246	01 34 28.179	1730	...	...	...	...	...	...	...	...	...	...
	30 32 46.51	786	59.2 (10.4)	42.0[b] (6.5)	18.0[b] (4.2)	13.7 (5.8)	28.5 (6.8)	17.3 (6.8)	50 (8.7)	31.5[b]	13.5[b]	8.90E+35
	3.6	2023	...	...	...	...	...	...	...	...	...	...
013429.0+304249	01 34 29.016	1730	<7.5	<8.5	<4.6	...	...	...	<5.6	<6.4	<3.5	<1.00E+35
	30 42 49.07	786	<10.1	<8.5	<6.6	...	...	...	<7.6	<6.4	<5.0	<1.36E+35
	1.2	2023	11.3 (4.6)	7.7 (4.0)	<10.2	...	...	...	4.3 (1.7)	2.9 (1.5)	<7.7	7.67E+34
013429.1+304212	01 34 29.135	1730	16.2 (5.9)	9.0[b] (3.0)	<17.8	...	...	...	13 (4.5)	6.8[b]	<13.4	2.28E+35
	30 42 12.44	786	<19.6	7.0[b] (2.7)	<9.3	...	...	...	<14.7	5.3[b]	<7.0	<2.63E+35
	1.2	2023	19.6 (5.8)	18.7 (5.6)	<12.2	...	...	...	7.5 (2.2)	7.2 (2.1)	<9.2	1.35E+35

TABLE 3—*Continued*

Source			Counts						Flux[a] (10^{-7} counts s^{-1} cm^{-2})			L[a] (ergs s^{-1})
CXO J	R.A., Decl., Uncertainty (arcsec)	ObsID	0.3–8.0	0.3–2.0	2.0–8.0	0.3–1.0	1.0–2.1	2.1–8.0	0.3–8.0	0.3–2.0	2.0–8.0	0.3–8.0
013429.7+305026	01 34 29.742	1730	...	...	...	...	...	...	...	...	...	...
	30 50 26.16	786	<10.2	<6.6	<10.1	...	...	...	<7.7	<5.0	<7.6	<1.38E+35
	1.0	2023	93.7 (10.8)	57.5 (8.7)	34.9 (7.1)	19.7 (5.6)	40.7 (7.5)	33.1 (6.9)	34 (3.9)	21 (3.1)	13 (2.5)	6.03E+35
013429.9+304236	01 34 29.917	1730	<4.6	<4.6	<4.6	...	...	...	<3.5	<3.5	<3.5	<6.30E+34
	30 42 36.39	786	<4.6	<4.6	<4.6	...	...	...	<3.5	<3.5	<3.5	<6.30E+34
	1.2	2023	6.0[b] (2.5)	4.5 (3.4)	<7.5	...	...	...	4.5[b]	1.7 (1.3)	<5.6	8.06E+34[b]
013429.9+305106	01 34 29.956	1730	...	...	...	...	...	...	...	...	...	...
	30 51 06.87	786	<8.5	<8.5	<4.6	...	...	...	<6.4	<6.4	<3.5	<1.15E+35
	1.0	2023	22.4 (5.9)	5.7 (3.6)	16.1 (5.2)	<1.9	10.9 (4.4)	11.6 (4.6)	8.1 (2.1)	2.1 (1.3)	5.8 (1.9)	1.46E+35
013430.4+305041	01 34 30.491	1730	...	...	...	...	...	...	...	...	...	...
	30 50 41.78	786	<4.6	<4.6	<4.6	...	...	...	<3.5	<3.5	<3.5	<6.30E+34
	1.0	2023	12.0 (4.7)	2.7 (2.9)	<13.8	...	...	...	4.3 (1.7)	0.98 (1.1)	<10.4	7.68E+34
013430.9+304510	01 34 30.904	1730	...	...	...	...	...	...	...	...	...	...
	30 45 10.0	786	<4.6	<4.6	<4.6	...	...	...	<3.5	<3.5	<3.5	<6.30E+34
	1.0	2023	19.2 (5.7)	11.5 (4.6)	9.3 (4.3)	...	...	...	7.4 (2.2)	4.4 (1.8)	3.6 (1.7)	1.32E+35
013432.0+303455	01 34 32.020	1730	102.7 (11.9)	28.4 (6.7)	67.9 (9.6)	2.4 (3.6)	29.6 (6.7)	73.2 (10.0)	85 (9.7)	24 (4.6)	57 (7.1)	1.52E+36
	30 34 55.00	786	...	...	...	...	...	...	...	...	...	...
	1.8	2023	...	...	...	...	...	...	...	...	...	...
013432.1+305158	01 34 32.148	1730	...	...	...	...	...	...	...	...	...	...
	30 51 58.81	786	<6.6	<6.6	<4.6	...	...	...	<5.0	<5.0	<3.5	<9.00E+34
	1.0	2023	68.5 (9.5)	53.2 (8.4)	13.4 (4.8)	18.8 (5.4)	38.9 (7.3)	12.5 (4.7)	93 (13)	68 (11)	20 (7.0)	1.66E+36
013432.2+304958	01 34 32.238	1730	...	...	...	...	...	...	...	...	...	...
	30 49 58.73	786	<6.6	<4.6	<6.6	...	...	...	<5.0	<3.5	<5.0	<9.00E+34
	1.0	2023	6.5 (3.8)	3.7 (3.2)	<8.5	...	...	...	2.3 (1.3)	1.3 (1.1)	<6.4	4.11E+34
013432.2+303159	01 34 32.277	1730	...	...	...	...	...	...	...	...	...	...
	30 31 59.23	786	27.0[b] (5.2)	18.0 (6.3)	<22.1	...	...	...	<20.3	15 (5.1)	<16.6	3.64E+35
	4.6	2023	...	...	...	...	...	...	...	...	...	...
013432.5+303928	01 34 32.523	1730	<18.2	<6.5	8.0[b] (2.8)	...	...	...	<13.7	<4.9	6.0[b]	<2.45E+35
	30 39 28.22	786	13.0[b] (3.6)	<8.3	12.0 (5.0)	...	...	...	9.8[b]	<6.2	9.2 (3.9)	1.75E+35[b]
	2.0	2023	<7.5	<4.6	<7.5	...	...	...	<5.6	<3.5	<5.6	<1.00E+35
013432.5+305035	01 34 32.595	1730	...	...	...	...	...	...	...	...	...	...
	30 50 35.41	786	<6.6	<4.6	<6.6	...	...	...	<5.0	<3.5	<5.0	<9.00E+34
	1.0	2023	35.8 (7.1)	13.7 (4.8)	21.4 (5.8)	0.7 (2.3)	13.8 (4.8)	21.2 (5.8)	15 (3.0)	6.4 (2.3)	8.8 (2.4)	2.67E+35
013432.7+303436	01 34 32.704	1730	54.6 (9.6)	33.7 (7.3)	18.0[b] (4.2)	10.2 (4.9)	29.4 (6.7)	18.8 (6.2)	51 (8.3)	29 (5.2)	13.5[b]	9.05E+35
	30 34 36.04	786	<4.8	<5.1	<4.6	...	...	...	<3.6	<3.8	<3.5	6.45E+34
	3.7	2023	...	...	...	...	...	...	...	...	...	...
013433.0+304638	01 34 33.021	1730	...	...	...	...	...	...	...	...	...	...
	30 46 38.00	786	<10.2	<10.2	<4.6	...	...	...	<7.7	<7.7	<3.5	<1.38E+35
	1.0	2023	33.6 (7.0)	36.0 (7.1)	<7.5	20.6 (5.7)	11.7 (4.6)	1.1 (2.7)	12 (2.5)	13 (2.6)	<5.6	2.16E+35
013433.6+305500	01 34 33.614	1730	...	...	...	...	...	...	...	...	...	...
	30 55 00.39	786	...	...	...	...	...	...	...	...	...	...
	1.7	2023	25.5 (6.6)	<12.6	22.0 (6.1)	<2.3	4.9 (3.6)	20.2 (6.0)	10 (2.7)	<9.5	8.7 (2.4)	1.79E+35
013433.7+304701	01 34 33.763	1730	...	...	...	...	...	...	...	...	...	...
	30 47 01.92	786	421.1 (27.4)	353.7 (22.4)	67.4 (16.6)	221.0 (16.9)	103.2 (12.5)	56.9 (13.1)	430 (27)	340 (22)	87 (18)	7.66E+36
	1.0	2023	819.6 (36.4)	781.9 (31.9)	37.6 (18.4)	467.7 (24.6)	265.9 (19.4)	101.0 (19.1)	280 (14)	280 (12)	3.0 (7.7)	5.00E+36

TABLE 3—*Continued*

Source			Counts						Flux[a] (10^{-7} counts s^{-1} cm^{-2})			L[a] (ergs s^{-1})
CXO J	R.A., Decl., Uncertainty (arcsec)	ObsID	0.3–8.0	0.3–2.0	2.0–8.0	0.3–1.0	1.0–2.1	2.1–8.0	0.3–8.0	0.3–2.0	2.0–8.0	0.3–8.0
013433.9+305021	01 34 33.929	1730	...	...	...	...	...	...	...	...	...	...
	30 50 21.42	786	3.1 (3.4)	<7.5	<9.1	...	...	...	2.6 (2.9)	<5.6	<6.8	4.56E+34
	1.0	2023	<4.6	<4.6	<4.6	...	...	...	<3.5	<3.5	<3.5	<6.30E+34
013434.1+305136	01 34 34.195	1730	...	...	...	...	...	...	...	...	...	...
	30 51 36.00	786	4.6 (4.3)	<8.3	<14.6	...	...	...	4.0 (3.7)	<6.2	<11.0	7.10E+34
	1.0	2023	11.0 (4.6)	5.0[b] (2.2)	4.5 (3.4)	...	...	...	4.0 (1.7)	3.8[b]	1.6 (1.3)	7.23E+34
013434.2+305254	01 34 34.217	1730	...	...	...	...	...	...	...	...	...	...
	30 52 54.82	786	3.4 (3.4)	<9.1	<7.5	...	...	...	5.6 (4.7)	<6.8	<5.6	1.01E+35
	1.1	2023	<4.6	<4.6	<4.6	...	...	...	<3.5	<3.5	<3.5	<6.30E+34
013435.0+304439	01 34 35.032	1730	...	...	...	...	...	...	...	...	...	...
	30 44 39.16	786	<10.2	<6.6	<10.1	...	...	...	<7.7	<5.0	<7.6	<1.38E+35
	1.0	2023	47.3 (8.1)	11.6 (4.6)	37.0 (7.2)	<1.9	10.7 (4.4)	36.9 (7.2)	17 (3.0)	4.3 (1.7)	14 (2.7)	3.11E+35
013435.0+304711	01 34 35.090	1730	...	...	...	...	...	...	...	...	...	...
	30 47 11.52	786	<8.5	<8.5	<4.6	...	...	...	<6.4	<6.4	<3.5	<1.15E+35
	1.0	2023	12.0[b] (3.5)	<10.1	9.6 (4.3)	...	...	...	9.0[b]	<7.6	3.5 (1.6)	1.61E+35[b]
013435.1+305034	01 34 35.107	1730	...	...	...	...	...	...	...	...	...	...
	30 50 34.33	786	7.3 (5.0)	<10.2	<18.0	...	...	...	6.7 (4.4)	<7.7	<13.5	1.20E+35
	1.0	2023	<6.0	<4.6	<6.0	...	...	...	<4.5	<3.5	<4.5	<8.10E+34
013435.1+305646	01 34 35.152	1730	...	...	...	...	...	...	...	...	...	...
	30 56 46.29	786	...	...	...	...	...	...	...	...	...	...
	1.5	2023	159.1 (14.9)	72.1 (10.0)	76.7 (10.3)	0.5 (3.8)	76.7 (10.2)	81.5 (11.2)	68 (6.4)	31 (4.3)	33 (4.5)	1.21E+36
013435.3+305208	01 34 35.372	1730	...	...	...	...	...	...	...	...	...	...
	30 52 08.81	786	<6.6	<6.6	<4.6	...	...	...	<5.0	<5.0	<3.5	<9.00E+34
	1.0	2023	<12.2	3.8 (3.2)	<6.6	...	...	...	<9.2	1.4 (1.2)	<5.0	<1.65E+35
013435.3+304946	01 34 35.389	1730	...	...	...	...	...	...	...	...	...	...
	30 49 46.10	786	<10.1	<8.5	<6.6	...	...	...	<7.6	<6.4	<5.0	<1.36E+35
	1.0	2023	5.6 (3.6)	3.5 (3.2)	<8.5	...	...	...	6.1 (3.8)	4.1 (3.4)	<6.4	1.09E+35
013436.0+303450	01 34 36.096	1730	63.7 (10.7)	37.3 (7.7)	21.6 (7.1)	3.1 (4.2)	42.9 (7.9)	23.8 (7.0)	61 (9.3)	32 (5.5)	21 (5.2)	1.08E+36
	30 34 50.24	786	...	...	...	...	...	...	...	...	...	...
	4.3	2023	...	...	...	...	...	...	...	...	...	...
013436.4+304713	01 34 36.487	1730	...	...	...	...	...	...	...	...	...	...
	30 47 13.99	786	67.0[b] (8.2)	20.0[b] (4.5)	47.0 (9.0)	...	...	...	50.3[b]	15.0[b]	43 (8.2)	9.01E+35[b]
	1.0	2023	65.3 (9.2)	<10.1	65.1 (9.2)	0.8 (2.3)	1.9 (2.7)	62.6 (9.0)	23 (3.3)	<7.6	24 (3.3)	4.20E+35
013436.6+304314	01 34 36.647	1730	...	...	...	...	...	...	...	...	...	...
	30 43 14.67	786	<8.5	<8.5	<4.6	...	...	...	<6.4	<6.4	<3.5	<1.15E+35
	1.1	2023	8.6 (4.3)	<7.5	7.0[b] (2.7)	...	...	...	3.2 (1.6)	<5.6	5.3[b]	5.72E+34
013437.4+305033	01 34 37.437	1730	...	...	...	...	...	...	...	...	...	...
	30 50 33.77	786	7.4 (4.6)	<9.7	<14.4	...	...	...	6.5 (4.0)	<7.3	<10.8	1.16E+35
	1.0	2023	<4.6	<4.6	<4.6	...	...	...	<3.5	<3.5	<3.5	<6.30E+34
013438.8+304538	01 34 38.831	1730	...	...	...	...	...	...	...	...	...	...
	30 45 38.78	786	108.9 (12.6)	96.6 (11.7)	29.0[b] (5.4)	30.9 (7.1)	50.1 (8.5)	26.6 (7.6)	89 (10)	78 (9.5)	21.8[b]	1.59E+36
	1.0	2023	213.3 (15.7)	156.0 (13.6)	58.5 (8.7)	48.6 (8.1)	108.7 (11.5)	55.9 (8.6)	77 (5.7)	56 (4.9)	21 (3.2)	1.38E+36
013438.8+305504	01 34 38.833	1730	...	...	...	...	...	...	...	...	...	...
	30 55 04.23	786	...	...	...	...	...	...	...	...	...	...
	0.7	2023	2429.1 (50.5)	1741.3 (42.8)	692.4 (27.5)	508.6 (23.6)	1270.8 (36.7)	648.6 (26.7)	1000 (21)	710 (18)	290 (11)	1.78E+37

TABLE 3—*Continued*

Source			Counts						Flux[a] (10^{-7} counts s^{-1} cm^{-2})			L[a] (ergs s^{-1})
CXO J	R.A., Decl., Uncertainty (arcsec)	ObsID	0.3–8.0	0.3–2.0	2.0–8.0	0.3–1.0	1.0–2.1	2.1–8.0	0.3–8.0	0.3–2.0	2.0–8.0	0.3–8.0
013438.9+305014	01 34 38.996	1730	...	...	...	...	...	...	...	...	...	...
	30 50 14.38	786	6.6 (4.7)	<7.5	<18.0	...	...	...	5.6 (4.0)	<5.6	<13.5	1.00E+35
	1.0	2023	<6.0	<4.6	<6.0	...	...	...	<4.5	<3.5	<4.5	<8.10E+34
013439.0+304115	01 34 39.028	1730	...	...	...	...	...	...	...	...	...	...
	30 41 15.12	786	<8.5	<8.5	<4.6	...	...	...	<6.4	<6.4	<3.5	<1.15E+35
	1.4	2023	24.3 (7.1)	<18.0	17.0[b] (4.1)	<2.7	9.8 (4.6)	15.0 (5.8)	9.4 (2.8)	<13.5	12.8[b]	1.69E+35
013439.8+305143	01 34 39.875	1730	...	...	...	...	...	...	...	...	...	...
	30 51 43.40	786	...	...	...	...	...	...	...	...	...	...
	1.0	2023	126.4 (12.4)	85.0 (10.3)	45.3 (7.9)	21.4 (5.8)	62.5 (9.0)	42.0 (7.7)	47 (4.6)	32 (3.9)	17 (2.9)	8.39E+35
013440.8+304409	01 34 40.846	1730	...	...	...	...	...	...	...	...	...	...
	30 44 09.58	786	<10.1	<8.5	<6.6	...	...	...	<7.6	<6.4	<5.0	<1.36E+35
	1.0	2023	27.8 ± 6.5	18.5 (5.4)	9.0[b] (3.0)	6.7 (3.8)	11.8 (4.6)	9.3 (4.3)	10 (2.4)	6.8 (2.0)	6.8[b]	1.84E+35
013441.0+304325	01 34 41.070	1730	...	...	...	...	...	...	...	...	...	...
	30 43 25.84	786	<8.5	<8.5	<4.6	...	...	...	<6.4	<6.4	<3.5	<1.15E+35
	1.1	2023	40.7 (7.9)	51.5 (8.7)	<12.1	30.5 (6.7)	6.8 (4.0)	3.0 (3.8)	15 (3.0)	19 (3.2)	<9.1	2.70E+35
013441.2+304330	01 34 41.207	1730	...	...	...	...	...	...	...	...	...	...
	30 43 30.37	786	20.4 (6.6)	24.7 (6.9)	<10.2	15.2 (5.2)	2.3 (3.2)	3.4 (4.1)	18 (5.7)	21 (5.9)	<7.7	3.18E+35
	1.1	2023	7.0[b] (2.7)	<15.5	<7.5	...	...	...	5.3[b]	<11.6	<5.6	9.51E+34[b]
013441.6+305033	01 34 41.653	1730	...	...	...	...	...	...	...	...	...	...
	30 50 33.89	786	10.1 (5.4)	<16.0	<13.8	...	...	...	13 (5.9)	<12.0	<10.4	2.33E+35
	1.0	2023	<7.5	<8.5	<4.6	...	...	...	<5.6	<6.4	<3.5	<1.00E+35
013442.0+305229	01 34 42.066	1730	...	...	...	...	...	...	...	...	...	...
	30 52 29.09	786	...	...	...	...	...	...	...	...	...	...
	1.1	2023	60.5 (9.0)	44.7 (7.8)	17.0 (5.3)	6.5 (3.8)	36.5 (7.1)	17.2 (5.4)	24 (3.6)	18 (3.1)	6.7 (2.1)	4.30E+35
013442.5+305249	01 34 42.515	1730	...	...	...	...	...	...	...	...	...	...
	30 52 49.33	786	...	...	...	...	...	...	...	...	...	...
	1.2	2023	68.2 (9.5)	33.0[b] (5.7)	35.3 (7.1)	5.2 (3.6)	27.2 (6.4)	35.2 (7.2)	26 (3.6)	24.8[b]	13 (2.7)	4.61E+35
013442.6+304927	01 34 42.669	1730	...	...	...	...	...	...	...	...	...	...
	30 49 27.39	786	<6.6	<4.6	<6.6	...	...	...	<5.0	<3.5	<5.0	<9.00E+34
	1.0	2023	7.2 (4.0)	<10.1	4.6 (3.4)	...	...	...	2.6 (1.4)	<7.6	1.6 (1.2)	4.57E+34
013442.7+305050	01 34 42.793	1730	...	...	...	...	...	...	...	...	...	...
	30 50 50.44	786	...	...	...	...	...	...	...	...	...	...
	1.0	2023	9.0[b] (3.0)	<6.6	8.2 (4.1)	...	...	...	<6.8	<5.0	2.9 (1.5)	<1.22E+35
013442.8+304505	01 34 42.840	1730	...	...	...	...	...	...	...	...	...	...
	30 45 05.86	786	50.4 (9.5)	31.7 (7.3)	18.0[b] (4.2)	10.7 (5.0)	20.9 (6.1)	18.0 (6.7)	41 (7.9)	26 (6.0)	13.5[b]	7.39E+35
	1.0	2023	77.9 (9.9)	56.6 (8.6)	21.1 (5.8)	18.8 (5.4)	37.8 (7.2)	21.2 (5.8)	28 (3.6)	21 (3.1)	7.6 (2.1)	5.06E+35
013443.1+304948	01 34 43.136	1730	...	...	...	...	...	...	...	...	...	...
	30 49 48.61	786	<4.6	<4.6	<4.6	...	...	...	<3.5	<3.5	<3.5	<6.30E+34
	1.0	2023	25.4 (6.3)	6.7 (3.8)	8.7 (4.1)	1.6 (2.7)	15.6 (5.1)	7.7 (4.1)	9.1 (2.3)	2.4 (1.4)	3.1 (1.5)	1.62E+35
013444.3+304702	01 34 44.363	1730	...	...	...	...	...	...	...	...	...	...
	30 47 02.90	786	<4.6	<4.6	<4.6	...	...	...	<3.5	<3.5	<3.5	<6.30E+34
	1.0	2023	26.9 (6.4)	16.8 (5.2)	10.7 (4.4)	1.8 (2.7)	15.8 (5.)1	9.2 (4.3)	9.6 (2.3)	6.0 (1.9)	3.8 (1.6)	1.71E+35
013444.5+304922	01 34 44.561	1730	...	...	...	...	...	...	...	...	...	...
	30 49 22.42	786	81.7 (12.1)	51.3 (9.1)	29.0[b] (5.4)	26.2 (7.0)	30.6 (7.1)	31.7 (8.2)	88 (12)	54 (9.1)	21.8[b]	1.57E+36
	1.0	2023	152.2 (13.4)	138.3 (12.8)	14.7 (5.0)	68.6 (9.4)	71.6 (9.5)	11.6 (4.7)	55 (4.9)	50 (4.6)	5.2 (1.8)	9.82E+35

TABLE 3—*Continued*

Source			Counts						Flux[a] (10^{-7} counts s^{-1} cm^{-2})			L[a] (ergs s^{-1})
CXO J	R.A., Decl., Uncertainty (arcsec)	ObsID	0.3–8.0	0.3–2.0	2.0–8.0	0.3–1.0	1.0–2.1	2.1–8.0	0.3–8.0	0.3–2.0	2.0–8.0	0.3–8.0
013444.6+305535	01 34 44.637	1730	...	...	...	...	...	...	...	...	...	...
	30 55 35.46	786	...	...	...	...	...	...	...	...	...	...
	1.3	2023	314.7 (19.2)	202.4 (15.5)	129.6 (12.8)	19.3 (5.8)	173.4 (14.3)	121.9 (12.5)	140 (8.3)	87 (6.7)	56 (5.6)	2.43E+36
013445.8+305222	01 34 45.853	1730	...	...	...	...	...	...	...	...	...	...
	30 52 22.43	786	...	...	...	...	...	...	...	...	...	...
	1.2	2023	10.5 (4.6)	<7.5	7.4 (4.0)	...	...	...	3.9 (1.7)	<5.6	2.8 (1.5)	6.95E+34
013446.7+304449	01 34 46.778	1730	...	...	...	...	...	...	...	...	...	...
	30 44 49.01	786	<8.5	<6.6	<6.6	...	...	...	<6.4	<5.0	<5.0	<1.15E+35
	1.0	2023	52.7 (8.4)	46.1 (7.9)	12.5 (4.8)	10.8 (4.4)	30.8 (6.6)	11.1 (4.6)	21 (3.3)	18 (3.0)	4.8 (1.9)	3.68E+35
013447.4+304957	01 34 47.471	1730	...	...	...	...	...	...	...	...	...	...
	30 49 57.53	786	...	...	...	...	...	...	...	...	...	...
	1.0	2023	12.4 (4.8)	5.7 (3.6)	6.6 (3.8)	...	...	...	4.4 (1.8)	2.1 (1.3)	2.4 (1.4)	7.95E+34
013447.4+303958	01 34 47.488	1730	...	...	...	...	...	...	...	...	...	...
	30 39 58.44	786	21.1 (7.3)	16.3 (6.2)	<17.2	7.2 (4.4)	8.4 (4.6)	4.4 (5.1)	17 (6.1)	13 (5.1)	<12.9	3.01E+35
	2.1	2023	...	...	...	...	...	...	...	...	...	...
013448.6+304706	01 34 48.629	1730	...	...	...	...	...	...	...	...	...	...
	30 47 06.55	786	<8.5	<4.6	<8.5	...	...	...	<6.4	<3.5	<6.4	<1.15E+35
	1.0	2023	7.3 (4.0)	<8.5	5.6 (3.6)	...	...	...	2.8 (1.5)	<6.4	2.1 (1.4)	4.98E+34
013449.0+304446	01 34 49.043	1730	...	...	...	...	...	...	...	...	...	...
	30 44 46.44	786	<8.5	<8.5	<4.6	...	...	...	<6.4	<6.4	<3.5	<1.15E+35
	1.1	2023	92.2 (10.8)	51.1 (8.3)	39.6 (7.5)	15.3 (5.1)	39.3 (7.4)	37.2 (7.4)	34 (4.0)	19 (3.0)	14 (2.7)	6.05E+35
013449.3+304808	01 34 49.314	1730	...	...	...	...	...	...	...	...	...	...
	30 48 08.96	786	<4.6	<4.6	<4.6	...	...	...	<3.5	<3.5	<3.5	<6.30E+34
	1.0	2023	7.3 (4.0)	7.8 (4.0)	<4.6	...	...	...	2.8 (1.5)	3.0 (1.5)	<3.5	5.03E+34
013449.5+305011	01 34 49.516	1730	...	...	...	...	...	...	...	...	...	...
	30 50 11.93	786	...	...	...	...	...	...	...	...	...	...
	1.1	2023	9.1 (4.3)	5.8 (3.6)	<9.1	...	...	...	3.3 (1.6)	2.1 (1.3)	<6.8	5.94E+34
013451.1+304356	01 34 51.128	1730	...	...	...	...	...	...	...	...	...	...
	30 43 56.76	786	<4.6	<4.6	<4.6	...	...	...	<3.5	<3.5	<3.5	<6.30E+34
	1.2	2023	80.4 (10.2)	63.3 (9.1)	17.1 (5.4)	7.3 (4.0)	58.3 (8.7)	14.5 (5.2)	30 (3.8)	24 (3.4)	6.3 (2.0)	5.37E+35
013451.8+304523	01 34 51.849	1730	...	...	...	...	...	...	...	...	...	...
	30 45 23.06	786	8.8 (4.6)	<12.2	<15.7	...	...	...	7.7 (4.0)	<9.2	<11.8	1.37E+35
	1.1	2023	<7.5	<8.5	<4.6	...	...	...	<5.6	<6.4	<3.5	<1.00E+35
013451.9+304615	01 34 51.938	1730	...	...	...	...	...	...	...	...	...	...
	30 46 15.84	786	137.5 (15.6)	77.6 (11.1)	57.0[b] (7.6)	24.5 (7.4)	60.1 (9.7)	55.0 (11.1)	120 (14)	6.7 (9.6)	42.8[b]	2.18E+36
	1.0	2023	121.3 (12.2)	85.2 (10.3)	35.9 (7.1)	25.5 (6.2)	59.5 (8.8)	36.2 (7.2)	48 (4.8)	34 (4.1)	14 (2.8)	8.56E+35
013452.2+305309	01 34 52.289	1730	...	...	...	...	...	...	...	...	...	...
	30 53 09.01	786	...	...	...	...	...	...	...	...	...	...
	1.6	2023	29.7 (7.2)	25.4 (6.3)	6.0[b] (2.5)	5.6 (3.8)	19.6 (5.7)	4.2 (4.1)	12 (3.0)	11 (2.6)	4.5[b]	2.21E+35
013452.3+305037	01 34 52.386	1730	...	...	...	...	...	...	...	...	...	...
	30 50 37.72	786	...	...	...	...	...	...	...	...	...	...
	1.2	2023	17.4 (5.4)	<13.8	11.8 (4.7)	...	...	...	7.1 (2.2)	<10.4	4.8 (1.9)	1.28E+35
013452.5+304241	01 34 52.595	1730	...	...	...	...	...	...	...	...	...	...
	30 42 41.74	786	<4.6	<4.6	<4.6	...	...	...	<3.5	<3.5	<3.5	<6.30E+34
	1.5	2023	16.2 (5.7)	9.0[b] (3.0)	<17.6	...	...	...	6.2 (2.2)	<6.8	<13.2	1.10E+35

TABLE 3—*Continued*

Source			Counts						Flux[a] (10^{-7} counts s^{-1} cm^{-2})			L[a] (ergs s^{-1})
CXO J	R.A., Decl., Uncertainty (arcsec)	ObsID	0.3–8.0	0.3–2.0	2.0–8.0	0.3–1.0	1.0–2.1	2.1–8.0	0.3–8.0	0.3–2.0	2.0–8.0	0.3–8.0
013453.2+305718	01 34 53.225	1730	...	...	...	...	...	...	...	...	...	...
	30 57 18.28	786	...	...	...	...	...	...	...	...	...	...
	2.0	2023	106.6 (12.6)	71.0 (10.0)	26.7 (6.7)	14.7 (5.6)	58.9 (9.1)	32.7 (8.1)	45 (5.3)	30 (4.2)	12 (2.9)	8.01E+35
013453.8+305744	01 34 53.843	1730	...	...	...	...	...	...	...	...	...	...
	30 57 44.79	786	...	...	...	...	...	...	...	...	...	...
	4.8	2023	13.0[b] (3.6)	14.4 (5.5)	<9.3	...	...	...	9.8[b]	6.2 (2.3)	<7.0	1.75E+35[b]
013455.3+304624	01 34 55.304	1730	...	...	...	...	...	...	...	...	...	...
	30 46 24.21	786	<6.6	<4.6	<6.6	...	...	...	<5.0	<3.5	<5.0	<9.00E+34
	1.2	2023	29.5 (6.7)	9.6 (4.3)	20.3 (5.8)	0.5 (2.3)	9.5 (4.3)	19.3 (5.7)	11 (2.5)	3.6 (1.6)	7.5 (2.1)	1.95E+35
013455.9+304814	01 34 55.922	1730	...	...	...	...	...	...	...	...	...	...
	30 48 14.77	786	...	...	...	...	...	...	...	...	...	...
	1.2	2023	16.4 (5.3)	11.7 (4.6)	<13.8	...	...	...	6.0 (2.0)	4.3 (1.7)	<10.4	1.07E+35
013456.1+304138	01 34 56.174	1730	...	...	...	...	...	...	...	...	...	...
	30 41 38.10	786	<6.6	<6.6	<4.6	...	...	...	<5.0	<5.0	<3.5	<9.00E+34
	2.0	2023	10.8 (4.7)	11.9 (4.7)	<6.6	...	...	...	4.6 (2.0)	4.9 (1.9)	<5.0	8.24E+34
013456.7+304556	01 34 56.798	1730	...	...	...	...	...	...	...	...	...	...
	30 45 56.01	786	5.9 (4.1)	<12.2	<9.7	...	...	...	6.5 (4.2)	<9.2	<7.3	1.17E+35
	1.3	2023	<6.0	<6.6	<4.6	...	...	...	<4.5	<5.0	<3.5	<8.10E+34
013456.9+304626	01 34 56.966	1730	...	...	...	...	...	...	...	...	...	...
	30 46 26.42	786	...	...	...	...	...	...	...	...	...	...
	1.3	2023	6.7 (3.8)	6.9 (3.8)	<4.6	...	...	...	2.5 (1.4)	2.6 (1.4)	<3.5	4.46E+34
013457.3+304319	01 34 57.344	1730	...	...	...	...	...	...	...	...	...	...
	30 43 19.44	786	<8.5	<8.5	<4.6	...	...	...	<6.4	<6.4	<3.5	<1.15E+35
	1.6	2023	9.0[b] (3.0)	8.9 (4.3)	<6.6	...	...	...	6.8[b]	3.4 (1.6)	<5.0	1.22E+35[b]
013457.7+304247	01 34 57.763	1730	...	...	...	...	...	...	...	...	...	...
	30 42 47.05	786	<4.6	<4.6	<4.6	...	...	...	<3.5	<3.5	<3.5	<6.30E+34
	1.8	2023	20.4 (6.0)	<6.0	21.7 (6.0)	<1.9	0.4 (2.3)	20.8 (5.9)	8.5 (2.5)	<4.5	9.1 (2.5)	1.51E+35
013458.5+304707	01 34 58.584	1730	...	...	...	...	...	...	...	...	...	...
	30 47 07.27	786	...	...	...	...	...	...	...	...	...	...
	1.3	2023	47.7 (8.3)	23.8 (6.1)	21.3 (5.9)	4.2 (3.4)	23.2 (6.0)	20.0 (5.9)	18 (3.2)	9.0 (2.3)	8.1 (2.2)	3.25E+35
013459.2+304608	01 34 59.236	1730	...	...	...	...	...	...	...	...	...	...
	30 46 08.02	786	...	...	...	...	...	...	...	...	...	...
	1.4	2023	20.5 (5.9)	8.7 (4.1)	9.1 (4.4)	2.5 (2.9)	7.5 (4.0)	10.2 (4.6)	7.6 (2.2)	3.2 (1.5)	3.4 (1.7)	1.36E+35
013500.5+305028	01 35 00.574	1730	...	...	...	...	...	...	...	...	...	...
	30 50 28.81	786	...	...	...	...	...	...	...	...	...	...
	1.6	2023	82.3 (10.5)	44.7 (7.9)	37.6 (7.5)	3.6 (3.4)	44.6 (7.8)	33.2 (7.2)	31 (4.0)	17 (3.0)	14 (2.9)	5.59E+35
013501.1+304345	01 35 01.127	1730	...	...	...	...	...	...	...	...	...	...
	30 43 45.33	786	85.6 (12.7)	53.6 (9.1)	<33.7	20.3 (6.6)	50.7 (8.8)	16.9 (7.9)	78 (11)	47 (8.0)	<25.3	1.40E+36
	1.2	2023	180.6 (14.9)	120.7 (12.1)	51.6 (8.6)	33.7 (7.1)	94.8 (10.9)	51.8 (8.8)	71 (5.9)	47 (4.7)	20 (3.4)	1.27E+36
013504.2+304344	01 35 04.228	1730	...	...	...	...	...	...	...	...	...	...
	30 43 44.50	786	<8.5	<8.5	<4.6	...	...	...	<6.4	<6.4	<3.5	<1.15E+35
	2.2	2023	13.4 (5.5)	8.0[b] (2.8)	<14.8	...	...	...	6.1 (2.4)	6.0[b]	<11.1	1.09E+35
013504.8+305034	01 35 04.820	1730	...	...	...	...	...	...	...	...	...	...
	30 50 34.15	786	...	...	...	...	...	...	...	...	...	...
	2.1	2023	8.0[b] (2.8)	8.9 (4.3)	<5.7	...	...	...	6.0[b]	3.6 (1.7)	<4.3	1.07E+35[b]

TABLE 3—*Continued*

Source			Counts						Flux[a] (10^{-7} counts s^{-1} cm^{-2})			L[a] (ergs s^{-1})
CXO J	R.A., Decl., Uncertainty (arcsec)	ObsID	0.3–8.0	0.3–2.0	2.0–8.0	0.3–1.0	1.0–2.1	2.1–8.0	0.3–8.0	0.3–2.0	2.0–8.0	0.3–8.0
013505.6+305004.....	01 35 05.685	1730	...	...	...	...	...	...	...	...	...	...
	30 50 04.47	786	...	...	...	...	...	...	...	...	...	...
	2.2	2023	42.8 (8.1)	13.9 (5.1)	25.2 (6.6)	<1.9	18.9 (5.6)	26.2 (6.5)	21 (3.9)	7.5 (2.6)	13 (3.2)	3.78E+35
013505.8+305429.....	01 35 05.889	1730	...	...	...	...	...	...	...	...	...	...
	30 54 29.06	786	...	...	...	...	...	...	...	...	...	...
	3.8	2023	30.6 (9.4)	23.4 (6.8)	<27.6	9.9 (5.1)	12.1 (5.3)	15.3 (7.0)	19 (4.9)	12 (3.3)	<20.7	3.44E+35
013507.3+305210.....	01 35 07.333	1730	...	...	...	...	...	...	...	...	...	...
	30 52 10.42	786	...	...	...	...	...	...	...	...	...	...
	2.9	2023	44.1 (8.3)	9.0 (4.3)	29.3 (6.9)	3.4 (3.4)	9.4 (4.4)	30.7 (7.1)	17 (3.3)	3.5 (1.7)	12 (2.8)	3.12E+35
013511.1+304257.....	01 35 11.170	1730	...	...	...	...	...	...	...	...	...	...
	30 42 57.48	786	...	...	...	...	...	...	...	...	...	...
	3.4	2023	29.3 (8.9)	12.4 (5.2)	<29.6	<3.2	20.6 (6.2)	12.0 (6.7)	13 (3.7)	5.1 (2.1)	<22.2	2.33E+35
013512.7+304514.....	01 35 12.718	1730	...	...	...	...	...	...	...	...	...	...
	30 45 14.46	786	...	...	...	...	...	...	...	...	...	...
	3.1	2023	22.9 (6.7)	14.8 (5.7)	9.0[b] (3.0)	1.4 (2.9)	12.4 (4.8)	9.4 (5.0)	9.6 (2.8)	6.0 (2.3)	6.8[b]	1.71E+35
013517.0+304407.....	01 35 17.030	1730	...	...	...	...	...	...	...	...	...	...
	30 44 07.11	786	...	...	...	...	...	...	...	...	...	...
	4.3	2023	20.6 (8.2)	18.6 (6.5)	<22.8	1.8 (3.8)	12.9 (5.3)	6.9 (6.1)	8.7 (3.3)	7.6 (2.6)	<17.1	1.55E+35
013517.5+304446.....	01 35 17.560	1730	...	...	...	...	...	...	...	...	...	...
	30 44 46.41	786	...	...	...	...	...	...	...	...	...	...
	4.2	2023	80.5 (11.6)	29.3 (7.0)	54.7 (9.3)	4.7 (4.3)	26.8 (6.7)	49.8 (9.3)	33 (4.7)	12 (2.8)	23 (3.9)	5.89E+35
013520.9+304236.....	01 35 20.996	1730	...	...	...	...	...	...	...	...	...	...
	30 42 36.08	786	...	...	...	...	...	...	...	...	...	...
	5.8	2023	25.4 (7.8)	18.0 (5.9)	<21.4	6.1 (4.1)	12.2 (5.0)	11.2 (5.7)	14 (3.8)	8.9 (2.8)	<16.1	2.57E+35

Notes.—Units of right ascension are hours, minutes, and seconds, and units of declination are degrees, arcminutes, and arcseconds. Table 3 is also available in machine-readable form in the electronic edition of the *Astrophysical Journal Supplement*.

[a] For sources with more than 100 counts, luminosity was computed from spectral fit; otherwise $\Gamma = 2$ and $N_H = 6 \times 10^{20}$ cm^{-2} are assumed.

[b] Most probable value; for details see § 2.

[c] The nucleus; because of pileup, counts and flux are not true values.

TABLE 4

Chandra Sources with Optical Counterparts

Source CXO J	Uncertainty (arcsec)	Counterpart (R.A., Decl.)	Magnitude/Colors			Remarks	Reference
			V	$B-V$	$U-B$		
013253.4+303817	6.1	01 32 53.30, +30 38 21.0	19.33	−0.14	−0.59		1
013253.9+303312	8.0	01 32 53.62, +30 33 06.4	19.62	1.51	...	M33d−676	2
013256.3+303558	15.4	01 32 56.10, +30 35 52.0	18.40	−0.10	−1.10	B30	1
		01 32 56.50, +30 35 50.0	19.27	−0.31	−0.30		1
		01 32 56.33, +30 35 52.4	18.19	−0.09	−0.89	B1 Ia/B30	3
		01 32 56.71, +30 35 49.5	19.44	−0.16	−1.02	O8−9	3
		01 32 57.13, +30 36 05.1	20.24	−0.13	−1.11		3
		01 32 56.41, +30 35 49.5	19.26	1.80	...	M33d−1785	2
		01 32 56.47, +30 36 01.1	20.10	1.70	...	M33d−798	2
013315.1+305317	8.1	01 33 15.00, +30 53 22.0	17.80	0.70	−0.90	B100, n	1
		01 33 15.30, +30 53 19.0	19.10	0.20	−0.70		1
		01 33 14.89, +30 53 24.9	19.61	−0.32	−0.84		4
		01 33 15.18, +30 53 18.2	18.45	−0.17	−0.69	Of or WN	4
		01 33 15.20, +30 53 25.0	17.8			B99	5
013327.9+303135	5.9	01 33 27.60, +30 31 37.0	20.83	−0.24	...		6
		01 33 27.90, +30 31 36.0	20.07	−0.13	...		6
		01 33 27.90, +30 31 34.0	19.68	−0.12	...		6
		01 33 27.80, +30 31 32.0	20.63	0.10	...		6
		01 33 27.90, +30 31 31.0	20.10	−0.22	−1.26		6
		01 33 27.90, +30 31 29.0	19.63	−0.17	...		6
013328.7+304746	4.5	01 33 28.80, +30 47 46.0	16.50	0.00	−0.70	B133	1
		01 33 28.97, +30 47 44.3	16.69	−0.08	−0.82	B1 Ia	4
		01 33 28.80, +30 47 46.0	16.73			B2.5 Ia	7
013333.6+303108	5.5	01 33 33.80, +30 31 14.0	19.12	−0.05	−1.10		6
		01 33 33.70, +30 31 12.0	20.32	−0.17	−1.07		6
013334.1+303210	1.9	01 33 34.00, +30 32 12.0	18.70	0.10	−1.30	n?	1
		01 33 34.20, +30 32 09.0	18.50	0.10	−1.20	B194	1
		01 33 34.20, +30 32 08.0	18.36	0.04	−1.21		6
		01 33 34.10, +30 32 08.3	20.28	0.21	−0.64		3
		01 33 34.12, +30 32 11.0	18.32	−0.06	−0.83		4
013336.0+303333	2.6	01 33 36.00, +30 33 31.0	20.48	−0.12	−0.50		6
013341.5+303220	3.2	01 33 41.50, +30 32 20.0	16.50	0.81	0.16		6
	3.2	01 33 41.30, +30 32 19.0	20.36	−0.05	−1.03		6
	3.2	01 33 41.30, +30 32 19.0	20.41	0.02	...		6
013358.4+303332	2.3	01 33 58.30, +30 33 33.0	19.52	−0.15	−1.05		6
013359.0+303425	1.8	01 33 59.20, +30 34 25.0	19.50	0.00	−1.10		1
		01 33 59.00, +30 34 26.0	19.56	−0.15	−1.15	Assoc. 54	6
013402.8+304151	1.0	01 34 02.91, +30 41 51.6	18.79	−0.20	−0.87		4
013408.3+304633	2.1	01 34 08.20, +30 46 36.0	19.20	0.10	−0.70		1
		01 34 08.50, +30 46 35.0	17.00	0.10	−0.90	B401	1
013416.3+305154	1.7	01 34 16.30, +30 51 56.0	16.40	0.00	−1.30	M	1
		01 34 16.30, +30 51 53.0	17.70	0.10	−1.30	B384, M	1
		01 34 16.46, +30 51 54.1	16.22	0.35	−0.72	B384?	4
013438.9+305014	22.9	01 34 38.60, +30 50 12.0	19.47	0.00	−0.84		1

Notes.—Units of right ascension are hours, minutes, and seconds, and units of declination are degrees, arcminutes, and arcseconds. Table 4 is also available in machine-readable form in the electronic edition of the *Astrophysical Journal Supplement*.

References.—(1) Ivanov et al. 1993; (2) Massey 1998; (3) Massey et al. 1995; (4) Massey et al. 1996; (5) Humphreys & Sandage 1980; (6) Regan & Wilson 1993; (7) Fabrika et al. 1997.

TABLE 5
Chandra-ROSAT Matches

Chandra Source		*ROSAT* Source			
CXO J	Uncertainty (arcsec)	Coordinates (R.A., Decl.)	Uncertainty (arcsec)	Name	HRI Rate (10^{-4} counts s^{-1})
013253.4+303817	6.1	01 32 53.400, +30 38 15.00	2.3	R027	20.10 ± 1.90
013253.9+303312	8.0	01 32 53.800, +30 33 10.00	2.6	R028	9.56 ± 1.30
013308.3+304802	4.8	01 33 08.700, +30 47 52.00	9.8	R040	...
013315.1+305317	8.2	01 33 15.100, +30 53 23.00	2.4	R049	188.00 ± 12.00
013323.8+303517	3.2	01 33 23.800, +30 35 16.00	4.2	R054	1.56 ± 0.43
013324.4+304403	1.5	01 33 24.300, +30 44 04.00	2.0	R055	67.00 ± 1.80
013327.7+304647	3.8	01 33 27.500, +30 46 51.00	5.4	R057	2.01 ± 0.54
013327.9+303135	6.0	01 33 27.800, +30 31 30.00	6.0	R058	2.22 ± 0.60
013328.7+304746	4.5	01 33 28.900, +30 47 47.00	3.8	R061	3.94 ± 0.62
013328.9+304216	1.1	01 33 28.900, +30 42 18.00	2.2	R062	10.00 ± 0.73
013329.4+304912	2.7	01 33 29.500, +30 49 14.00	3.1	R064	10.10 ± 0.90
013330.5+303404	2.9	01 33 30.600, +30 34 04.00	4.6	R066	1.23 ± 0.37
013331.1+303333	1.7	01 33 31.200, +30 33 32.00	2.2	R067	14.80 ± 0.89
013333.6+303108	5.5	01 33 33.700, +30 31 06.00	4.3	R070	2.81 ± 0.55
013334.1+303210	2.0	01 33 34.100, +30 32 09.00	2.0	R071	92.20 ± 2.10
013335.9+303627	1.1	01 33 35.900, +30 36 27.00	2.5	R074	3.84 ± 0.49
013336.0+303333	2.7	01 33 35.900, +30 33 31.00	4.3	R075	1.52 ± 0.40
013336.4+303742	1.0	01 33 36.400, +30 37 42.00	3.5	R077	1.32 ± 0.36
013337.5+304718	1.6	01 33 37.500, +30 47 21.00	4.3	R080	2.30 ± 0.49
013341.8+303848	1.0	01 33 41.800, +30 38 48.00	2.2	R084	7.75 ± 0.64
013343.4+304630	1.9	01 33 43.200, +30 46 33.00	2.5	R087	5.88 ± 0.62
013346.5+303748	0.9	01 33 46.600, +30 37 48.00	2.3	R092	6.20 ± 0.59
013350.5+303821	1.0	01 33 50.400, +30 38 18.00	3.4	R098	5.40 ± 1.30
013354.8+303310	1.4	01 33 55.000, +30 33 08.00	2.2	R106	10.70 ± 0.76
013356.7+303729	0.9	01 33 56.800, +30 37 28.00	2.4	R110	2.64 ± 0.40
013356.8+303706	1.0	01 33 56.800, +30 37 06.00	3.4	R109	1.14 ± 0.34
013357.0+303500	1.5	01 33 57.100, +30 35 01.00	4.4	R111	1.07 ± 0.33
013357.1+305134	5.7	01 33 57.300, +30 51 37.00	5.8	R112	3.26 ± 1.00
013358.4+303332	2.3	01 33 58.600, +30 33 31.00	3.7	R114	1.47 ± 0.38
013358.7+305003	2.1	01 33 58.700, +30 50 09.00	5.3	R115	3.44 ± 0.67
013401.2+303135	2.0	01 34 01.200, +30 31 36.00	3.0	R120	3.99 ± 0.56
013401.5+303136	2.0	01 34 01.200, +30 31 36.00	3.0	R120	3.99 ± 0.56
013402.0+303004	2.8	01 34 02.400, +30 30 08.00	12.4	R122	...
013407.9+303555	1.8	01 34 07.900, +30 35 53.00	3.5	R124	1.37 ± 0.35
013408.3+304633	2.1	01 34 08.500, +30 46 35.00	4.3	R126	2.22 ± 0.51
013409.8+305044	2.1	01 34 10.300, +30 50 52.00	17.1	R128	...
013410.5+303946	1.0	01 34 10.600, +30 39 47.00	2.7	R129	1.70 ± 0.35
013410.6+304223	1.6	01 34 10.800, +30 42 25.00	2.4	R130	5.22 ± 0.56
013414.1+305352	2.9	01 34 13.700, +30 53 52.00	17.1	R132	...
013416.9+303425	4.2	01 34 17.400, +30 34 22.00	5.0	R137	1.42 ± 0.42
013425.4+302821	6.9	01 34 25.400, +30 28 14.00	11.9	R143	3.94 ± 1.00
013426.6+303737	5.0	01 34 26.000, +30 37 35.00	11.5	R145	...
013428.1+303246	10.1	01 34 28.400, +30 32 54.00	11.9	R146	...
013429.7+305026	0.9	01 34 29.100, +30 50 27.00	12.8	R147	11.8 ± 3.10
013432.1+305158	1.1	01 34 32.800, +30 51 54.00	31.8	R150	...
013436.0+303450	11.7	01 34 36.400, +30 34 48.00	3.9	R154	5.56 ± 0.75
013438.7+304538	0.9	01 34 38.600, +30 45 28.00	14.6	R156	...
013439.8+305143	0.9	01 34 40.100, +30 51 48.00	4.7	R158	3.13 ± 1.10
013445.0+304927	0.9	01 34 45.200, +30 49 24.00	10.5	R161	5.01 ± 1.10
013500.9+304346	1.5	01 35 01.300, +30 43 50.00	6.3	R168	5.18 ± 1.80

Notes.—Units of right ascension are hours, minutes, and seconds, and units of declination are degrees, arcminutes, and arcseconds. *ROSAT* data from Haberl & Pietsch (2001). Table 5 is also available in machine-readable form in the electronic edition of the *Astrophysical Journal Supplement*.

TABLE 6

Chandra–XMM-Newton MATCHES

Chandra SOURCE		*XMM-Newton* SOURCE		
CXO J	Uncertainty (arcsec)	Coordinates (R.A., Decl.)	Flux (ergs cm^{-2} s^{-1})	X-Ray ID
013253.4+303817	2.6	1 32 53.46, 30 38 14.9	1.32E−13 ± 2.9E−15	X-1, SB1, LCB5, HP27
013253.9+303312	3.0	1 32 53.82, 30 33 12.1	1.14E−13 ± 2.8E−15	X-2, SB2, LCB6, HP28
013308.3+304802	2.5	1 33 08.21, 30 48 04.3	1.12E−14 ± 1.1E−15	LCB10, HP40
013315.1+305317	0.7	1 33 15.03, 30 53 17.9	1.06E−12 ± 1.3E−14	X-4, SB5, LCB13, HP49
013321.7+303858	1.4	1 33 21.66, 30 38 58.8	3.85E−15 ± 7.3E−16	...
013321.9+303921	1.4	1 33 22.02, 30 39 22.3	3.05E−15 ± 7.1E−16	...
013323.8+303517	1.6	1 33 23.86, 30 35 18.0	6.66E−15 ± 7.7E−16	HP54
013323.9+304821	3.2	1 33 23.79, 30 48 20.1	1.03E−14 ± 1.1E−15	...
013324.4+304401	0.7	1 33 24.31, 30 44 02.8	5.13E−13 ± 6.0E−15	X-5, SB6, LCB15, HP55
013325.5+303618	1.4	1 33 25.47, 30 36 17.1	4.43E−15 ± 7.5E−16	...
013327.7+304645	1.3	1 33 27.69, 30 46 47.4	4.66E−15 ± 6.4E−16	...
013327.9+303135	2.3	1 33 27.88, 30 31 36.1	2.99E−15 ± 4.0E−16	HP58
013328.7+304746	2.4	1 33 28.78, 30 47 44.5	7.48E−15 ± 7.1E−16	HP61
013329.0+304216	1.0	1 33 28.92, 30 42 16.9	2.45E−14 ± 9.9E−16	SB8, LCB18, HP62
013329.2+304537	1.6	1 33 29.21, 30 45 38.7	5.79E−15 ± 9.7E−16	...
013329.2+304508	1.1	1 33 29.19, 30 45 09.1	2.14E−14 ± 1.2E−15	SB9, LCB17, HP63
013329.4+304912	1.7	1 33 29.31, 30 49 10.7	1.73E−14 ± 1.0E−15	...
013330.5+303404	1.5	1 33 30.56, 30 34 04.1	1.80E−14 ± 1.2E−15	HP66
013331.1+303333	1.1	1 33 31.19, 30 33 33.3	3.88E−14 ± 1.2E−15	X-14, SB11, LCB20, HP67
013333.0+304920	3.0	1 33 32.70, 30 49 17.5	5.50E−15 ± 9.9E−16	...
013333.6+303108	2.2	1 33 33.70, 30 31 10.3	8.22E−15 ± 8.9E−16	HP70
013334.1+303714	1.0	1 33 34.16, 30 37 14.8	3.13E−15 ± 6.8E−16	...
013334.1+303210	0.7	1 33 34.07, 30 32 11.6	6.82E−13 ± 6.2E−15	X-7, SB12, LCB21, HP71
013334.5+303556	1.1	1 33 34.53, 30 35 55.0	2.42E−15 ± 4.7E−16	...
013335.9+303627	1.0	1 33 35.89, 30 36 27.6	1.01E−14 ± 6.4E−16	SB13, LCB22, HP74
013336.0+303333	1.4	1 33 35.86, 30 33 31.9	5.31E−15 ± 7.0E−16	HP75
013336.3+303742	1.0	1 33 36.27, 30 37 42.0	1.13E−14 ± 9.4E−16	HP77
013337.4+304718	1.2	1 33 37.32, 30 47 18.6	1.75E−14 ± 1.3E−15	LCB23, HP80
013339.2+304049	1.0	1 33 39.17, 30 40 51.0	4.96E−15 ± 8.0E−16	...
013340.0+304323	1.0	1 33 40.01, 30 43 22.4	4.18E−15 ± 8.0E−16	...
013341.5+303220	1.5	1 33 41.54, 30 32 19.7	1.39E−14 ± 9.7E−16	...
013341.5+304136	1.0	1 33 41.48, 30 41 35.2	4.33E−15 ± 6.7E−16	...
013341.8+303848	1.0	1 33 41.80, 30 38 48.8	1.49E−14 ± 8.6E−16	SB14, LCB24, HP84
013342.5+304253	1.0	1 33 42.36, 30 42 53.7	7.05E−15 ± 8.8E−16	HP86
013343.4+304630	1.1	1 33 43.26, 30 46 30.7	1.43E−14 ± 9.4E−16	LCB25, HP87
013346.5+303748	1.0	1 33 46.52, 30 37 50.0	2.06E−14 ± 1.3E−15	SB15, LCB26, HP92
013351.0+303937	0.7	1 33 50.84, 30 39 37.1	1.10E−11 ± 2.8E−14	X-8 (nuc), SB16, LCB28, HP102
013354.6+304519	1.1	1 33 54.67, 30 45 21.4	2.08E−15 ± 3.6E−16	HP103?
013354.8+303309	1.1	1 33 54.89, 30 33 11.4	2.84E−14 ± 1.0E−15	X-13, SB17, LCB29, HP106
013356.8+303729	1.0	1 33 56.75, 30 37 30.0	2.33E−14 ± 1.4E−15	LCB30, HP110
013356.8+303706	1.0	1 33 56.77, 30 37 08.4	8.74E−15 ± 9.9E−16	HP109
013357.2+305136	3.5	1 33 56.93, 30 51 37.1	4.62E−15 ± 8.0E−16	LCB31, HP112
013358.1+303200	1.6	1 33 57.80, 30 32 03.5	3.90E−15 ± 7.3E−16	...
013358.4+303333	1.3	1 33 58.49, 30 33 35.0	4.87E−15 ± 5.1E−16	HP114
013358.8+305004	1.5	1 33 58.70, 30 50 04.6	8.76E−15 ± 9.3E−16	LCB32, HP115
013359.0+303425	1.2	1 33 59.24, 30 34 26.5	4.23E−15 ± 6.7E−16	...
013400.0+303057	2.0	1 34 00.15, 30 30 59.1	3.70E−15 ± 7.4E−16	...
013400.2+304218	1.0	1 34 00.26, 30 42 18.7	3.65E−15 ± 5.6E−16	Part of HP121
013402.0+303004	1.4	1 34 02.00, 30 30 05.3	3.00E−14 ± 1.4E−15	HP122
013402.6+304939	2.1	1 34 02.75, 30 49 41.9	4.20E−15 ± 7.3E−16	...
013402.8+304151	1.0	1 34 02.86, 30 41 51.7	5.40E−15 ± 8.6E−16	Part of HP121
013407.8+303553	1.2	1 34 07.76, 30 35 54.5	7.82E−15 ± 7.6E−16	HP124
013408.4+304632	1.5	1 34 08.28, 30 46 34.5	5.21E−15 ± 4.8E−16	LCB34, HP126
013409.7+303259	1.8	1 34 09.57, 30 32 58.8	2.23E−15 ± 5.9E−16	...
013409.9+303219	1.3	1 34 09.99, 30 32 20.9	3.14E−15 ± 5.3E−16	...
013410.3+305346	2.4	1 34 10.30, 30 53 45.3	4.33E−15 ± 7.1E−16	...
013410.5+303946	1.0	1 34 10.41, 30 39 46.5	2.64E−14 ± 1.4E−15	HP129
013410.6+304223	1.0	1 34 10.61, 30 42 25.1	1.41E−14 ± 7.3E−16	LCB35, HP130
013412.8+303554	1.4	1 34 12.90, 30 35 56.1	3.87E−15 ± 7.0E−16	...
013416.3+305154	1.3	1 34 16.51, 30 51 55.0	2.46E−15 ± 4.6E−16	HP134?
013416.7+305101	1.2	1 34 16.71, 30 51 01.8	4.67E−15 ± 7.3E−16	HP139?
013417.0+303425	1.9	1 34 17.08, 30 34 25.8	7.08E−15 ± 8.2E−16	LCB36, HP137

TABLE 6—*Continued*

Chandra Source		*XMM-Newton* Source		
CXO J	Uncertainty (arcsec)	Coordinates (R.A., Decl.)	Flux (ergs cm^{-2} s^{-1})	X-Ray ID
013419.2+304942	1.0	1 34 19.48, 30 49 41.1	2.09E−15 ± 5.7E−16	...
013421.1+303928	1.6	1 34 20.94, 30 39 31.4	1.86E−15 ± 4.9E−16	...
013421.2+304932	1.0	1 34 21.13, 30 49 32.4	6.14E−15 ± 7.3E−16	...
013423.5+305426	1.7	1 34 23.31, 30 54 23.8	1.15E−15 ± 5.0E−16	...
013423.8+303847	1.9	1 34 23.81, 30 38 46.3	8.54E−15 ± 9.2E−16	...
013424.5+304306	1.2	1 34 24.55, 30 43 07.2	2.19E−15 ± 5.7E−16	...
013425.4+302821	2.4	1 34 25.72, 30 28 18.0	9.35E−15 ± 9.3E−16	HP143
013426.5+304446	1.0	1 34 26.42, 30 44 46.4	5.93E−15 ± 7.1E−16	...
013426.6+303737	2.3	1 34 26.58, 30 37 40.3	3.34E−15 ± 6.1E−16	LCB37, HP145
013427.0+304314	1.0	1 34 26.93, 30 43 14.2	7.47E−15 ± 7.5E−16	...
013428.1+303246	3.6	1 34 28.16, 30 32 48.0	7.61E−15 ± 8.5E−16	LCB39, HP146
013429.1+304212	1.2	1 34 29.08, 30 42 16.0	1.18E−15 ± 4.1E−16	...
013429.7+305026	1.0	1 34 29.72, 30 50 27.2	6.19E−15 ± 7.3E−16	HP147
013432.0+303455	1.8	1 34 31.99, 30 34 53.6	2.02E−14 ± 1.5E−15	...
013432.1+305158	1.0	1 34 32.06, 30 51 59.7	2.38E−14 ± 1.2E−15	HP150
013432.5+305035	1.0	1 34 32.44, 30 50 37.4	3.36E−15 ± 6.7E−16	...
013432.7+303436	3.7	1 34 32.44, 30 34 37.0	4.91E−15 ± 7.2E−16	...
013435.0+304439	1.0	1 34 34.89, 30 44 40.2	4.83E−15 ± 7.4E−16	...
013435.1+305646	1.5	1 34 35.09, 30 56 47.0	2.75E−14 ± 1.7E−15	...
013436.0+303450	4.3	1 34 35.92, 30 34 50.2	1.08E−14 ± 9.6E−16	LCB41, HP154
013438.8+304538	1.0	1 34 38.67, 30 45 40.1	1.66E−14 ± 9.8E−16	HP156
013438.8+305504	0.7	1 34 38.74, 30 55 05.2	1.90E−13 ± 3.6E−15	X-9a, LCB42, HP157
013439.8+305143	1.0	1 34 39.87, 30 51 44.4	7.83E−15 ± 8.1E−16	HP158
013441.0+304325	1.1	1 34 40.93, 30 43 28.5	4.84E−15 ± 4.5E−16	...
013442.0+305229	1.1	1 34 41.98, 30 52 28.9	4.40E−15 ± 7.5E−16	...
013442.5+305249	1.2	1 34 42.41, 30 52 49.2	8.22E−15 ± 8.6E−16	...
013442.8+304505	1.0	1 34 42.67, 30 45 06.7	9.84E−15 ± 8.9E−16	...
013444.6+305535	1.3	1 34 44.60, 30 55 36.5	2.83E−14 ± 1.6E−15	HP160
013447.4+303958	2.1	1 34 47.30, 30 40 01.1	3.62E−15 ± 7.3E−16	...
013449.0+304446	1.1	1 34 48.98, 30 44 47.9	9.09E−15 ± 8.8E−16	...
013449.3+304808	1.0	1 34 49.42, 30 48 09.5	1.71E−15 ± 4.0E−16	...
013451.1+304356	1.2	1 34 51.04, 30 43 58.5	3.43E−15 ± 6.7E−16	...
013451.9+304615	1.0	1 34 51.87, 30 46 16.8	8.83E−15 ± 9.2E−16	LCB46, HP165
013453.2+305718	2.0	1 34 53.25, 30 57 18.2	1.26E−14 ± 1.2E−15	HP163?
013458.5+304707	1.3	1 34 58.42, 30 47 08.6	4.11E−15 ± 7.4E−16	...
013500.5+305028	1.6	1 35 00.33, 30 50 28.9	6.54E−15 ± 9.1E−16	...
013505.6+305004	2.1	1 35 05.68, 30 50 06.5	8.13E−15 ± 9.2E−16	...
013505.8+305429	3.8	1 35 05.84, 30 54 28.6	2.79E−15 ± 8.4E−16	...
013507.3+305210	2.9	1 35 07.31, 30 52 09.8	4.50E−15 ± 8.8E−16	...
013512.7+304514	3.1	1 35 12.77, 30 45 14.6	2.30E−15 ± 7.4E−16	...
013517.5+304446	4.2	1 35 17.74, 30 44 46.7	8.61E−15 ± 1.5E−15	...

Notes.—Units of right ascension are hours, minutes, and seconds, and units of declination are degrees, arcminutes, and arcseconds. *XMM-Newton* data from Pietsch et al. (2004). Table 6 is also available in machine-readable form in the electronic edition of the *Astrophysical Journal Supplement*.

REFERENCES

Alexander, D. M., et al. 2003, AJ, 126, 539
Calzetti, D., Kinney, A. L., Ford, H., Doggett, J., & Long, K. S. 1995, AJ, 110, 2739
Chandar, R., Bianchi, L., & Ford, H. C. 1999, ApJS, 122, 431
———. 2001, A&A, 366, 498
Colbert, E. J. M., Heckman, T. M., Ptak, A. F., Strickland, D. K., & Weaver, K. A. 2004, ApJ, 602, 231
Dickey, J. M., & Lockman, F. J. 1990, ARA&A, 28, 215
Dubus, G., Charles, P. A., & Long, K. S. 2004, A&A, 425, 95
Engargiola, G., Plambeck, R. L., Rosolowsky, E., & Blitz, L. 2003, ApJS, 149, 343
Fabrika, S. N., Sholukhova, O. N., & Zakharova, S. A. 1997, Bull. Spec. Astrophys. Obs., 43, 133
Freedman, W. L., Wilson, C. D., & Madore, B. F. 1991, ApJ, 372, 455
Gebhardt, K., et al. 2001, AJ, 122, 2469
Gehrels, N. 1986, ApJ, 303, 336
Ghavamian, P., Blair, W. P., Long, K. S., Sasaki, M., Gaetz, T. J., & Plucinsky, P. P. 2005, AJ, 130, 539
Gilfanov, M. 2004, MNRAS, 349, 146
Gordon, S. M., Duric, N., Kirshner, R. P., Goss, W. M., & Viallefond, F. 1999, ApJS, 120, 247
Grimm, H.-J., Gilfanov, M., & Sunyaev, R. 2002, A&A, 391, 923
———. 2003, MNRAS, 339, 793
Haberl, F., & Pietsch, W. 2001, A&A, 373, 438
Hippelein, H., Haas, M., Tuffs, R. J., Lemke, D., Stickel, M., Klaas, U., & Völk, H. J. 2003, A&A, 407, 137
Hodge, P. W., Balsley, J., Wyder, T. K., & Skelton, B. P. 1999, PASP, 111, 685
Humphreys, R. M., & Sandage, A. 1980, ApJS, 44, 319
Ivanov, G. R., Freedman, W. L., & Madore, B. F. 1993, ApJS, 89, 85
Jarrett, T. H., Chester, T., Cutri, R., Schneider, S. E., & Huchra, J. P. 2003, AJ, 125, 525
Kilgard, R. E., et al. 2005, ApJS, 159, 214
Kim, D., & Fabbiano, G. 2003, ApJ, 586, 826
———. 2004, BAAS, 204, 15.02
Kim, D.-W., Fabbiano, G., & Trinchieri, G. 1992, ApJS, 80, 645

Kim, D.-W., et al. 2004a, ApJS, 150, 19
———. 2004b, ApJ, 600, 59
Kong, A. K. H., DiStefano, R., Garcia, M. R., & Greiner, J. 2003, ApJ, 585, 298
Kong, A. K. H., Garcia, M. R., Primini, F. A., Murray, S. S., Di Stefano, R., & McClintock, J. E. 2002, ApJ, 577, 738
Kraft, R. P., Burrows, D. N., & Nousek, J. A. 1991, ApJ, 374, 344
La Parola, V., Damiani, F., Fabbiano, G., & Peres, G. 2003, ApJ, 583, 758
Li, J., Ma, J., Zhou, X., Jiang, Z., Yang, Y., & Chen, J. 2004, A&A, 420, 89
Long, K. S., Charles, P. A., Blair, W. P., & Gordon, S. M. 1996, ApJ, 466, 750
Macri, L. M., Stanek, K. Z., Sasselov, D. D., Krockenberger, M., & Kaluzny, J. 2001, AJ, 121, 861
Magrini, L., Cardwell, A., Corradi, R. L. M., Mampaso, A., & Perinotto, M. 2001, A&A, 367, 498
Markert, T. H., & Rallis, A. D. 1983, ApJ, 275, 571
Massey, P. 1998, ApJ, 501, 153
Massey, P., Armandroff, T. E., Pyke, R., Patel, K., & Wilson, C. D. 1995, AJ, 110, 2715
Massey, P., Bianchi, L., Hutchings, J. B., & Stecher, T. P. 1996, ApJ, 469, 629
Massey, P., & Johnson, O. 1998, ApJ, 505, 793
Mochejska, B. J., Kaluzny, J., Krockenberger, M., Sasselov, D. D., & Stanek, K. Z. 1998, Acta Astron., 48, 455
Parmar, A. N., et al. 2001, A&A, 368, 420
Peres, G., Reale, F., Collura, A., & Fabbiano, G. 1989, ApJ, 336, 140
Pietsch, W., Misanovic, Z., Haberl, F., Hatzidimitriou, D., Ehle, M., & Trinchieri, G. 2004, A&A, 426, 11
Prestwich, A. H., Irwin, J. A., Kilgard, R. E., Krauss, M. I., Zezas, A., Primini, F., Kaaret, P., & Boroson, B. 2003, ApJ, 595, 719
Regan, M. W., & Wilson, C. D. 1993, AJ, 105, 499
Sasaki, M., Haberl, F., & Pietsch, W. 2000a, A&AS, 143, 391
———. 2000b, A&AS, 147, 75
Supper, R., Hasinger, G., Lewin, W. H. G., Magnier, E. A., van Paradijs, J., Pietsch, W., Read, A. M., & Trümper, J. 2001, A&A, 373, 63
Trinchieri, G., Fabbiano, G., & Peres, G. 1988, ApJ, 325, 531
Yokogawa, J., Imanishi, K., Tsujimoto, M., Nishiuchi, M., Koyama, K., Nagase, F., Corbet, R. H. D. 2000, ApJS, 128, 491